Compound-nuclear reaction cross sections from surrogate measurements

Jutta E. Escher, Jason T. Harke, Frank S. Dietrich, Nicholas D. Scielzo,
Ian J. Thompson, and Walid Younes
Lawrence Livermore National Laboratory, Livermore, California 94550, USA

(published 13 March 2012)

Nuclear reaction cross sections are important for a variety of applications in the areas of astrophysics, nuclear energy, and national security. When these cross sections cannot be measured directly or predicted reliably, it becomes necessary to develop indirect methods for determining the relevant reaction rates. The *surrogate nuclear reactions* approach is such an indirect method. First used in the 1970s for estimating (n, f) cross sections, the method has recently been recognized as a potentially powerful tool for a wide range of applications that involve compound-nuclear reactions. The method is expected to become an important focus of inverse-kinematics experiments at rare-isotope facilities. The present paper reviews the current status of the surrogate approach. Experimental techniques employed and theoretical descriptions of the reaction mechanisms involved are presented and representative cross section measurements are discussed.

DOI: 10.1103/RevModPhys.84.353 PACS numbers: 24.87.+y, 24.60.Dr, 25.85.Ec, 24.50.+g

CONTENTS

I. Introduction 353
II. Compound-nuclear reactions in basic and applied physics 355
A. Nuclear astrophysics 355
B. Nuclear energy 356
C. Radiochemistry for national security 356
III. Compound-nuclear cross sections from surrogate reactions 357
A. Hauser-Feshbach formalism for compound reactions 357
B. The surrogate strategy 358
1. Ideal approach 359
2. Modeling approach 359
3. Approximations 359
4. "Serendipitous" ("matching") approach 360
IV. Early surrogate work 360
V. Modern surrogate experiments 363
A. Surrogate experiments in France 364
1. Experimental setup 364
2. ^{230}Th, ^{231,233}Pa neutron-induced fission cross sections 364
3. Results for ^{241}Am(n, f) and ^{242,243}Cm(n, f) from surrogate reactions 365
B. STARS/LiBerACE experiments 367
1. STARS/LiBerACE experimental setup 367
2. Results for ^{237}Np(n, f) and ^{236}U(n, f) using the Weisskopf-Ewing approximation 367
3. Surrogate ratio experiments 368
4. Results for ^{230,231}Th(n, f) 369
5. Results for ^{237}U(n, f) 369
6. Results for ^{239}U(n, f) 369
7. Results for ^{238}Pu(n, f) 369
C. Results from other groups 369
VI. Validity of the Approximations 370
A. Experimental tests for (n, f) cross sections 370
B. Insights from theory: Spin dependence of fission probabilities 371
C. Fission cross sections from a Weisskopf-Ewing analysis 373
D. Fission cross sections from a ratio approach 373
VII. Modeling approach 374
A. Modeling approach for low-energy (n, f) reactions 374
B. Extension of the method to higher neutron energy 376
C. Comments on the modeling approach 377
VIII. Surrogate reactions for (n, γ) 378
A. Challenges for surrogate measurements of $(\boldsymbol{n}, \boldsymbol{\gamma})$ cross sections 378
B. Experimental efforts for $(\boldsymbol{n}, \boldsymbol{\gamma})$ 378
1. Weisskopf-Ewing approach to $(\boldsymbol{n}, \boldsymbol{\gamma})$ 379
2. Ratio measurements 380
C. Theoretical case studies for (n, γ) cross sections 381
1. Spin-parity mismatch and Weisskopf-Ewing approximation for $(\boldsymbol{n}, \boldsymbol{\gamma})$ cross sections 382
2. Ratios of coincidence probabilities 384
3. Using surrogate data to normalize calculated cross sections 385
IX. Toward a comprehensive theory of surrogate reactions 385
A. Theory of surrogate-reaction mechanisms 386
1. Pickup reactions 387
2. Inelastic scattering 387
3. Stripping reactions 388
4. Charge-exchange reactions 390
5. Two-nucleon transfer reactions 390
B. Width-fluctuation corrections 391
C. Tests of the theory predictions 391
D. Accuracy of compound-nucleus formation cross sections 392
E. Preequilibrium neutron emission in the desired reaction 393
X. Concluding remarks 394

I. INTRODUCTION

Nuclear reaction data play an important role in nuclear physics applications. Cross sections for reactions of neutrons and light, charged particles with target nuclei across the

isotopic chart, taking place at energies from several keV to tens of MeV, are required for nuclear astrophysics, national security, and nuclear-energy applications. Not all relevant data can be directly measured in the laboratory or easily determined by calculations.

Direct measurements may encounter a variety of difficulties: The energy regime relevant for a particular application is often inaccessible: cross sections for charged-particle reactions, e.g., become vanishingly small as the relative energy of the colliding nuclei decreases. For astrophysical purposes, such as descriptions of stellar environments and evolution, reaction rates at energies below 100 keV are needed. Furthermore, many important reactions involve unstable nuclei which are too difficult to produce with currently available techniques or are too short lived to serve as targets in present-day setups. Producing all relevant isotopes will remain challenging even for radioactive-beam facilities.

Cross section calculations are nontrivial since they often require a thorough understanding of both direct and statistical reaction mechanisms (as well as their interplay) and a detailed knowledge of nuclear structure. Nuclear-structure models can provide only limited information and little is known about optical-model potentials, level densities, and spectroscopy relevant to nuclei outside the valley of stability.

To overcome these limitations, several indirect methods have been employed in recent years. Approaches such as the ANC (asymptotic normalization coefficient) method (Xu *et al.*, 1994; Azhari *et al.*, 1999; Gagliardi *et al.*, 1999; Mukhamedzhanov, Gagliardi, and Tribble, 2001; Timofeyuk, Johnson, and Mukhamedzhanov, 2003; Timofeyuk and Descouvemont, 2005), Coulomb dissociation (Baur, Bertulani, and Rebel, 1986; Baur and Rebel, 1996; Baur, Hencken, and Trautmann, 2003), and the Trojan-horse method (Baur, 1986; Typel and Baur, 2003; Wolter and Typel, 2003; Baur and Typel, 2004; Pizzone and Spitaleri, 2008) have yielded valuable cross section information for various direct reactions. These methods focus on direct reactions, i.e., fast reactions (time scale $\approx 10^{-22}$ sec) that involve simple rearrangements of the constituents of the target and projectile nuclei.

The present review focuses on a complementary method, the *surrogate nuclear reaction method*, which aims at determining reaction cross sections for compound-nuclear reactions that involve difficult-to-produce targets. In a compound reaction, target and projectile nuclei combine to form a highly excited, intermediate system, the compound nucleus, which subsequently decays. The reaction proceeds on a relatively slow time scale ($\gg 10^{-22}$ sec), as the formation of a compound nucleus involves the excitation of many degrees of freedom. Apart from observing the constraints of basic conservation laws (energy, angular momentum), the formation and decay of a compound nucleus are considered to be independent of each other in first order (''Bohr hypothesis''); this independence is exploited in the surrogate-reaction approach. To obtain experimental information on the decay of the compound nucleus (B^*) occurring in the reaction of interest ($a + A \rightarrow B^* \rightarrow c + C$), this nucleus is produced via an alternative, ''surrogate'' reaction ($d + D \rightarrow B^* + b$) that involves a projectile-target combination ($d + D$) that is experimentally more accessible (see Fig. 1). The decay of B^* is observed in coincidence with the outgoing direct-reaction particle b. The measured compound-nuclear decay probabilities can then be combined with calculated formation cross sections for the compound nucleus in the desired reaction to yield the relevant reaction cross section.

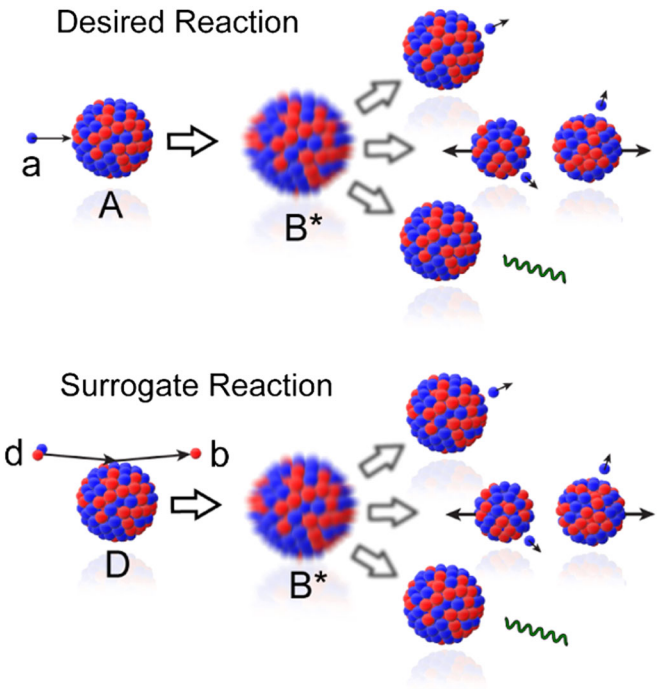

FIG. 1 (color online). Schematic representation of the desired (top) and surrogate (bottom) reaction mechanisms. The basic idea of the surrogate approach is to replace the first step of the desired reaction, $a + A$, by an alternative (surrogate) reaction, $d + D \rightarrow b + B^*$, that is experimentally easier to access yet populates the same compound nucleus. The subsequent decay of the compound nucleus into the relevant channel, $c + C$, can then be measured and used to extract the desired cross section. Three typical decay channels are shown here: neutron evaporation, fission, and γ emission.

Originally introduced in the 1970s (Cramer and Britt, 1970a; Britt and Wilhelmy, 1979), the surrogate approach has recently received renewed attention (Younes and Britt, 2003b; 2003c; Petit *et al.*, 2004; Boyer *et al.*, 2006; Harke *et al.*, 2006; Escher and Dietrich, 2006; Escher *et al.*, 2007; Jurado *et al.*, 2008; Escher and Dietrich, 2010; Kessedjian *et al.*, 2010). A sizable number of surrogate experiments aimed at obtaining (n, f) cross sections has been carried out over the years, and recent efforts have also considered (n, γ) cross sections. In principle, the method can also provide information about the charged-particle or two-neutron exit channels, or for reactions induced by charged particles, but, to date, little effort has been devoted to those cases.

In this paper, we review the present status of the surrogate method. In Sec. II, we have compiled representative examples from the areas of nuclear astrophysics, nuclear energy, and national security to illustrate the importance of cross sections for reactions on unstable targets for a wide variety of applications. The surrogate idea and formalism are detailed in Sec. III. The majority of the surrogate experiments carried out so far have focused on (n, f) cross sections. The early work, carried out in the 1970s, is summarized in Sec. IV, and the more recent experiments are reviewed in Sec. V. We

investigate the validity of the approximations that are typically used in these applications in Sec. VI and discuss recent steps that move beyond these approximate approaches in Sec. VII. Applications of the surrogate method to (n, γ) reactions are relatively new. In Sec. VIII, we review the challenges involved and the insights gained from recent (n, γ) experiments and theoretical work. Applications of the surrogate approach to a wide range of compound-nuclear reactions requires a comprehensive description of the reactions involved. We discuss the ingredients of such a theory in Sec. IX. We offer concluding remarks in Sec. X.

II. COMPOUND-NUCLEAR REACTIONS IN BASIC AND APPLIED PHYSICS

Many areas of basic and applied nuclear physics require cross sections for compound-nuclear reactions. Here we discuss some representative examples of interest to astrophysics, nuclear energy, and national security.

A. Nuclear astrophysics

Nuclear astrophysics addresses some of the most compelling questions in nature: What are the origins of the elements necessary for life? What is the age of the Universe? How did the Sun, the stars, our Galaxy form and evolve? We have acquired a basic, but incomplete understanding of the processes that drive stellar evolution and that are responsible for the synthesis of the elements (Rolfs and Rodney, 1988). Much effort is now devoted to developing detailed models of these processes and to formulate predictions, e.g., for isotopic abundances, that can be compared to astrophysical observations.

A prime example of the progress being made, and one in which compound-nuclear reaction cross sections play a crucial role, is our understanding of the synthesis of the heavy elements ($A > 56$). It is well known that nucleosynthesis of heavy elements beyond ^{56}Fe takes place primarily by neutron capture on lighter seed nuclei in the *s* (slow neutron capture) and *r* (rapid neutron capture) processes (Burbidge *et al.*, 1957; Rolfs and Rodney, 1988; Wallerstein *et al.*, 1997), with other processes contributing to the abundances of some specific isotopes. The basic nuclear mechanisms involved in the *s* and *r* processes are generally agreed upon, but many open questions remain. Current efforts address challenges such as identifying the site (or sites) of the *r* process, working out the details of the known *s*-process environments, and determining the signatures and contributions from additional processes. New astrophysical observations and increasingly sophisticated models of astrophysical phenomena present a unique opportunity for significant advances in these areas. Providing the requisite nuclear physics input is a major motivation for studies of unstable nuclei at radioactive-beam facilities around the world (National Research Council, 2003; Dean *et al.*, 2005; Ahearne *et al.*, 2006). These studies are expected to provide much-needed information on the structure of and reactions with unstable nuclei.

Cross sections for compound-nuclear reactions on radioactive targets, for instance, are required input for *s*-process models. The *s* process takes place under conditions in which the time interval between successive neutron captures is longer than the average lifetime for β decay (Rolfs and Rodney, 1988). As a result, the *s* process proceeds through nuclides in and very near the valley of stability. Reliable rates for neutron reactions along the *s*-process path are important input parameters for stellar models. Of particular interest are neutron captures on *s*-process branch points, unstable nuclei with a lifetime long enough to allow the *s* process to proceed by either neutron capture or β decay. The strength with which one path dominates over the other depends on environmental variables, such as neutron density, temperature, and pressure, as well as on nuclear properties, specifically capture rates and β-decay lifetimes. To reduce uncertainties in simulations of astrophysical environments, nuclear properties need to be known.

Specifically, spectroscopic observations of stars and high-precision isotope ratio measurements on presolar meteoritic grains provide constraints on stellar evolutionary models and serve as probes for the detailed conditions at the *s*-process site if the requisite reaction cross sections are known. The ^{96}Zr/^{94}Zr abundance ratio, for instance, is sensitive to the neutron density and temperature of the neutron production site in asymptotic giant branch stars (Lugaro *et al.*, 2003; Herwig, 2005). The temperature, in turn, is affected by mixing processes in the convective zones of such stars. The conclusions that can be drawn about the details of these mechanisms are limited by uncertainties in the neutron-capture rate for the unstable ^{95}Zr isotope, which has a half-life of 64 days. The ^{95}Zr(n, γ) cross section has not been measured, and current evaluations give cross sections that differ by factors of two to three in the energy region of interest (CSISRS, 2010). Similarly, cross sections for neutron capture on the *s*-process branch points ^{85}Kr ($t_{1/2} = 10.8$ days) and ^{86}Rb ($t_{1/2} = 18.65$ days) affect the abundances of nearby *s*-only isotopes. The production rates of the latter have been calculated with different stellar evolution models and are being used to understand the processes described by these models, such as neutron generation and hydrodynamic mixing in stars (Lugaro *et al.*, 2003). Other astrophysically significant *s*-process branch points can be used to probe additional aspects of the stellar environment under consideration, provided the relevant nuclear physics input is available. Most neutron-capture rates for branch points have not been measured as the nuclear lifetimes are too short.

Improved neutron-capture cross sections in a given mass region can significantly affect the predicted abundance distributions, both locally and also, through propagation along the *s*-process path, for heavier isotopes (Pignatari *et al.*, 2010). Beyond being important for gaining a more detailed description of the *s*-process environments, reliable *s*-process abundances are crucial for our understanding of the *r* (rapid neutron-capture) process. Models of the *r* process have to be validated by observables, i.e., they have to reproduce measured isotopic abundances. Typically, *r*-process abundances are inferred by subtracting calculated *s*-process abundances from measured total abundances. This requires detailed calculations to predict *s*-process abundances, and, of course, reliable cross sections for neutron captures along the *s*-process path (Travaglio *et al.*, 2004).

The *r* process takes place in an environment with high temperature ($T > 10^9$ K) and high neutron flux

($> 10^{20}/\mathrm{cm}^2$ sec). In such conditions, the average time between neutron captures is much shorter than the lifetime for β decay and reaction flows can proceed to very neutron-rich nuclei. When the strong neutron flux subsides, these neutron-rich nuclei decay back towards the valley of stability and produce relative isotopic abundances characteristic of the process. Despite the significant effort that has been devoted to the study of the *r* process, there are large gaps in our understanding of this process. Unknowns include the exact path along the nuclear chart of the neutron captures and β decays involved, and the astrophysical site(s) of the process. Candidate sites include core-collapse supernovae and neutron-star mergers (Arnould, Goriely, and Takahashi, 2007; Beun *et al.*, 2009).

β-decay half-lives and nuclear masses, which determine nucleon separation energies, are considered to be the most important nuclear physics inputs for *r*-process models, as they determine the neutron-capture path in scenarios that assume (n, γ) and (γ, n) reactions to be in equilibrium with each other. For some astrophysical models, e.g., those considering cold *r*-process scenarios (Wanajo, 2007), it is not appropriate to invoke the equilibrium assumption; the simulations then require neutron-capture rates for nuclei far off stability. Given the large number of reactions involved, calculations are and will remain essential for determining the relevant cross sections. Cross sections for both compound and direct-capture mechanisms are required (Mathews *et al.*, 1983; Goriely, 1997; Descouvemont and Rauscher, 2006; Rauscher, 2008). To test the reaction predictions, and to obtain complementary experimental information, measurements for selected capture rates will be very valuable. Global variations of capture rates have been shown to influence final abundance distributions (Goriely, 1998; Rauscher, 2005) and recent work indicates that modifying rates for captures on very specific nuclei may induce significant changes in the predicted abundances across a wide range of isotopes (Surman and Engel, 2001; Beun *et al.*, 2009; Surman *et al.*, 2009).

In addition, the rp (rapid proton capture) (Schatz *et al.*, 1998) and the γ (or p) (Arnould and Goriely, 2003) processes, which can produce various neutron-deficient isotopes, involve compound-nuclear reactions on both stable and unstable target nuclei. In some cases, reactions on target excited states are relevant as well. Only a small number of the relevant charged-particle capture cross sections, and their inverse reactions, have been measured.

B. Nuclear energy

The generation of electricity from nuclear fission is likely to play an increasingly important role in satisfying the ever-growing worldwide demand for energy. The use of nuclear energy avoids much of the pollution and CO_2 emission that results from the burning of fossil fuels. However, before a renaissance in nuclear energy can occur, concerns regarding reactor safety, waste handling, proliferation resistance, and economic competitiveness have to be carefully considered. Advanced nuclear-energy systems such as Generation-IV reactors, innovative nuclear-fuel cycles, and accelerator-driven systems, are actively being investigated to address these issues. Even more sophisticated technologies that take advantage of the high-energy neutrons from fusion reactions to initiate fission are being proposed as a long-term energy solution (Moses *et al.*, 2009; Tanaka, 2009).

The Generation-IV reactor designs take advantage of advances in nuclear technology. Several thermal-reactor and fast-reactor concepts are being researched and significant reactor modeling must be performed to optimize the strategies for efficient waste transmutation, the recycling of actinides in a closed fuel cycle, and the use of alternative fuel cycles. An important component of the research and development for these reactor concepts is the improvement of the fundamental nuclear data (Colonna *et al.*, 2010). The transuranic nuclides, for example, play a much more prominent role in these new designs and yet the available cross section data is quite limited. In addition, neutron-capture reactions could be used to incinerate long-lived fission fragments and therefore limit the challenges associated with the reactor waste.

The thorium-uranium fuel cycle is an appealing alternative to the conventional uranium-plutonium fuel cycle because of reduced buildup of radiotoxic heavy transuranium isotopes. In addition, thorium is monoisotopic so no isotopic separation is needed and is 3 to 4 times more abundant that uranium in the Earth's crust. Although the concept for a thorium-based fuel cycle is not new, much of the basic nuclear data required for design calculation either are not sufficiently precise or are altogether absent. Improved determination of neutron-induced cross sections for many thorium, protactinium, and uranium isotopes is needed to reach the desired accuracy standards.

Sensitivity studies (Aliberti *et al.*, 2006) indicate that high quality, reliable cross section data are needed for neutron-induced reactions for a wide variety of radioactive isotopes covering neutron energies from thermal up to tens of MeV. In particular, capture and fission reactions on many of the isotopes of thorium, uranium, plutonium, and the minor actinides (such as ^{237}Np, $^{241-243}$Am, and $^{244-245}$Cm), as well as certain long-lived fission fragments, are of interest. Many of these cross sections are extremely challenging to measure directly but significantly contribute to uncertainties in the reliable design and safe operation of a nuclear-energy system.

The surrogate-reaction method provides new opportunities to determine many of the needed cross sections. In fact, several cross section measurements on short-lived thorium and protactinium isotopes of importance for the thorium-uranium fuel cycle have already been performed (Petit *et al.*, 2004; Boyer *et al.*, 2006; Nayak *et al.*, 2008; Goldblum *et al.*, 2009). The (n, f) cross sections for ^{241}Am and $^{243-244}$Cm (Kessedjian *et al.*, 2010), and for ^{238}Pu(n, f) (Ressler *et al.*, 2011), of interest for nuclear-waste transmutation, have also recently been determined. It is anticipated that the surrogate-reaction approach will continue to provide valuable cross section results on isotopes for which there is limited, poor quality, or no data of use for nuclear-energy applications.

C. Radiochemistry for national security

Radiochemical data and interpretations are relevant to several national security areas (Mortensen, Scott, and

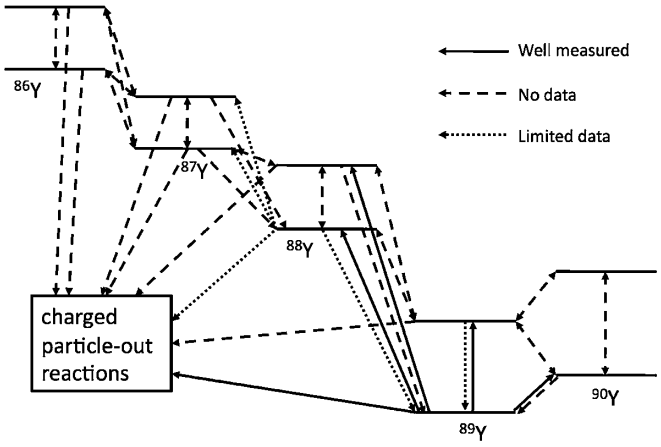

FIG. 2. Yttrium reaction network showing isomeric states and partial level schemes of ^{86}Y, ^{87}Y, ^{88}Y, ^{89}Y, and ^{90}Y and associated reaction channels. Most cross sections are unknown or poorly constrained.

Colgate, 2003; Kreisler, 2007; May *et al.*, 2008). For instance, various aspects of nuclear explosive device performance are determined through the application of radiochemistry. During the underground test program, select naturally occurring elements (or separated isotopes of these elements) were used and recovered after irradiation (Mortensen, Scott, and Colgate, 2003). Results are typically presented as isotopic ratios (such as $^{87}\mathrm{Y}/^{88}\mathrm{Y}$ produced from the stable isotope of the naturally occurring element). From the measured activity and prior knowledge of the amount of loaded detector material, performance aspects could be inferred by comparing the measured isotope ratios with those calculated using particle fluences from one of the design codes and appropriately averaged cross section sets that have been prepared for this purpose.

Many relevant reactions are dominated by compound-nuclear processes. Reactions that produce a given radio isotope are of interest, as well as those that destroy it. An example that illustrates the problem is shown in Fig. 2. The yttrium reaction network encompasses neutron-induced reactions [(n,γ), $(n,2n)$, (n,n'), and (n,p)] on the ground and long-lived (isomeric) excited states for several isotopes. Very few reactions have well-measured cross sections (represented by solid lines). Limited data are available for some reactions (dotted lines), but for most reactions, no data exist (dashed lines).

The yttrium reaction network considered here includes neutron-deficient isotopes close to the valley of stability; the primary challenge in calculating reliable cross sections lies in the proper description of the isomeric states. As in astrophysical environments, relevant reaction flows can also proceed farther into regions of unstable nuclei. Reactions on fission fragments that are more than a few nucleons away from the valley of stability, are of interest as well.

In the absence of measurements, Hauser-Feshbach reaction calculations are used to determine the cross sections of interest. Such calculations can reproduce measured cross sections (when available) to good accuracy. For $(n,2n)$, (n,n'), and (n,p) reactions in the energy range from 0.01 to 20 MeV, 10%–20% uncertainties are not uncommon. For neutron-capture reactions, the error is typically higher (30%–50%). With suitably developed systematics, cross sections on unstable targets adjacent to the nuclei used to construct the local systematics are expected to exhibit somewhat larger uncertainties. But as one reaches regions of the periodic chart farther removed from the valley of stability, one has to resort to extrapolation of the local systematics, or develop microscopic models that predict the necessary statistical model ingredients. Both approaches lead to uncertainties that have not yet been quantified.

In regions far removed from stability, little experimental data exist that can constrain or test the predictions. Neutron-induced reactions cannot presently be measured for such short-lived nuclei, but future experiments at radioactive-beam facilities will make it possible to study these isotopes in inverse-kinematics setups. Indirect approaches, such as the surrogate reactions method, will be required to interpret these experiments so that they can provide data to constrain the calculated cross sections.

III. COMPOUND-NUCLEAR CROSS SECTIONS FROM SURROGATE REACTIONS

The surrogate approach is designed to provide indirect information on cross sections that are difficult to measure directly or calculate accurately. We briefly review the statistical Hauser-Feshbach description relevant to the approach and indicate how surrogate data can be employed to determine or constrain the cross sections of interest.

A. Hauser-Feshbach formalism for compound reactions

The formalism appropriate for describing compound-nucleus reactions is the statistical Hauser-Feshbach theory (Hauser and Feshbach, 1952; Vogt, 1968; Fröbrich and Lipperheide, 1996; Thompson and Nunes, 2009). The average cross section per unit energy in the outgoing channel for reactions proceeding to an energy region in the final nucleus described by a level density is given by

$$\frac{d\sigma_{\alpha\chi}^{\mathrm{HF}}(E_a)}{dE_\chi} = \pi\lambda\!\!\!^{-2}_{\alpha}\sum_{J\pi}\omega_\alpha^J \sum_{\ell s\ell' s' I'} \frac{T^J_{\alpha\ell s}T^J_{\chi\ell' s'}\rho_{I'}(U')W_{\alpha\chi}(J)}{\sum'_{\chi''\ell''s''} T^J_{\chi''\ell''s''} + \sum_{\chi''\ell''s''I''}\int T^J_{\chi''\ell''s''}(E_{\chi''})\rho_{I''}(U'')dE_{\chi''}}. \tag{1}$$

Here α denotes the entrance channel $a+A$ and χ represents the relevant exit channel $c+C$, E_a is the kinetic energy of the projectile, and $\lambda\!\!\!^{-}_{\alpha}$ is the reduced wavelength in the incident channel. The spin of the incident particle is i, the target spin is I, the channel spin is $\vec{s}=\vec{i}+\vec{I}$, and the compound-nucleus angular momentum and parity are $J\pi$. The statistical-weight factor ω_α^J is $(2J+1)/[(2i+1)\times(2I+1)]$. Similarly, the spin of the outgoing particle is i',

the spin of the residual nucleus is I', and the channel spin for χ is $\vec{s}' = \vec{i}' + \vec{I}'$. The quantities ℓ and ℓ' are the relative orbital angular momentum in the entrance and exit channels, respectively. The transmission coefficients are written as $T^J_{\alpha ls}$ and $\rho_{I'}(U')$ denotes the density of levels of spin I' at excitation energy U' in the residual nucleus. All energetically possible final channels χ'' have to be taken into account, thus the denominator includes contributions from decays to discrete levels in the residual nuclei (given by the first sum in the denominator, $\sum'$) as well as contributions from decays to regions described by a level density in the residual nuclei (given by the second sum in the denominator which involves an energy integral of transmission coefficients and level densities in the residual nuclei). Width fluctuation corrections $W_{\alpha\chi}$ are included in order to account for correlations between the incident and outgoing reaction channels (Moldauer, 1961; Hilaire, Lagrange, and Koning, 2003). In writing Eq. (1), we have suppressed the parity quantum number except for that of the compound nucleus. In fact, the level density depends in principle on parity (although this dependence is usually ignored), and all sums over quantum numbers must respect parity conservation.

Very often the width fluctuations are unimportant $[W_{\alpha\chi}(J) \approx 1]$. In this case, for each total spin and parity $J\pi$, the expression factors into a product of two terms, one of which contains the transmission coefficients for the entrance channel. The other factor describes the probability of decay into the exit channel; i.e., it is the sum over exit-channel transmission coefficients divided by the denominator representing the decay into all energetically available channels. This factored form embodies the essential assumptions of the Hauser-Feshbach model, that formation and decay of the compound nucleus are independent processes, and that the total spin and parity of the compound system must be conserved.

Ingredients required to carry out Hauser-Feshbach cross section calculations include nuclear binding energies, spins, and parities of both ground and excited nuclear states, γ-branching ratios for these states, nuclear level densities, and transmission coefficients for particles, photons, and fission. Much effort has been devoted to develop the requisite models and codes, and to formulate parameter recommendations (Capote *et al.*, 2009). The approach has been successfully employed to reproduce cross sections for which some data are available. It complements measurements and makes predictions possible in the absence of data. The uncertainties of the calculated cross sections depend on the amount and quality of the available experimental constraints. For instance, neutron resonance measurements provide average level spacings and thus constraints for the level densities near the neutron separation energy. Average radiative widths provide information on the product of the level density and the γ-ray strength function, which is relevant to capture cross section calculations. Typically, the most valuable constraints come from actual cross section measurements, even if these exist for energies somewhat removed from the energy range of interest.

In the absence of constraining data, one has to rely on systematics or on extrapolations, which typically leads to significantly increased uncertainties in the calculated cross sections. Microscopic calculations of relevant quantities are valuable, in particular, if one extends the calculations to reactions on isotopes far removed from the valley of stability, but the uncertainties are difficult to quantify at present.

In typical applications that require cross sections for neutron-induced reactions, the formation of the compound nucleus is reasonably well described (see the discussion in Sec. IX.D), while a reliable description of the decay is more challenging, since the competition between all possible decay channels has to be properly captured in the calculated decay probabilities. It is the objective of the surrogate approach to determine or constrain the probabilities for decay into the channels of interest.

B. The surrogate strategy

Although the cross section expressed in Eq. (1) is differential in the outgoing-channel energy, this is not actually the quantity of interest. For the (n, f) reaction, we need the cross section integrated over all final-state energies, which for fission correspond to the energies of the transition states built on top of the fission barriers. For radiative capture, we usually need only the integral over the energy spectrum of primary γ rays emitted from the compound nucleus. We integrate over all energies E_χ of the final-state channel and, in a first approximation, neglect the width fluctuation correlations. The primary effect of the correlations is an enhancement of the elastic scattering cross section. Because of the requirement of flux conservation, the inelastic and reaction cross sections are reduced, although this depletion rarely exceeds 10%–20%, even at relatively low energies (below approximately 2 MeV). As the excitation energy of the compound nucleus (CN) increases and many reaction channels become available, the effect of the width fluctuations becomes quickly negligible for the nonelastic channels (see also the discussion in Sec. IX.B)

This allows us to write the cross section for the desired reaction as

$$\sigma_{a\chi}(E_a) = \sum_{J,\pi} \sigma^{\mathrm{CN}}_\alpha(E_{\mathrm{ex}}, J, \pi) G^{\mathrm{CN}}_\chi(E_{\mathrm{ex}}, J, \pi), \tag{2}$$

where $\sigma^{\mathrm{CN}}(E_{\mathrm{ex}}, J, \pi) = \sigma(a + A \rightarrow B^*)$ denotes the cross section for forming the compound nucleus at excitation energy E_{ex} with angular momentum and parity quantum numbers $J\pi$ and $G^{\mathrm{CN}}_\chi(E_{\mathrm{ex}}, J, \pi)$ is the branching ratio for the decay of this compound state into the desired exit channel χ. The kinetic energy E_a of the projectile a is related to the excitation energy of the compound nucleus E_{ex}, via

$$E_a = \frac{\mathcal{A}_A + \mathcal{A}_a}{\mathcal{A}_A}(E_{\mathrm{ex}} - S_a), \tag{3}$$

where the factor $(\mathcal{A}_A + \mathcal{A}_a)/\mathcal{A}_A$ accounts for the nuclear-recoil energy imparted on a nucleus consisting of $\mathcal{A}_A$ nucleons by a projectile consisting of $\mathcal{A}_a$ nucleons, and S_a is the energy required for separating particle a from the compound nucleus B.

In typical applications, the formation cross sections for the individual spins $\sigma^{\mathrm{CN}}_\alpha(E_{\mathrm{ex}}, J, \pi)$, can be calculated to reasonable accuracy by using optical potentials (see Sec. IX.D),

while the theoretical decay probabilities $G_\chi^{\rm CN}(E_{\rm ex}, J, \pi)$ are often quite uncertain. The objective of the surrogate method is to determine or constrain these probabilities via an indirect measurement. Equation (2) is just a simplified form of Eq. (1) in the absence of width-fluctuation corrections, in which the factorization representing independence of formation and decay of the compound system has been made explicit. Because of the independence hypothesis, we can replace the formation factor $\sigma_\alpha^{\rm (CN)}$ in Eq. (2) by a factor representing any other mechanism that we expect to form an equilibrated compound nucleus. This is the feature we exploit in developing the surrogate-reaction technique.

In a surrogate experiment, the compound nucleus B^* is produced via an alternative (surrogate), direct reaction $d + D \rightarrow b + B^*$ and the decay of B^* is observed in coincidence with the outgoing particle b. The probability for forming B^* in the surrogate reaction (with specific values for $E_{\rm ex}$, J, π) is $F_\delta^{\rm CN}(E_{\rm ex}, J, \pi)$, where δ refers to the entrance-channel reaction $D(d, b)$. The quantity

$$P_{\delta\chi}(E_{\rm ex}) = \sum_{J,\pi} F_\delta^{\rm CN}(E_{\rm ex}, J, \pi) G_\chi^{\rm CN}(E_{\rm ex}, J, \pi), \tag{4}$$

which gives the probability that the compound nucleus B^* was formed with energy $E_{\rm ex}$ and decayed into channel χ, can be obtained experimentally, by measuring N_δ, the total number of surrogate events, and $N_{\delta\chi}$, the number of coincidences between the direct-reaction particle and the observable that identifies the relevant exit channel:

$$P_{\delta\chi}^{\rm exp}(E_{\rm ex}) = \frac{N_{\delta\chi}}{N_\delta \epsilon_\chi}. \tag{5}$$

Here ϵ_χ is the efficiency for detecting the exit-channel χ for the reactions in which the outgoing direct-reaction particle b is detected. The efficiency for detecting b cancels in the ratio and does not need to be determined. To simplify the notation, we have suppressed here, and throughout the next few sections, the dependence of the coincidence probability $P_{\delta\chi}^{\rm exp}(E_{\rm ex})$ on the angle θ_b of the outgoing direct-reaction particle b. The angular dependence of $P_{\delta\chi}^{\rm exp}(E_{\rm ex})$ arises from the fact that the population $F_\delta^{\rm CN}(E_{\rm ex}, J, \pi)$ of the compound nucleus depends on the angular-momentum transferred in the surrogate reaction, and hence on θ_b. This dependence is made explicit in Sec. IX, where theoretical predictions for the populations are considered.

To determine the desired cross section from a surrogate measurement, one can pursue the following strategies:

1. Ideal approach

Ideally, one calculates the spin-parity distribution, $F_\delta^{\rm CN}(E_{\rm ex}, J, \pi)$, in Eq. (4) from a suitable theory that describes the formation of the compound nucleus following the direct reaction $d + D \rightarrow b + B^*$. Given a reliable prediction of the quantities $F_\delta^{\rm CN}(E_{\rm ex}, J, \pi)$, and a sufficient range of experimental data $P_{\delta\chi}(E_{\rm ex})$ (for a range of energies and angles of the outgoing particle b, and possibly for various exit channels), it might be possible to extract the $G_\chi^{\rm CN}(E_{\rm ex}, J, \pi)$ which can then be used to calculate the desired cross section using Eq. (2). At this time, this idealized approach has not been implemented since a combination of possible reaction mechanisms, predicted $F_\delta^{\rm CN}$, and experimental data has not been available to unambiguously extract useful branching ratios.

2. Modeling approach

More realistically, the decay of the compound nucleus is modeled in a Hauser-Feshbach-type calculation that makes use of independently available (but typically incomplete) nuclear-structure information. The $G_\chi^{\rm CN}(E, J, \pi)$ obtained from such modeling are combined with calculated $F_\delta^{\rm CN}(E_{\rm ex}, J, \pi)$ to yield a prediction for $P_{\delta\chi}(E_{\rm ex})$. Fitting the latter to surrogate data provides further constraints on the $G_\chi^{\rm CN}$ which can then be employed in the calculation of the desired cross section. Steps towards developing this modeling approach were taken by Andersen, Back, and Bang (1970), Back *et al.* (1974b), and Younes and Britt (2003b and 2003c) for measurements designed to yield (n, f) cross sections.

3. Approximations

The majority of surrogate applications to date has relied on invoking approximations, such as the Weisskopf-Ewing limit of the Hauser-Feshbach theory, or the surrogate ratio method (Escher and Dietrich, 2006; 2010).

In the *Weisskopf-Ewing* (WE) limit of the Hauser-Feshbach theory, the branching ratios are independent of angular momentum and parity, $G_\chi^{\rm CN}(E_{\rm ex}, J, \pi) \rightarrow \mathcal{G}_\chi^{\rm CN}(E_{\rm ex})$, and the cross section expression for the desired reaction becomes

$$\sigma_{\alpha\chi}^{\rm WE}(E_a) = \sigma_\alpha^{\rm CN}(E_{\rm ex}) \mathcal{G}_\chi^{\rm CN}(E_{\rm ex}). \tag{6}$$

Here $\sigma_\alpha^{\rm CN}(E_{\rm ex})$ denotes the cross section for forming the compound nucleus at energy $E_{\rm ex}$,

$$\sigma_\alpha^{\rm CN}(E_{\rm ex}) \equiv \sum_{J\pi} \sigma_\alpha^{\rm CN}(E_{\rm ex}, J, \pi), \tag{7}$$

which can be calculated using a suitable optical potential. The Weisskopf-Ewing approximation greatly simplifies the application of the surrogate method: The branching ratios $\mathcal{G}_\chi^{\rm CN}$ can be directly obtained from the measured coincidence probabilities $P_{\delta\chi}$ [since $\sum_{J\pi} F_\delta^{\rm CN}(E_{\rm ex}, J, \pi) = 1$],

$$P_{\delta\chi}(E_{\rm ex}) = \mathcal{G}_\chi^{\rm CN}(E_{\rm ex}), \tag{8}$$

and the desired cross section can be written as

$$\sigma_{\alpha\chi}^{\rm CN}(E_{\rm ex}) = \sigma_\alpha^{\rm CN}(E_{\rm ex}) P_{\delta\chi}(E_{\rm ex}). \tag{9}$$

Thus, in this approximation, calculating the direct-reaction probabilities $F_\delta^{\rm CN}(E_{\rm ex}, J, \pi)$ or modeling the compound-nuclear decay is not required.

The term ''absolute surrogate method'' is sometimes used to distinguish analyses of surrogate data that determine the coincidence probabilities via Eq. (5) from *ratio analyses* that determine only a ratio of probabilities, as described next. In this review, we reserve the term ''Weisskopf-Ewing'' approximation to describe the above approach, and use the term ''ratio approach'' for applications that employ ratio analyses in addition to invoking the Weisskopf-Ewing approximation.

The *surrogate ratio approach* (Harke *et al.*, 2006; Escher and Dietrich, 2006; 2010) is an approximation that makes use of the surrogate idea and requires the (approximate) validity of the Weisskopf-Ewing limit. In this approach, the ratio

$$R(E) = \frac{\sigma_{\alpha_1\chi_1}(E)}{\sigma_{\alpha_2\chi_2}(E)} \tag{10}$$

of the cross sections of two compound-nuclear reactions, $a_1 + A_1 \rightarrow B_1^* \rightarrow c_1 + C_1$ and $a_2 + A_2 \rightarrow B_2^* \rightarrow c_2 + C_2$, is determined in two surrogate experiments. An independent determination of one of the cross sections can then be used to deduce the other. In the Weisskopf-Ewing limit,

$$R(E) = \frac{\sigma_{\alpha_1}^{\mathrm{CN1}}(E)\mathcal{G}_{\chi_1}^{\mathrm{CN1}}(E)}{\sigma_{\alpha_2}^{\mathrm{CN2}}(E)\mathcal{G}_{\chi_2}^{\mathrm{CN2}}(E)}. \tag{11}$$

For most cases of interest, the compound-nucleus formation cross sections $\sigma_{\alpha_1}^{\mathrm{CN1}}$ and $\sigma_{\alpha_2}^{\mathrm{CN2}}$ can be calculated reliably by using an optical model. To determine $\mathcal{G}_{\chi_1}^{\mathrm{CN1}}(E)/\mathcal{G}_{\chi_2}^{\mathrm{CN2}}(E)$, two experiments are carried out that create the relevant compound nuclei (CN1 and CN2, respectively). For each experiment, the number of coincidence events $N_{\delta_1\chi_1}^{\mathrm{CN1}}$ and $N_{\delta_2\gamma_2}^{\mathrm{CN2}}$ is measured. The ratio of the branching ratios into the desired channels for the compound nuclei created in the two reactions is given by

$$\frac{\mathcal{G}_{\chi_1}^{\mathrm{CN1}}(E)}{\mathcal{G}_{\chi_2}^{\mathrm{CN2}}(E)} = \frac{P_{\delta_1\chi_1}^{\mathrm{CN1}}(E)}{P_{\delta_2\chi_2}^{\mathrm{CN2}}(E)} = \frac{N_{\delta_1\chi_1}^{\mathrm{CN1}}(E)}{N_{\delta_2\chi_2}^{\mathrm{CN2}}(E)} \frac{N_{\delta_2}^{\mathrm{CN2}}(E)}{N_{\delta_1}^{\mathrm{CN1}}(E)} \frac{\epsilon_{\chi_2}(E)}{\epsilon_{\chi_1}(E)}, \tag{12}$$

where ϵ_χ denotes the efficiency for detecting the relevant exit channel. The experimental conditions are adjusted such that the relative number of reaction events $N_{\delta_1}^{\mathrm{CN1}}/N_{\delta_2}^{\mathrm{CN2}}$ can be determined from the relative beam intensities, target thickness, and live times of the two experiments. The ratio of detection efficiencies $\epsilon_{\chi_2}/\epsilon_{\chi_1}$ can typically be determined accurately and for fission measurements is nearly unity. The ratio of the decay probabilities then simply equals the ratio of the coincidence events and $R(E)$ becomes

$$R^{\mathrm{exp}}(E) = \frac{\sigma_{\alpha_1}^{\mathrm{CN1}}(E)N_{\delta_1\chi_1}^{\mathrm{CN1}}(E)}{\sigma_{\alpha_2}^{\mathrm{CN2}}(E)N_{\delta_2\chi_2}^{\mathrm{CN2}}(E)}, \tag{13}$$

where we have set $N_{\delta_1}^{\mathrm{CN1}}/N_{\delta_2}^{\mathrm{CN2}} = 1$ and $\epsilon_{\chi_2}/\epsilon_{\chi_1} = 1$ to simplify the notation. One advantage of this method is that it eliminates the need to accurately measure N_δ, the total number of surrogate-reaction events; determining N_δ can be difficult when target impurities are present.

The meaning of the energy E in the above equations remains to be specified. Typically, the energy dependence of a compound-nucleus formation cross section $\sigma_\alpha^{\mathrm{CN}} = \sigma(a + A \rightarrow B^*)$ is characterized by the kinetic energy of the projectile E_a while a branching ratio is normally given as a function of the excitation energy of the compound nucleus, $\mathcal{G}_\chi^{\mathrm{CN}}(E_{\mathrm{ex}})$. In a compound-nucleus reaction, those two values are related via the separation energy S_a of the particle a in B^*; see Eq. (3). While either E_{ex} or E_a can be used to uniquely specify the energy dependence of such a reaction, the choice to select one or the other energy to "match" in the ratio has certain implications for the type of corrections that have to be taken into account. This is discussed in Sec. V.B.3.

4. "Serendipitous" ("matching") approach

A primary challenge for the surrogate approach lies in accounting for the spin-parity mismatch between the desired and surrogate reactions. The situation simplifies greatly when it is possible to identify a surrogate reaction (i.e., a reaction mechanism, projectile-target combination, beam energy, outgoing-particle angle) that approximately reproduces the spin-parity distribution of the desired reaction, that is when

$$F_\delta^{\mathrm{CN}}(E_{\mathrm{ex}}, J, \pi) \approx F_\alpha^{\mathrm{CN}}(E_{\mathrm{ex}}, J, \pi) \equiv \frac{\sigma_\alpha^{\mathrm{CN}}(E_{\mathrm{ex}}, J, \pi)}{\sum_{J',\pi'}\sigma_\alpha^{\mathrm{CN}}(E_{\mathrm{ex}}, J', \pi')} \tag{14}$$

holds for all possible (J, π) combinations. Here F_α^{CN} is the compound-nuclear spin-parity population in the desired reaction. In this limit, we find

$$\sigma_{\alpha\chi}(E_a) \approx \sigma_\alpha^{\mathrm{CN}}(E_{\mathrm{ex}})P_{\delta\chi}^{\mathrm{exp}}(E_{\mathrm{ex}}). \tag{15}$$

The compound-nuclear formation cross section $\sigma_\alpha^{\mathrm{CN}}(E_{\mathrm{ex}})$ defined in Eq. (7), can be calculated using an optical potential, and $P_{\delta\chi}^{\mathrm{exp}}(E_{\mathrm{ex}})$ is determined from the experiment. While it is sometimes argued that a given surrogate experiment approximately satisfies Eq. (14), there has not been sufficient evidence to support such claims.

IV. EARLY SURROGATE WORK

The surrogate approach was first used in the 1970s to extract (n, f) cross sections for various actinides from transfer reactions with t and ^{3}He projectiles on neighboring (long-lived) nuclei, followed by fission (Cramer and Britt, 1970a; Britt and Wilhelmy, 1979). The experimental fission probabilities P_f were determined using Eq. (5). Utilizing the Weisskopf-Ewing approximation, cross sections were determined using Eq. (9) by simply multiplying the measured P_f values by an estimated cross section for the formation of the compound nucleus in the neutron-induced reaction of interest. The results of this approach typically agreed with direct measurements (where available) to within 10%–20% at energies $\gtrsim 1$ MeV but showed larger deviations at lower energies. Below we summarize the results of the early experiments from which the surrogate approach has evolved.

The first time fission probabilities were measured using a direct reaction instead of a neutron-induced reaction was in 1959 (Northrop, Stokes, and Boyer, 1959). The absolute fission probabilities P_f were determined from Eq. (5) for ^{239}Pu and ^{233,235,238}U from the relative number of particle-fission coincidence counts $N_{\delta f}$ and particle-singles counts N_δ after accounting for the fission-fragment detection efficiency ϵ_f. The excitation energy of the resulting nucleus following a nuclear reaction that releases energy Q is determined from

$$E_{\mathrm{ex}} = E_a - E_b - E_r + Q, \tag{16}$$

where E_a is the energy of the incident beam, E_b is the ejectile particle energy (corrected for energy loss in apparatus dead layers), and E_r is the recoil energy imparted to the nucleus. It

was pointed out that light-ion reactions, such as (d, p), have the advantage that P_f can be determined both above and below the neutron separation energy. The energy of the emitted proton was determined using a ΔE-E telescope consisting of a thin transmission ion chamber backed by a NaI (Tl) detector. Fission fragments were detected using a single proportional counter. The targets were 2 mg/cm^2 of actinide oxide vacuum evaporated on a 200 μg/cm^2 gold backing. Backgrounds from carbon, oxygen, and the gold backing were accounted for and subtracted by measuring (d, p) on other targets. They even noted that the probability for fission from the (d, p) reaction at 2 MeV for the different nuclei have the same ratios as the neutron-induced reaction. These early results were believed to be accurate to 10%–20%.

In the following years, similar techniques were routinely used to study fission properties induced by direct reactions. Measurements were performed using (d, pf), $(\alpha, \alpha' f)$, (t, pf), (t, df), (^{3}He, df), and (^{3}He, tf) reactions to determine fission thresholds, the excitation-energy dependence of the fission probabilities, and/or the fission-fragment angular anisotropies for many different actinides (Wilkins, Unik, and Huizenga, 1964; Britt *et al.*, 1965; Britt and Plasil, 1966; Specht, Fraser, and Milton, 1966; Britt, Rickey, and Hall, 1968; Wolf, Vandenbosch, and Loveland, 1968; Britt and Cramer, 1969, 1970; Cramer and Britt, 1970b; Back *et al.*, 1974a, 1974b; Gavron *et al.*, 1975; Van Der Plicht *et al.*, 1980; Wu *et al.*, 1981; David *et al.*, 1987; Sinha *et al.*, 1992). These experiments used semiconductor detectors for both light-ion and fission-fragment detection. For example, Britt, Rickey, and Hall (1968), identified light ions using a ΔE-E telescope consisting of a 310-μm surface-barrier silicon detector backed by either a 2-mm or 3-mm-thick lithium-drifted silicon detector while fission fragments were observed in coincidence using an array of eight phosphorus-diffused silicon detectors. In this particular measurement, protons from (d, pf) and (t, pf) reactions were detected with a FWHM energy resolution of 120 keV. Typical targets consisted of 150–2000 μg/cm^2 of actinide oxides deposited on a thin carbon or gold backing. Reactions off of ^{12}C and ^{16}O nuclei in the target were often used to calibrate the ΔE-E telescope response. In some cases, additional targets were run to measure the backgrounds from these light contaminants and in other cases the impact of the contamination was estimated by interpolating values under the obvious light-ion contaminant peaks as is shown in Fig. 3 [from Cramer and Britt (1970b)]. The typical FWHM energy resolution that was obtained was 100–200 keV for 10–20 MeV protons, deuterons, and tritons, and 300–500 keV for 30–40 MeV ^{3}He and ^{4}He ions and was limited by the intrinsic resolution of the detectors, the kinematic spread due to finite detector solid angles, and other effects such as incident beam properties.

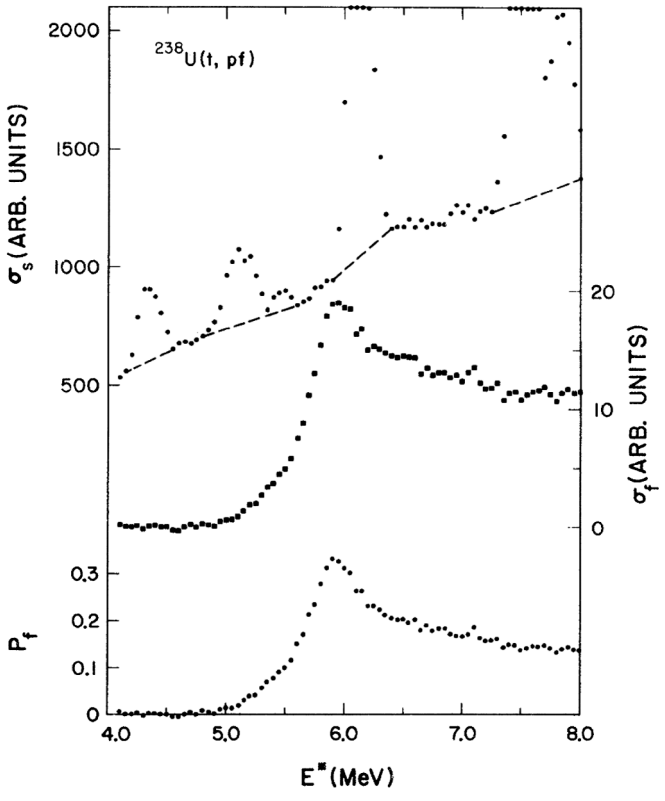

FIG. 3. Determination of fission coincidence probabilities for the ^{240}U compound nucleus in an early surrogate experiment. The proton-singles spectra N_δ for ^{238}U(t, p) is shown at the top with interpolated dashed lines to determine the spectrum under the clearly visible peaks from (t, p) reactions on ^{12}C and ^{16}O. The ratio of this spectrum to the $N_{\delta f}$ spectrum shown below it results in P_f, shown at the bottom. From Cramer and Britt, 1970b.

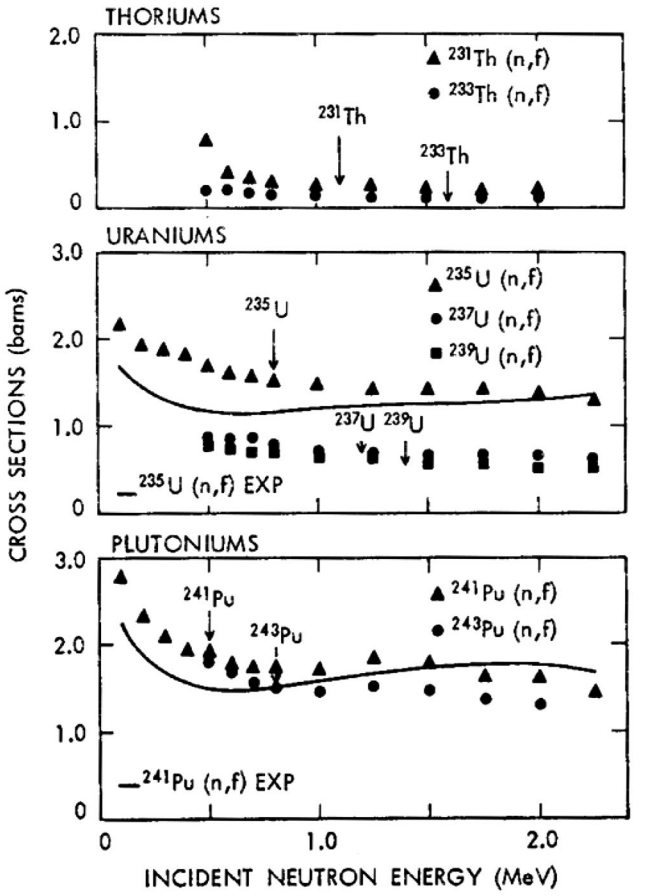

FIG. 4. The (n, f) cross sections determined using the Weisskopf-Ewing approximation to analyze (t, pf) data. The solid lines show the results of the direct measurements that existed at the time. The agreement above 1 MeV is quite good. From Cramer and Britt, 1970a.

This resolution was adequate to observe the desired energy-dependent features of P_f and evolution of the fission-fragment anisotropy. In these studies, the fission probabilities obtained from (t, pf) and (d, pf) reactions were found to be qualitatively similar to the fission probabilities deduced from (n, f) measurements (Britt and Cramer, 1970).

Cramer and Britt (1970a) were the first to use probabilities from light-ion reactions to infer (n, f) cross sections; they employed (t, pf) reactions to determine cross sections for short-lived actinides. The light-ion telescope detected scattered protons at back angles to minimize the effect of target impurities. The use of an 18-MeV t beam limited the accessible energy range to just a few MeV above the neutron separation energy because of t breakup.

The (n, f) cross sections $\sigma_{(n,f)}$, for the short-lived isotopes ^{231,233}Th, ^{237,239}U, and ^{243}Pu, were determined for neutron energies of 0.5–2.25 MeV from the product of the estimated compound-nuclear formation cross sections σ_n^{CN}, and the measured values of P_f using the Weisskopf-Ewing approximation. The reliability of the surrogate approach was investigated by also determining ^{235}U and ^{241}Pu cross sections and comparing the results to direct measurement.

As can be seen in Fig. 4, the resulting (n, f) cross section estimates agreed with the then available direct measurements to about 10%–20% for incident-neutron energies above about 1 MeV, but resulted in 20%–40% discrepancies below 1 MeV. These discrepancies were attributed to large uncertainties in the low-energy optical-model calculations employed and the neglect of the difference in the angular-momentum populations of the compound nucleus in the surrogate (transfer reaction) and "desired" (neutron-induced) reactions. The cross section uncertainties were estimated to be 10% from the determination of P_f, 5%–20% from the optical-model calculations, and 5%–20% from angular-momentum effects.

This method was subsequently used with $(^3\mathrm{He}, df)$ and $(^3\mathrm{He}, tf)$ reactions on a variety of actinide targets to infer (n, f) cross sections for 34 actinide nuclei at energies up to 6 MeV (Britt and Wilhelmy, 1979). The highest energy that could be reached was limited by the rapid decrease in cross section caused by the Coulomb barrier for outgoing charged particles and the increase in background from carbon and

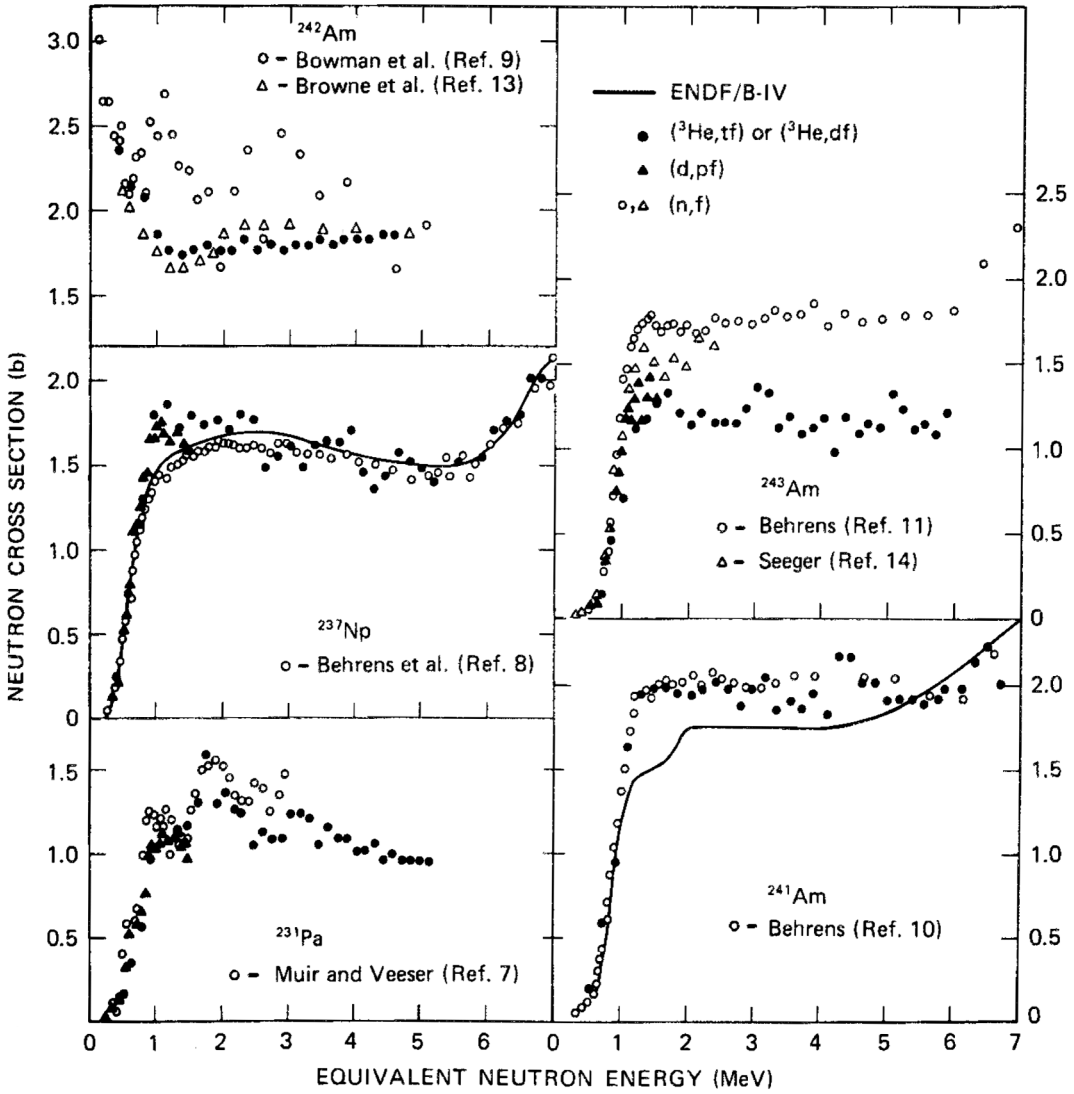

FIG. 5. The (n, f) cross sections for ^{241,242,243}Am, ^{237}Np, and ^{231}Pa determined using the Weisskopf-Ewing approximation to analyze $(^3\mathrm{He}, tf)$ data. The results were compared to direct (n, f) cross sections and ENDF/B-IV evaluations. From Britt and Wilhelmy, 1979.

oxygen in the target. Figure 5 shows a comparison of selected results to the direct measurements and ENDF/B-IV cross section evaluations that were available at the time. For these measurements, the compound-nuclear formation cross section was crudely estimated to be a constant 3.1 barns: This value was found to reproduce the available directly measured results. Recent optical-model calculations give formation cross sections that are about 10% higher, and energy dependent; a comparison is shown in Fig. 7 of (Younes and Britt, 2003c).

Results with significantly better energy resolutions were obtained for (d, pf) reactions using the Saclay Q3D magnetic spectrometer (Blons *et al.*, 1988). Protons were detected with FWHM energy resolutions of 7–12 keV to study fission probabilities and fission-fragment angular distributions for reactions on the ^{229,230,232}Th and ^{233,236}U isotopes. A detailed comparison to the fission probabilities determined from (n, f) measurements with a similar energy resolution (Blons *et al.*, 1984) showed overall agreement between the two reactions, although the excellent energy resolution revealed some differences that were attributed to the higher angular-momentum imparted to the compound nucleus from the (d, pf) reaction.

V. MODERN SURROGATE EXPERIMENTS

In recent years, surrogate cross section measurements have received renewed interest. Experiments have been carried out at the Tandem facility at the Institute de Physique Nucléaire d'Orsay (IPN Orsay) in France and at the 88-inch Cyclotron at Lawrence Berkeley National Laboratory (LBNL) in the United States of America. In addition, measurements have been performed at a Pelletron accelerator in Mumbai, India, and researchers in Japan and elsewhere have initiated research in this area.

The researchers in France implemented an experimental setup similar to that of the early experiments, with charged-particle detectors located at backward angles, and fission detectors located at various forward and backward angles relative to the beam direction. The French experiments used ^{3}He-induced transfer reactions to identify several compound nuclei in the same experiment by detecting various light-ion ejectiles. Cross sections were obtained using a Weisskopf-Ewing analysis. Experiments to determine cross sections for Th, Pa, and Cm isotopes relevant to the thorium-uranium fuel cycle and transmutation of nuclear waste have been carried out.

The American group, referred to as the STARS/LiBerACE Collaboration, has developed an apparatus that employs annular silicon detectors to detect the direct-reaction ejectiles at forward angles and fission fragments at backward angles (Lesher *et al.*, 2010). The ejectiles are detected at forward angles to minimize the angular-momentum imparted to the struck nucleus (to better match the angular momentum of the neutron-induced reaction) and to maximize the counting rate. Various light-ion beams have been used for inelastic scattering and one-nucleon or two-nucleon transfer reactions. Cross section results have also been determined using the

TABLE I. Summary of the cross sections examined in the last decade (ordered by isotope) using the surrogate reactions method. The neutron energy (E_n) range covered, surrogate-reaction used, type of measurement (absolute vs ratio), and publication reference are listed.

Desired reaction	E_n range (MeV)	Surrogate reaction	Type	Reference
		(n, f) cross sections		
^{230}Th(n, f)	0.5–10	^{232}Th(^{3}He, α))	absolute	Petit *et al.* (2004)
^{230}Th(n, f)	0.22–25	^{232}Th(^{3}He, α))	ratio	Goldblum *et al.* (2009)
^{231}Th(n, f)	0.36–25	^{232}Th(^{3}He, ^{3}He$'$)	ratio	Goldblum *et al.* (2009)
^{231}Pa(n, f)	0.5–10	^{232}Th(^{3}He, t)	absolute	Petit *et al.* (2004)
^{233}Pa(n, f)	0.5–10	^{232}Th(^{3}He, p)	absolute	Petit *et al.* (2004)
^{233}Pa(n, f)	11.5–16.5	^{232}Th(^{6}Li, α)	ratio	Nayak *et al.* (2008)
^{233}U(n, f)	0.4–18	^{234}U(α, α')	ratio	Lesher *et al.* (2009)
^{236}U(n, f)	0–20	^{238}U(^{3}He, α)	absolute, ratio	Lyles *et al.* (2007a)
^{237}U(n, f)	0–13	^{238}U(d, d')	ratio	Plettner *et al.* (2005)
^{237}U(n, f)	0–20	^{238}U(α, α')	ratio	Harke *et al.* (2006)
^{239}U(n, f)	0–20	^{238}U(^{18}O, ^{16}O)	ratio	Burke *et al.* (2011)
^{237}Np(n, f)	10–20	^{238}U(^{3}He, t)	absolute, ratio	Basunia *et al.* (2009)
^{238}Pu(n, f)	0–20	^{239}Pu(α, α')	ratio	Ressler *et al.* (2011)
^{241}Am(n, f)	0–10	^{243}Am(^{3}He, α)	absolute	Kessedjian *et al.* (2010)
^{242}Cm(n, f)	0–10	^{243}Am(^{3}He, t)	absolute	Kessedjian *et al.* (2010)
^{243}Cm(n, f)	0–3	^{243}Am(^{3}He, d)	absolute	Kessedjian *et al.* (2010)
		(n, γ) cross sections		
^{155}Gd(n, γ)	0.05–3.0	^{156}Gd(p, p')	absolute, ratio	Scielzo *et al.* (2010)
^{157}Gd(n, γ)	0.05–3.0	^{158}Gd(p, p')	absolute, ratio	Scielzo *et al.* (2010)
^{161}Dy(n, γ)	0.13–0.56	^{162}Dy(^{3}He, ^{3}He$'$)	ratio	Goldblum *et al.* (2010)
^{170}Yb(n, γ)	0.165–0.405	^{171}Yb(^{3}He, ^{3}He$'$)	ratio	Goldblum *et al.* (2008)
^{170}Yb(n, γ)	0.225–0.465	^{172}Yb(^{3}He, α)	ratio	Goldblum *et al.* (2008)
^{171}Yb(n, γ)	0.12–0.24	^{171}Yb(d, p)	ratio	Hatarik *et al.* (2010)
^{233}Pa(n, γ)	0–1	^{232}Th(^{3}He, p)	absolute	Boyer *et al.* (2006)
^{235}U(n, γ)	0.9–3.3	^{235}U(d, p)	ratio	Allmond *et al.* (2009)
^{237}U(n, γ)	0.2–1.0	^{238}U(α, α')	absolute, ratio	Bernstein *et al.* (2006); Young *et al.* (2007)

Weisskopf-Ewing approximation. In addition, the group has introduced an approach, referred to as the surrogate ratio method, to determine a cross section relative to a known (reference) one. This method, described in Sec. III.B, has the advantage that backgrounds from target contaminants and some of the model dependence of the analysis are reduced. Limits of the Weisskopf-Ewing and ratio approaches are currently being experimentally and theoretically investigated.

In India, a slightly different approach to determining cross sections from a ratio of (^{6}Li, α) and (^{6}Li, d) reactions has been developed (Nayak *et al.*, 2008).

A summary of the surrogate-reaction measurements published in the past decade by these groups is shown in Table I. In this section, the initial experimental efforts for determining cross sections for neutron-induced fission are described. Additional efforts to determine (n, γ) cross sections by identifying the capture channel using γ-ray detectors are discussed in Sec. VIII.

A. Surrogate experiments in France

1. Experimental setup

The experimental setup at IPN Orsay consists of two silicon ΔE-E telescopes and an array of photovoltaic cells surrounding the target (Petit *et al.*, 2004). A schematic of the apparatus is shown in Fig. 6. The telescopes (150 and 300 μm fully depleted silicon detectors backed by 5-mm-thick lithium-drifted silicon detectors), located at 90° and 130° with respect to the beam axis, enable light-ion identification and energy measurement with ≈ 100 keV (FWHM)

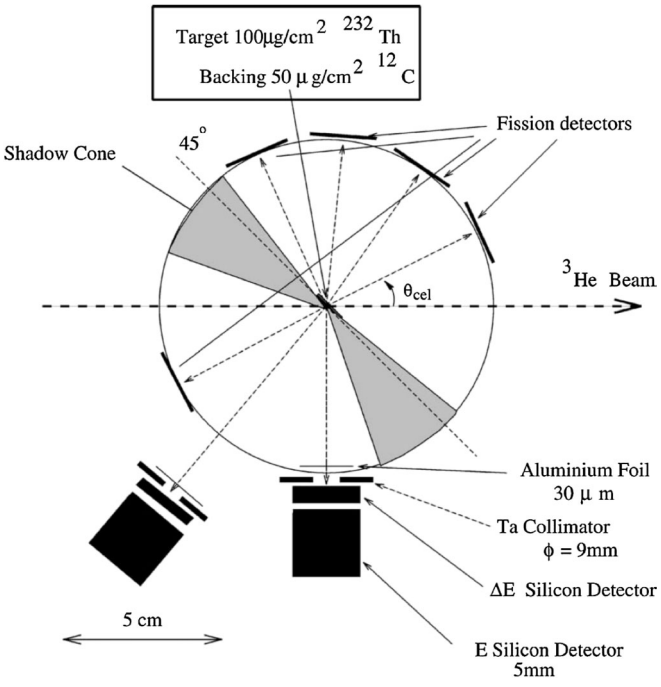

FIG. 6. Experimental setup at IPN Orsay. A ^{3}He beam strikes a target at the center of the chamber. Silicon telescopes located at 90° and 130° with respect to the beam detect light ions and an array of photovoltaic cells detects fission fragments. From Petit *et al.*, 2004.

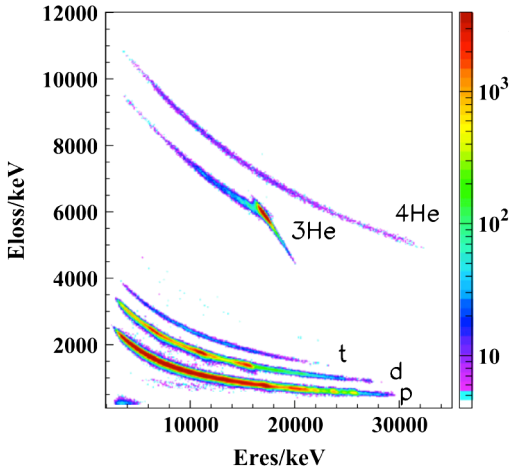

FIG. 7 (color online). The energy deposited in a ΔE-E silicon-detector telescope enables clear identification of the various light-ion exit channels. From Kessedjian *et al.*, 2010.

resolution. The particle identification following ^{3}He bombardment of a ^{232}Th target is shown in Fig. 7. Fission fragments were detected using five sets of three 20×40 mm^2 photovoltaic cells arranged in the reaction plane defined by the beam and silicon telescopes. For each set of photovoltaic cells, one was in, one was above, and one was below the reaction plane. The cells were located at a radius of 5 cm from the target and covered a solid angle of nearly 25% of 4π.

The (n, f) cross sections are determined in the Weisskopf-Ewing limit by multiplying the measured fission probabilities P_f by a calculated compound-nucleus formation cross section as prescribed in Eq. (9). Determining P_f requires measuring the number of particle-singles events N_δ the number of particle-fission coincidences events $N_{\delta f}$ and the fission-fragment detection efficiency (ϵ_f) as shown in Eq. (5). The telescopes were placed at backward angles to minimize backgrounds in the N_δ measurement. At large angles, peaks from reactions on light contaminants are kinematically shifted out of the energy region of interest and the elastic-scattering cross section is greatly reduced. The fission-fragment detection efficiency deviates by a few percent from the geometric solid angle subtended by the detectors because of an excitation-energy-dependent anisotropy in the fission-fragment emission directions (Petit *et al.*, 2004; Kessedjian *et al.*, 2010). The compound-nucleus formation cross section for this work has been calculated using modern semimicroscopic neutron-nucleus optical-model potentials (Bauge, Delaroche, and Girod, 1998; Bauge *et al.*, 2000; Bauge, Delaroche, and Girod, 2001). The model incorporates the deformation and rotational spectra of the target nuclei.

2. ^{230}Th, ^{231,233}Pa neutron-induced fission cross sections

The cross section for ^{233}Pa, an actinide with a half-life of only 27 days, is of great importance for the ^{232}Th-^{233}U reactor fuel cycle but had previously been measured at only four neutron energies (Tovesson *et al.*, 2002). The surrogate-reaction method identified the desired compound nuclei for the ^{230}Th(n, f), ^{231}Pa(n, f), and ^{233}Pa(n, f) reactions by detecting the α, t, and p exit channels from ^{3}He-induced

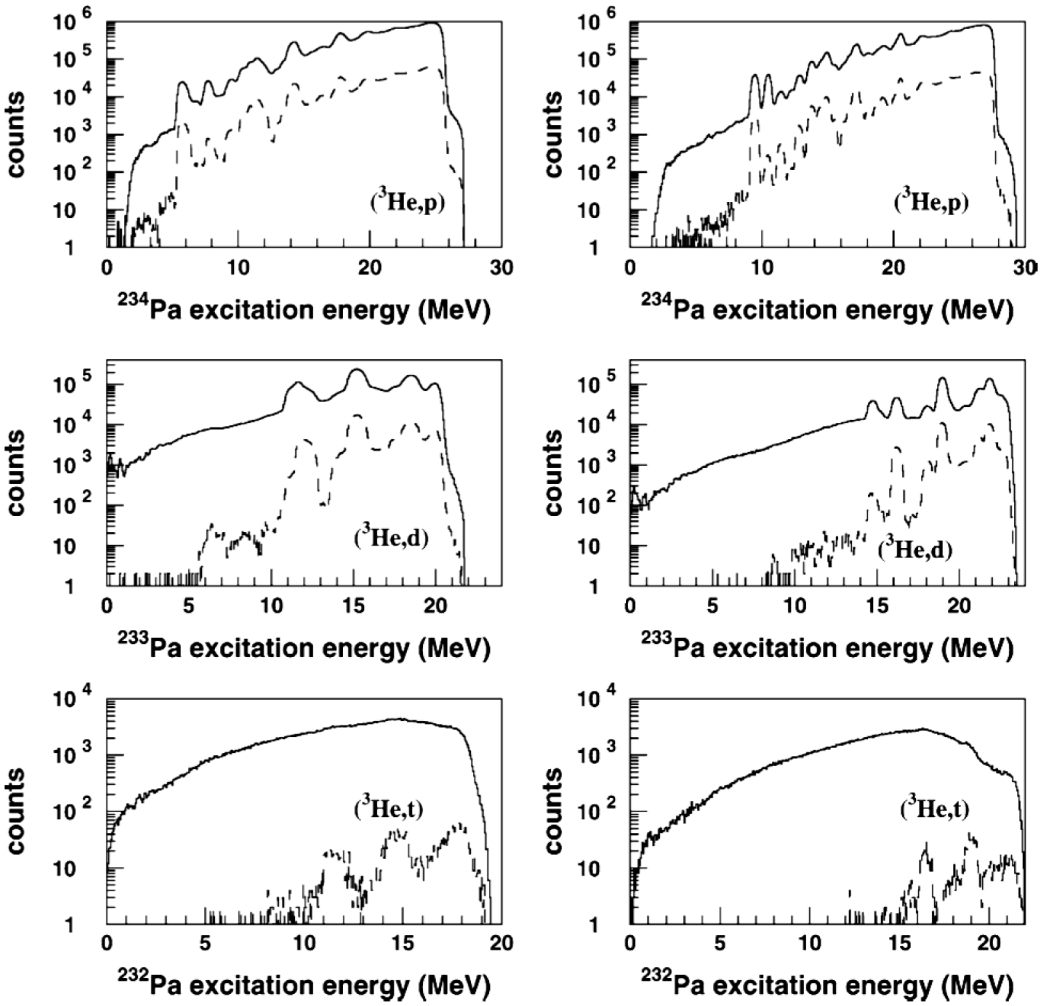

FIG. 8. Particle-singles spectra for various exit channels from ^{3}He reactions on a ^{232}Th target. The data on the left (right) correspond to the particles detected with the telescope at 90° (130°). The solid lines show data collected with the target and the dashed lines show data from the 50-μg/cm^2 carbon backing alone. From Petit *et al.*, 2004.

reactions on a target of 100 μg/cm^2 of ^{232}Th deposited on a 50-μg/cm^2 carbon backing (Petit *et al.*, 2004). The particle-singles spectra for several exit channels, shown in Fig. 8, reveal the size of the corrections required due to the carbon backing.

The results for ^{230}Th and ^{231}Pa were compared to directly measured data to verify the validity of the technique. The ^{230}Th(n, f) results are shown in Fig. 9 and compared to direct measurements and evaluations. Good agreement with the direct measurement is seen at energies below 7 MeV. At higher energies, the results differ somewhat from direct measurement but follow the trends of the ENDF/B-VI and JENDL-3 evaluations. The ^{231}Pa(n, f) cross section determined from the surrogate measurement is compared to direct measurements and evaluations. Again, good agreement with direct measurement is seen up to approximately 6 MeV.

The surrogate-reaction method allowed the ^{233}Pa(n, f) cross section to be determined for the first time at neutron energies up to 10 MeV. The results of the surrogate experiment are compared to a direct measurement (Tovesson *et al.*, 2002) and to evaluations in Fig. 9. The surrogate results differ in magnitude by nearly a factor of 2 from the earlier ENDF/B-VI evaluation but show the onset of first-chance fission at the same energy. They are in closer agreement with the magnitude predicted by the JENDL-3 evaluation over the energy range of 2–6 MeV, although the latter predicts an earlier onset of fission.

3. Results for ^{241}Am(n, f) and ^{242,243}Cm(n, f) from surrogate reactions

The neutron-induced fission cross sections for ^{241}Am, ^{242}Cm, and ^{243}Cm were obtained from (^{3}He, α), (^{3}He, t), and (^{3}He, d) reactions, respectively, on a ^{243}Am target that consisted of ≈ 100 μg/cm^2 of ^{243}Am deposited on a 75-μg/cm^2 carbon backing. Carbon backgrounds were measured and subtracted off by collecting data with a blank carbon backing. The cross sections obtained using the surrogate-reaction method in the Weisskopf-Ewing approximation are shown in Fig. 10. The ^{241}Am(n, f) cross section agrees remarkably well over the entire measurement range of 0–10 MeV with direct measurement (Dabbs, Johnson, and Bemis, 1983) and the ENDF/B-VII, JENDL 3.3, and JEFF 3.1 evaluations. In the energy region of overlap, the ^{242}Cm(n, f)

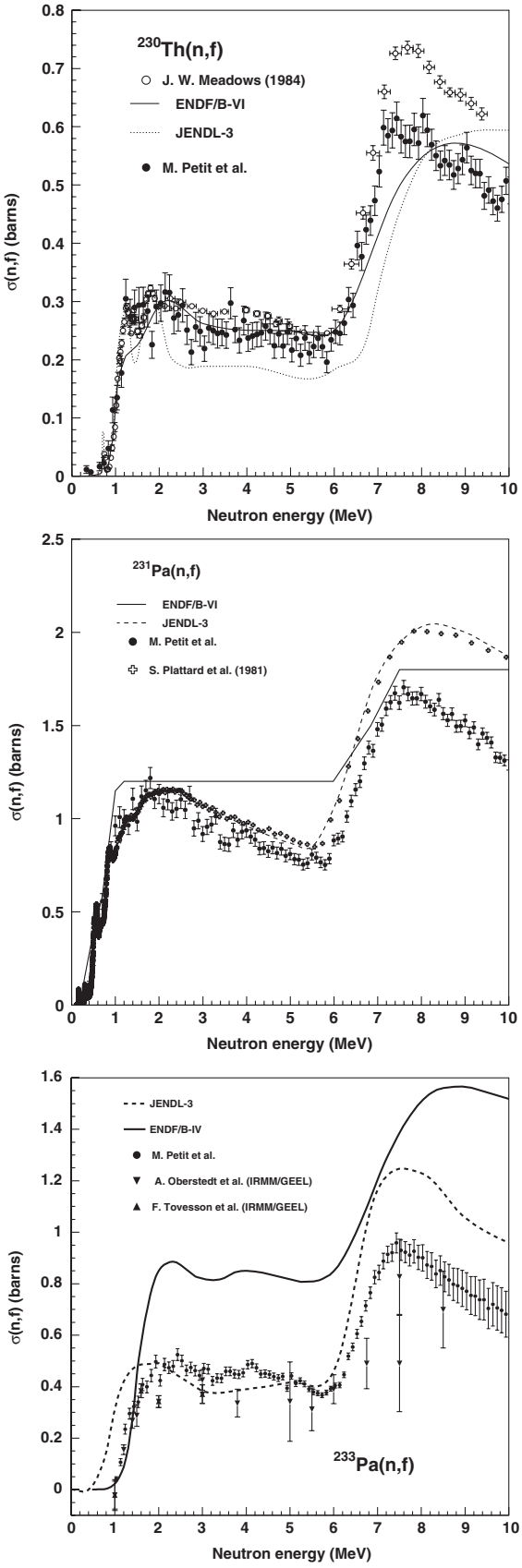

FIG. 9. The ^{230}Th(n, f), ^{231}Pa(n, f), and ^{233}Pa(n, f) cross sections determined using ^{232}Th(^{3}He, x) surrogate reactions (Petit *et al.*, 2004) are compared to direct measurements (Plattard *et al.*, 1981; Meadows, 1983; Tovesson *et al.*, 2002; 2004), and the ENDF/B-VI and JENDL-3 evaluations. From Petit *et al.*, 2004.

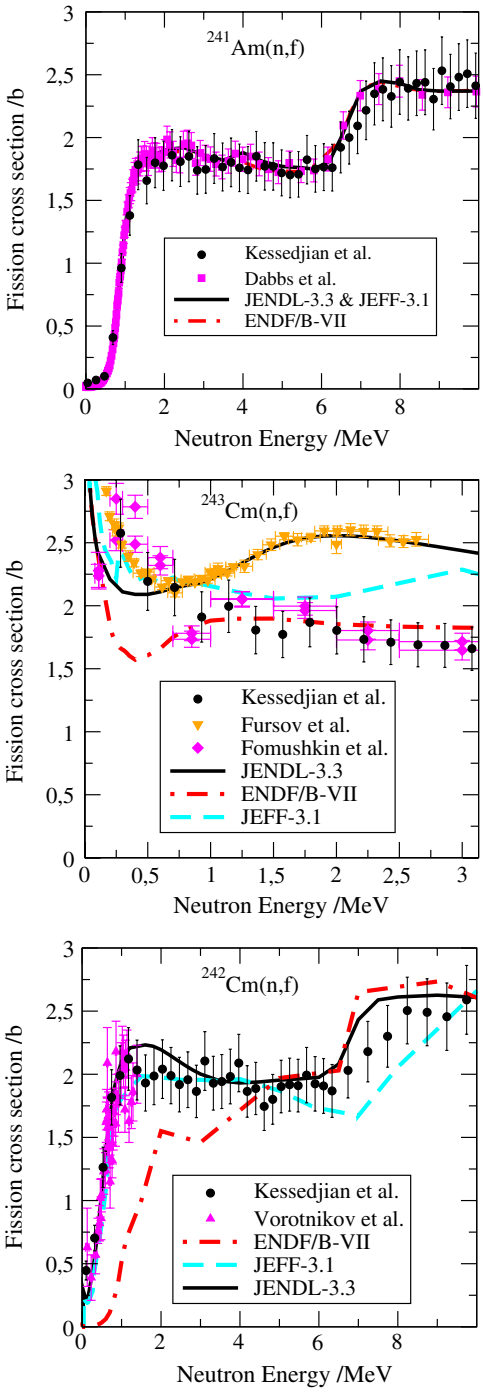

FIG. 10 (color online). Results for ^{241}Am(n, f), ^{243}Cm(n, f), and ^{242}Cm(n, f) determined from detecting ^{4}He, d and t exit channels, respectively, from ^{3}He bombardment of an ^{243}Am target. The surrogate-reaction results by Kessedjian *et al.* are compared to direct measurements (Dabbs, Johnson, and Bemis, 1983; Vorotnikov *et al.*, 1984; Fomushkin *et al.*, 1990; Fursov *et al.*, 1997) and evaluations. From Kessedjian *et al.* 2010.

cross section agrees with an existing direct measurement (Vorotnikov *et al.*, 1984), but the surrogate-reaction measurement covers a much broader range of energies. The result is consistent with the evaluations over the energy range of 4–10 MeV, where no direct measurement exists. As for the ^{243}Cm(n, f) cross section, the surrogate reactions result agrees with the measurement of Fomushkin *et al.* (1990).

Kessedjian *et al.* (2010) suggest that the more recent measurement (Fursov *et al.*, 1997) is overestimated at energies above 0.7 MeV as it would imply a total compound cross section that is significantly larger than what is expected from optical-model calculations and local systematics.

These results demonstrate that few-nucleon transfer reactions using a ^{3}He beam can serve as a powerful tool to successfully determine fission cross sections in the actinide region using the surrogate-reaction method. In general, the results are in good agreement with known data in the energy region that covers first-chance fission. In several cases, the results call into question the existing evaluations.

B. STARS/LiBerACE experiments

1. STARS/LiBerACE experimental setup

In contrast to the small area silicon detectors used in the early work from the 1970s and more recently by the French group, the STARS/LiBerACE Collaboration uses highly segmented large-area silicon detectors for light-ion detection. Initial experiments were conducted at the Wright Nuclear Structure Laboratory at Yale University (Plettner *et al.*, 2005). More recently, the Silicon Telescope Array for Reaction Studies (STARS) was developed (Lesher *et al.*, 2010) and subsequent measurements were performed at the 88-Inch Cyclotron at the Lawrence Berkeley National Laboratory. This system has been used to study a wide variety of topics in fundamental and applied nuclear physics, such as reactions (Clark *et al.*, 2005; Harke *et al.*, 2006; Lyles *et al.*, 2007a; Gibelin *et al.*, 2008; Scielzo *et al.*, 2008; Allmond *et al.*, 2009; Basunia *et al.*, 2009; Lesher *et al.*, 2009; Hatarik *et al.*, 2010; Scielzo *et al.*, 2010) and structure (Wiedeking *et al.*, 2008a; 2008b; Bender *et al.*, 2009; Ressler *et al.*, 2010). In the following sections, the apparatus and surrogate experiments that employ variants of the Weisskopf-Ewing approach are described. In addition, an auxiliary array of high-purity germanium (HPGe) detectors called the Livermore Berkeley Array for Collaborative Experiments (LiBerACE) can be used with STARS for γ-ray detection and is described in Sec. VIII. A schematic drawing of the detector systems is shown in Fig. 11.

The STARS ΔE-E particle telescope consists of two or more annular highly-segmented silicon detectors. Each detector is a Micron S1 or S2 detector (Micron, 2010), ranging in thickness from 65 to 1000 μm and segmented into 48 rings on one side and 16 sectors on the other for position sensitivity. These detectors are used to identify the outgoing particles and determine the energy and scattering angle. A thin aluminum shield is placed in front of the silicon telescope to protect it from damage from fission fragments and δ electrons. The silicon detectors can be placed at various distances from the target and typically cover an angle range from 35° to 65°. Placing detectors downstream of the target maximizes the counting statistics because the outgoing particles are somewhat forward focused in the laboratory frame. The light-ion detection efficiency can be an important consideration when coincident γ-ray detection is required. In these experiments, it is often challenging to collect the desired number of coincident events and the incident beam intensity is typically limited to $\sim$1 particle nA by the rates in the surrounding LiBerACE γ-ray detectors.

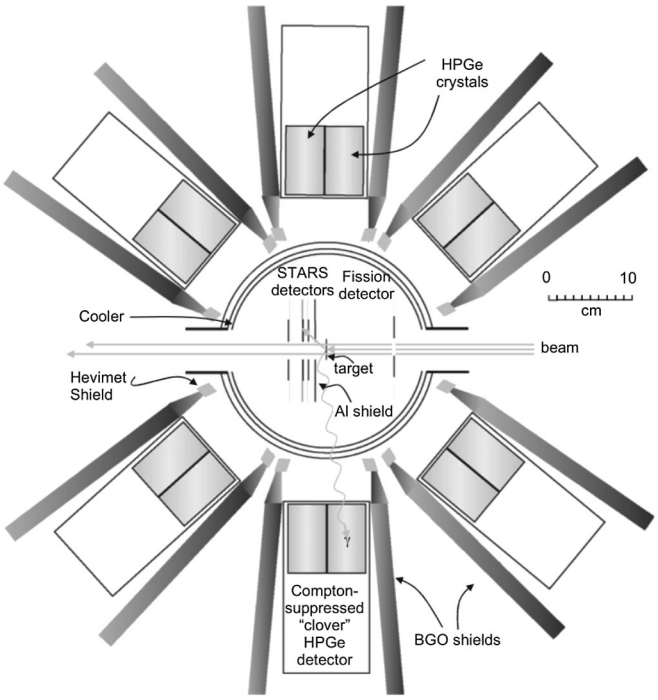

FIG. 11. A cross section of a typical STARS/LiBerACE experimental configuration is shown. The scattering chamber houses the targets and particle detectors. The LiBerACE HPGe detectors surround the scattering chamber.

An additional 140-μm-thick S2 detector is used upstream of the target location (typically covering an angular range from 106° to 131°) to detect fission fragments in coincidence with scattered particles. Figure 12 shows a typical example of the fission-fragment energy spectrum detected using STARS (Allmond *et al.*, 2009).

The silicon telescope is calibrated using α lines from a spectroscopy-grade ^{226}Ra source and reactions that populate the ground and excited states of the energies of the target nucleus or light nuclei such as ^{12}C or ^{16}O. Energy lost in apparatus dead layers is determined using the Energy Loss and Straggling Tool (ELAST) (Lesko, 1984) or the Stopping and Range of Ions in Matter (SRIM) (Ziegler, 2004) programs and the nuclear-recoil energy is calculated based on the reaction kinematics.

2. Results for ^{237}Np(n, f) and ^{236}U(n, f) using the Weisskopf-Ewing approximation

The ^{237}Np(n, f) cross section was determined using ^{238}U(^{3}He, t) as the surrogate reaction by bombarding a self-supporting 760 μg/cm^2 ^{238}U target with a 42-MeV ^{3}He beam (Basunia *et al.*, 2009). The use of a self-supporting target greatly reduced the particle-singles background that results from reactions on a carbon backing. The results obtained using the Weisskopf-Ewing approximation are compared to the cross section obtained by Shcherbakov *et al.* (2002) and the ENDF/B-VII.0 and JENDL3.3 evaluations in Fig. 13. There is good agreement over the accessible energy range (which was limited to 10–20 MeV equivalent neutron energy by the requirement that the tritons stop in the second

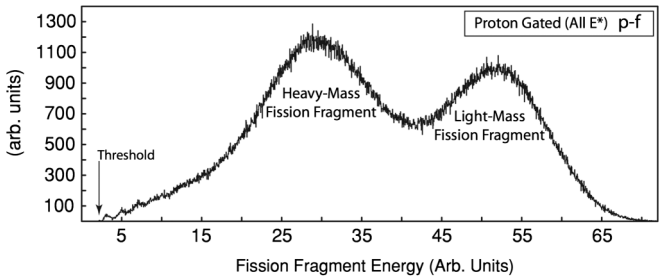

FIG. 12. The proton-gated fission spectra from a ^{235}U(d, p) surrogate experiment. The light and heavy mass fission-fragments peaks are indicated. From Allmond *et al.*, 2009.

detector of the ΔE-E telescope). This result is interesting because at energies greater than 10 MeV, preequilibirum effects (such as neutron emission prior to damping into a compound nucleus) were thought to become significant contributors to the cross section and would lower the cross section determined by surrogate reactions by 10%–20%. No clear preequilibrium effect is seen for this reaction.

The surrogate result, when divided by the directly measured ^{235}U(n, f) cross section, is compared to the ratio $\sigma[^{237}\mathrm{Np}(n, f)]/\sigma[^{235}\mathrm{U}(n, f)]$ measured by Tovesson and Hill (2007) in Fig. 13(b). The results are consistent across the entire energy range shown, with uncertainties of 5%–10% for the surrogate data.

In the same experiment, the ^{238}U$(^3\mathrm{He}, \alpha)$ reaction was studied as a surrogate for ^{236}U(n, f) (Lyles *et al.*, 2007a). For equivalent neutron energies above ≈ 6 MeV, the cross section result deviated significantly from the known cross section due to particle-singles backgrounds from reactions on light-element (such as hydrocarbon or oxidative) contamination in the target. When the cross section was determined relative to the results of the ^{235}U$(^3\mathrm{He}, \alpha)$ reaction [which served as a surrogate for the ^{233}U(n, f) reaction] measured in the same experiment, the higher-energy results were consistent with the known ^{233}U(n, f) cross section. At low energies,

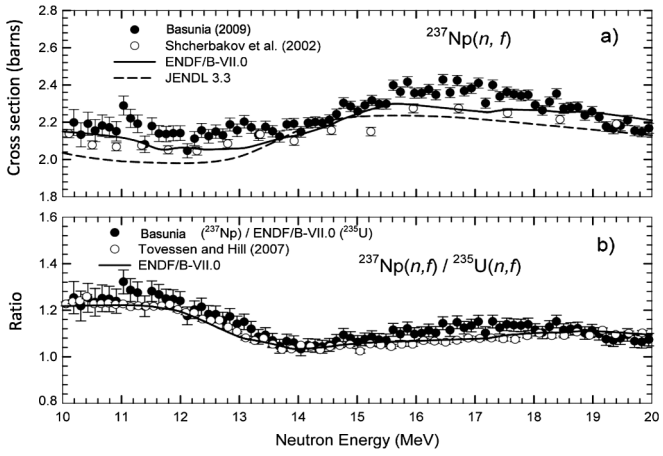

FIG. 13. The ^{237}Np(n, f) cross section determined from a surrogate experiment at STARS/LiBerACE. (a) Results from Basunia *et al.* (2009), Shcherbakov *et al.* (2002), ENDF/B-VII.0 and JENDL3.3, for the ^{237}Np(n, f) cross section from 10–20 MeV. (b) A comparison of the surrogate ratio result to measurements by Tovesson and Hill (2007).

the results were sensitive to angular-momentum effects and this is discussed in Sec. VI.A.

3. Surrogate ratio experiments

The surrogate ratio method was introduced (Plettner *et al.*, 2005) to overcome the difficulties associated with measuring the total number of observed direct-reaction events N_δ because of backgrounds from target backings or contaminants. In addition, there are indications that the effects of small to moderate violations of the Weisskopf-Ewing assumptions can be reduced in a ratio approach. The ratio $N_{\delta 2}/N_{\delta 1}$ can be determined from the direct-reaction cross section integrated over the detector solid angle σ_δ and the experimental parameters of the areal target thickness ρ_T, integrated beam current Q, light-ion detection efficiency ϵ_δ, and live time L_t through the relation

$$\frac{N_{\delta 2}(E)}{N_{\delta 1}(E)} = \frac{\sigma_{\delta 2}(E)\epsilon_{\delta 2}\rho_{T2}Q_2L_{t2}}{\sigma_{\delta 1}(E)\epsilon_{\delta 1}\rho_{T1}Q_1L_{t1}}. \tag{17}$$

Although the quantities σ_δ may be unknown for each reaction individually, if the same direct reaction is used on similar target nuclei to form similar compound nuclei, one expects $\sigma_{\delta 2}/\sigma_{\delta 1} \approx 1$ to hold. If the experimental geometry is identical as well, the ratio of the efficiencies $\epsilon_{\delta 2}(E)/\epsilon_{\delta 1}(E) \approx 1$. Equation (17) then simplifies to

$$\frac{N_{\delta 2}(E)}{N_{\delta 1}(E)} \approx \frac{\rho_{T2}Q_2L_{t2}}{\rho_{T1}Q_1L_{t1}} \tag{18}$$

and $R(E)$ from Eq. (13) can be determined from measurement of the ratio $N_{\delta 2f}/N_{\delta 1f}$ and a handful of easily accessible experimental properties.

The ratio $R(E)$ can be defined at either the same equivalent neutron energy E_n in the numerator and denominator or the same excitation energy E_{ex}. Of course, the two energies are simply related by Eq. (3). However, when cross sections for two nuclei with different separation energies and/or reactions with different reaction Q values are compared, the energy choice can introduce additional uncertainty in either the ratio of formation cross sections or the ratio of exit-channel branching ratios. The S_n and Q value differences in surrogate reactions is typically a few hundreds of keV but could be several MeV in an extreme case.

For (n, f) cross sections, most ratio comparisons have been performed at E_{ex} because the ratio $G_f^{\mathrm{CN1}}/G_f^{\mathrm{CN2}}$ is obtained from an experiment that measures quantities in terms of E_{ex}. The energy dependence of the ratio of the formation cross sections $\sigma_n^{\mathrm{CN1}}/\sigma_n^{\mathrm{CN2}}$, which appears in Eq. (11), has to be taken into account explicitly. If instead E_n is chosen, then $\sigma_n^{\mathrm{CN1}}/\sigma_n^{\mathrm{CN2}} \approx 1$ at all energies (for reactions on similar targets) but any excitation-energy dependence of the experimental quantities ϵ_δ and N_δ would cause the ratios $\epsilon_{\delta 2}/\epsilon_{\delta 1}$ and $N_{\delta 2}/N_{\delta 1}$ to deviate from unity in ways that may be difficult to measure or estimate.

Experiments using the surrogate ratio method have been performed to determine the ^{230,231}Th (Goldblum *et al.*, 2009), ^{237,239}U(n, f) (Harke *et al.*, 2006; 2011), and ^{238}Pu (Ressler *et al.*, 2011) cross sections. The validity of the ratio method was also tested by comparing results obtained from a ratio of ^{234}U$(\alpha, \alpha' f)$ to ^{236}U$(\alpha, \alpha' f)$ to the ratio of known cross

sections of ^{233}U(n, f) to ^{235}U(n, f) (Lesher *et al.*, 2009). The results and interpretation of this test is discussed in Sec VI.A.

4. Results for ^{230,231}Th(n, f)

The ^{230}Th(n, f) and ^{231}Th(n, f) cross sections were determined using the surrogate ratio method relative to the well-measured ^{234}U(n, f) and ^{235}U(n, f) cross sections, respectively, using (^{3}He, ^{3}He$'$) and (^{3}He, α) reactions on ^{232}Th and ^{236}U targets. The results show consistency with direct measurements (Muir and Veeser, 1971; Meadows, 1988), the earlier French surrogate measurements (Petit *et al.*, 2004), and the Evaluated Nuclear Data File (ENDF) evaluations up to energies of ≈ 7 MeV. Above this energy, there is some disagreement in the ^{230}Th cross sections. The (n, f) cross section for ^{231}Th had never been directly measured before because of its short half-life ($t_{1/2} = 25.52$ h). The results of this surrogate experiment confirm the general cross section prediction of the evaluations.

5. Results for ^{237}U(n, f)

The $(\alpha, \alpha' f)$ reactions were used as the surrogate reactions on long-lived ^{236,238}U targets to determine the ratio of the ^{235}U(n, f) and ^{237}U(n, f) cross sections. Only a single heroic measurement of the ^{237}U ($t_{1/2} = 6.75$ days) cross section had previously been attempted. It covered only a limited energy range and is described in McNally *et al.* (1974). The ^{237}U(n, f) cross section results from the surrogate ratio method show the expected structure of the first-chance, second-chance, and third-chance fission channels as can be seen in Fig. 14. Good agreement was found with the surrogate-method results of Younes and Britt (2005).

6. Results for ^{239}U(n, f)

Two-neutron transfer reactions provide a promising way to access nuclei further from stability. In the past, (t, p) reactions were used for this reaction. However, because tritium beams are currently unavailable, the (^{18}O, ^{16}O) reaction was used to determine the ^{239}U(n, f) cross section. Two neutrons were transferred to ^{234}U and ^{238}U to create the compound nuclei ^{236}U and ^{240}U that are formed in ^{235}U(n, f) and ^{239}U(n, f) reactions (Burke *et al.*, 2011).

The use of a 250-MeV ^{18}O beam presents several challenges. Many reaction channels are energetically accessible, resulting in exit-channel particles ranging from protons to neon with only a small fraction being the desired ^{16}O nuclei. A higher-Z projectile also results in larger energy-loss and kinematic corrections and the intrinsic resolution of the detectors is worse at higher energies due to charge-collection statistics. The energetic ^{18}O projectiles also cause significant radiation damage to the silicon detectors, resulting in a deterioration in response over the course of the experiment that must be monitored and taken into account. The ^{239}U(n, f) cross section obtained (Burke *et al.*, 2011) is consistent with the cross section from a different surrogate reaction, deduced by Younes and Britt (2005). Both results are significantly lower in the second-chance and third-chance fission regions than the ENDF/B-VII evaluation, indicating the need for an updated evaluation of the ^{239}U(n, f) cross section.

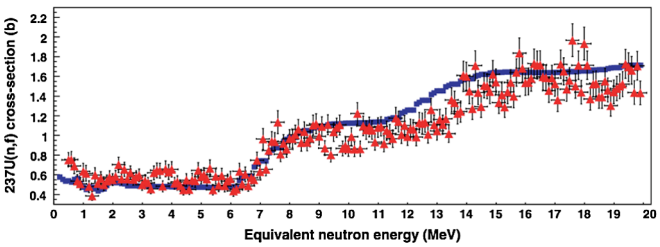

FIG. 14 (color online). The ^{237}U(n, f) cross section determined from a ^{238}U$(\alpha, \alpha' f)$ surrogate experiment (Burke *et al.*, 2006) (shown as triangles with statistical and systematic uncertainties) is compared to an earlier result (Younes and Britt, 2005) (shown as squares without uncertainties). From Burke *et al.*, 2006.

7. Results for ^{238}Pu(n, f)

A ratio approach was recently employed to determine the ^{238}Pu(n, f) cross section relative to the known ^{234}U(n, f) and ^{235}U(n, f) cross sections (Ressler *et al.*, 2011). Several prior direct measurements for the ^{238}Pu(n, f) cross section had resulted in a fairly well-established low-energy cross section (up to about 5 MeV), while showing disagreement at higher energies. Surrogate measurements using (α, α') reactions were performed to address the discrepancies at the higher energies. Alpha-fission fragment coincidence probabilities for the ^{239}Pu compound nucleus were determined relative to coincidence probabilities for the ^{235,236}U compound nuclei. The cross sections extracted from the two surrogate measurements were similar for neutron energies above 5 MeV. In the 5–10 MeV energy range, they agree with a recent direct measurement, but at energies above that they lie 20% higher than any of the direct measurements. The differences that are observed below 5 MeV are likely related to the breakdown of the Weisskopf-Ewing approximation that underlies the surrogate ratio approach.

C. Results from other groups

An alternative approach was used by Nayak *et al.* (2008) to determine the ^{233}Pa(n, f) cross section at energies of 11.5–16.5 MeV. In this experiment, a single self-supporting ^{232}Th target was bombarded by a 38-MeV ^{6}Li beam. By detecting d and α particles to identify ^{232}Th(^{6}Li, α)^{234}Pa and ^{232}Th(^{6}Li, d)^{236}U reactions, the ^{234}Pa and ^{236}U compound nuclei fission probabilities were measured. Although it may have been possible to independently infer the two (n, f) cross sections, a ratio of the two cross sections was used to determine the ^{233}Pa cross section relative to the known ^{235}U cross section. By taking a ratio of two reactions on the *same target*, systematic uncertainties due to target thickness, beam current, and dead time were eliminated. Nayak *et al.* (2008) also surmised that taking a ratio of cross sections minimized the effects of the spin-parity mismatch and discrepancies due to preequilibrium. Although this seems to be valid here, there is no evidence to suggest that this is more generally the case for another pair of reactions.

The ^{233}Pa(n, f) cross section was determined at excitation energies of 17–22 MeV. The ratio of entrance-channel cross sections was calculated using the EMPIRE-2.19 code (Herman *et al.*, 2007) and the exit-channel probabilities were measured

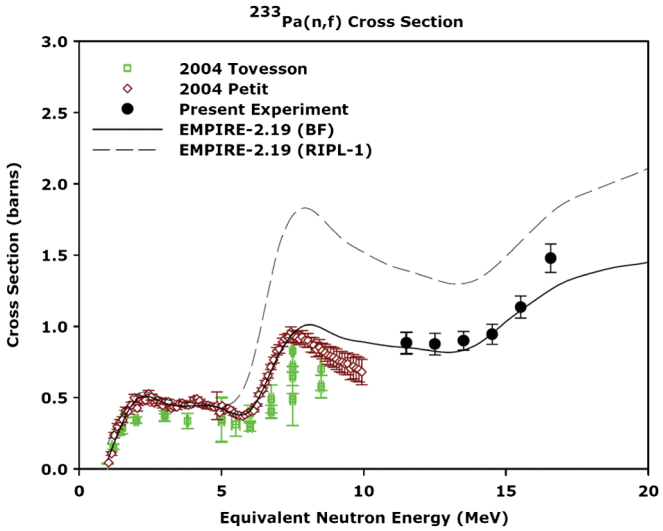

FIG. 15 (color online). Cross section for ^{233}Pa(n, f) determined using a hybrid surrogate approach (dots) and compared to other results from experiment and the EMPIRE-2.19 code. From Nayak *et al.*, 2008.

for ^{234}Pa and ^{236}U using the absolute surrogate-reaction method. The results, shown in Fig. 15, are consistent with the cross sections determined by Petit *et al.* (2004); Tovesson and Hill (2007) and with calculations using the EMPIRE-2.19 code (Nayak *et al.*, 2008).

VI. VALIDITY OF THE APPROXIMATIONS

Experimentally, it is not feasible to determine the branching ratios $G_\chi^{\mathrm{CN}}(E, J, \pi)$ for individual $J\pi$ values and test under which conditions the Weisskopf-Ewing limit is applicable. The use of the Weisskopf-Ewing or ratio approximations in the analysis of surrogate experiments is typically justified *a posteriori* by comparing the extracted cross sections to direct measurement where available. However, it is possible to carry out calculations to predict the behavior of the branching ratios $G_\chi^{\mathrm{CN}}(E, J, \pi)$ as a function of energy, angular momentum, and parity, and to draw some conclusions about the limitations of the Weisskopf-Ewing and ratio approximations. Such calculations have been carried out for the decay of several uranium isotopes by fission and γ emission (Escher and Dietrich, 2006; Chiba and Iwamoto, 2010; Escher and Dietrich, 2010), and for lighter systems (Zr, Gd, Ir, Au) decaying via γ emission (Forssén *et al.*, 2007; Chiba and Iwamoto, 2010; Escher and Dietrich, 2010).

Below we focus on applications to fission cross sections. We highlight representative experiments that shed light on the validity of the Weisskopf-Ewing and ratio approaches and discuss the findings of recent theoretical work. Tests of the approximations for capture cross sections are considered in Sec. VIII.

A. Experimental tests for (n, f) cross sections

The early surrogate work (see Sec. IV), aimed at determining (n, f) cross sections for a series of actinide targets, included measurements for a few known cases. The resulting cross sections agreed with direct (n, f) measurements to about 10%–20% for incident-neutron energies above 1 MeV, while more serious discrepancies were observed for lower energies. The differences were attributed to a combination of experimental uncertainties, uncertainties in the low-energy neutron-nucleus optical potentials available at the time, and the use of the Weisskopf-Ewing approximation.

Indications for the violation of the Weisskopf-Ewing approximation at low neutron energies were also found in more recent work by Lyles *et al.* (2007a, 2007b), who extracted the ^{236}U(n, f) cross section from a ^{238}U$(^3$He, $\alpha)$ measurement. The outgoing α particle was stopped at forward angles relative to the beam, and the measured α-fission coincidence probability $P_{\alpha f}(E)$ was found to depend on the angle at which the particle was detected. The angular-momentum transfer between projectile and target, and thus the spin-parity population of the compound nucleus ^{237}U, depends on this angle. The effect is shown in Fig. 16 for the associated (n, f) cross section, obtained in the Weisskopf-Ewing approximation. A 20° variation in the angle was observed to result in changes in the fission probability, and thus the cross section, of up to a factor of 2.

Lyles *et al.* (2007a and 2007b) also examined the validity of the surrogate ratio approach. Compound nuclei ^{237}U and ^{234}U were produced using $(^3$He, $\alpha)$ reactions on neighboring isotopes, and fission products from their decay were observed in coincidence with the outgoing α particles. The relative α-fission probabilities were used to estimate the ratio $\sigma[^{236}\mathrm{U}(n, f)]/\sigma[^{233}\mathrm{U}(n, f)]$ and, subsequently, the ^{236}U(n, f) cross section. The resulting cross section showed agreement for energies above about 4 MeV, while significant deviations occurred at lower energies [see Fig. 12 of Lyles *et al.* (2007a)].

The ratio approach was further studied by Lesher *et al.* (2009) who carried out an inelastic scattering experiment

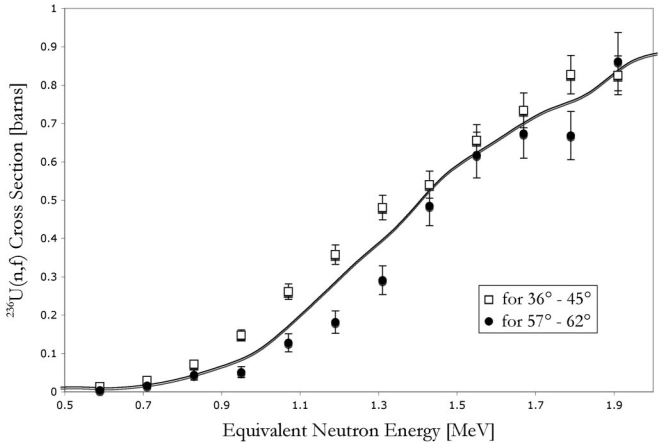

FIG. 16. ^{236}U(n, f) cross section obtained from a Weisskopf-Ewing analysis of surrogate ^{238}U$(^3$He, $\alpha)$ measurements. Data represented by open squares correspond to events for which the outgoing α particle was observed at 36° to 45°, while filled circles correspond to an angular range of 57° to 62°. The solid line is the cross section that results from averaging over all experimentally accessible angles, 36° to 62°. The fact that the extracted cross section depends on the angle of the outgoing α particle is an indication that the Weisskopf-Ewing approximation is violated.

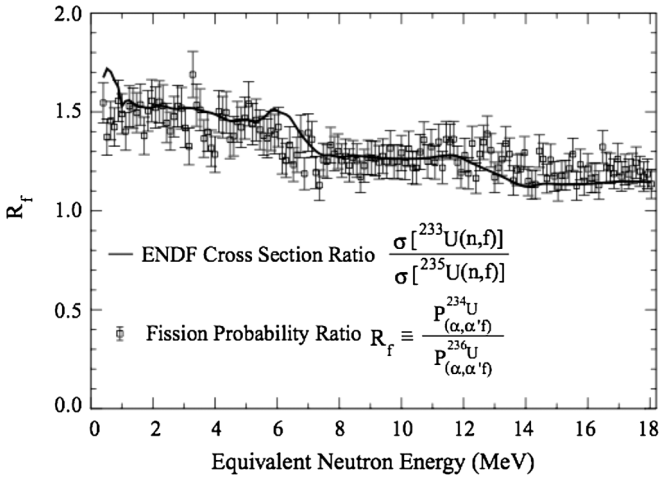

FIG. 17. Experimental test of the surrogate ratio method for neutron-induced fission, for ^{233,235}U targets, for which the compound-formation cross sections are expected to be almost identical. The ratio of measured fission probabilities (squares) is compared to the ratio $\sigma[^{233}\mathrm{U}(n,f)]/\sigma[^{235}\mathrm{U}(n,f)]$ of evaluated fission cross sections (solid line). From Lesher *et al.*, 2009.

with α particles to determine the ratio $R_f^{\mathrm{exp}} = P^{234U}_{(\alpha,\alpha' f)}/P^{236U}_{(\alpha,\alpha' f)}$ of the fission probabilities associated with the decays of ^{234}U and ^{236}U nuclei. In Fig. 17, R_f^{exp} is compared to the ratio of $\sigma[^{233}\mathrm{U}(n,f)]/\sigma[^{235}\mathrm{U}(n,f)]$, with cross sections obtained from ENDF evaluations. Overall, one observes an acceptable level of agreement between the cross section ratio and the surrogate results. The former lies within the error bars of the latter, except for low energies, $E_n < 1$ MeV.

While many (n,f) cross sections that have been obtained from a Weisskopf-Ewing or ratio analysis of surrogate data deviate significantly from directly measured cross sections for neutron energies below about 1 MeV, one can find exceptions. Most notably, the French collaboration's measurements of (n,f) cross sections for minor actinides [see Sec. V.A and Petit *et al.* (2004); Kessedjian *et al.* (2010)] were seen to be in excellent agreement with direct measurements, even at very low energies ($E_n < 1$ MeV). This might be an indication that the experimental conditions selected for these measurements resulted in spin-parity populations of the compound nuclei involved that are similar to the spin-parity distributions occurring in the neutron-induced reactions.

B. Insights from theory: Spin dependence of fission probabilities

The branching ratios $G_\chi^{\mathrm{CN}}(E,J,\pi)$ can be extracted from a calculation of the (n,f) cross section and their $J\pi$ dependence can be studied. For the fission case, this was done by Escher and Dietrich (2006) and, more recently, by Chiba and Iwamoto (2010). In Escher and Dietrich (2006), the branching ratios $G^{\mathrm{CN}}_{\chi=\mathrm{fission}}(E,J,\pi)$ were extracted from a full Hauser-Feshbach calculation of the ^{235}U(n,f) reaction that was calibrated to an evaluation of experimental data. The model used a deformed optical potential and the level schemes, level densities, gamma strength functions, fission-model parameters, and preequilibrium parameters were

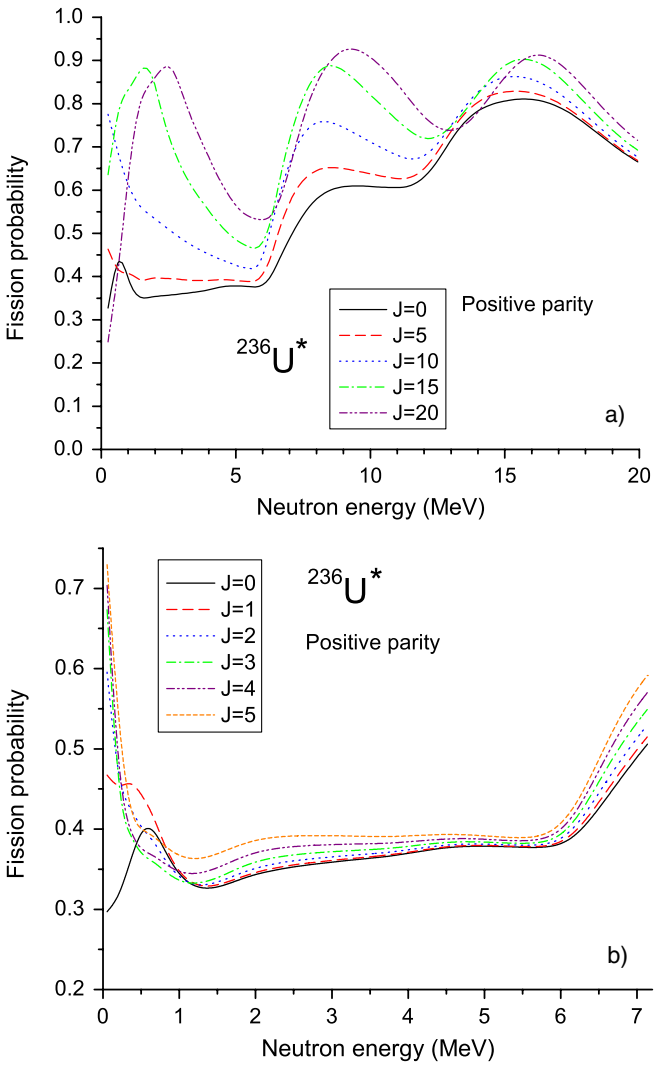

FIG. 18 (color online). Calculated branching ratios $G^{\mathrm{CN}}_{\mathrm{fission}}(E,J,\pi)$ for fission of ^{236}U*, as a function of the laboratory neutron energy in the $^{235}\mathrm{U}+n$ system. Results are shown for positive-parity states with total angular momenta $J = 0$, 5, 10, 15, 20 (top panel) and $J = 0$, 1, 2, 3, 4, 5 (bottom panel) in the compound nucleus ^{236}U*. From Escher and Dietrich, 2006.

adjusted to reproduce the available data on n-induced fission for energies from $E_n = 0$ to 20 MeV. In Fig. 18 we reproduce the extracted $G^{\mathrm{CN}}_{\mathrm{fission}}(E,J,\pi)$ for fission proceeding through positive-parity states in the compound nucleus ^{236}U. Figure 18(a) shows the $G^{\mathrm{CN}}_{\mathrm{fission}}(E,J,\pi)$ for $J = 0$, 5, 10, 15, 20 for neutron energies $E_n = 0$–20 MeV, where $E_n = E(^{236}\mathrm{U}) - S_n(^{236}\mathrm{U})$. We observe that the branching ratios exhibit a significant $J\pi$ dependence, in particular, for low neutron energies, $E_n = 0$–5 MeV. Similarly strong $J\pi$ dependences were observed by Younes and Britt (2003b), as well as a dependence on the discrete transition state above the barrier at low E_n. With increasing energy, the differences decrease, although the discrepancies become more pronounced near the thresholds for second-chance and third-chance fission. The branching ratios for negative parity states are very similar to those for positive states [cf. Fig. 8 of Escher and Dietrich (2006)]. Furthermore, fission probabilities for the decay of the compound nucleus ^{234}U exhibit the

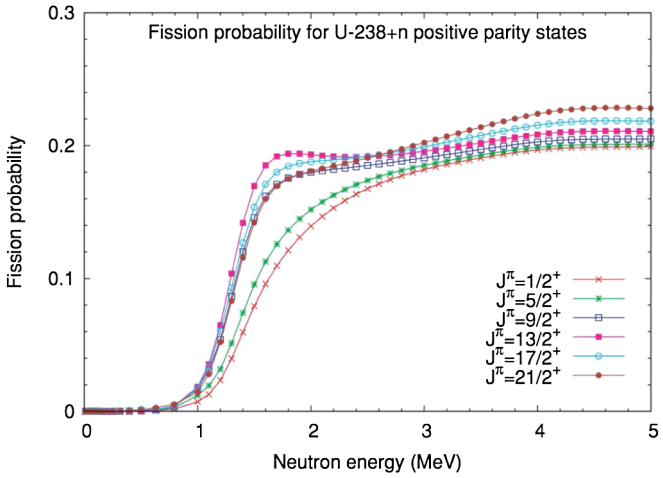

FIG. 19 (color online). Calculated branching ratios $G^{\mathrm{CN}}_{\mathrm{fission}}(E, J, \pi)$ for fission of ^{239}U*, as a function of the laboratory neutron energy in the $^{238}\mathrm{U} + n$ system. Results are shown for positive-parity states with total angular momenta $J = 1/2, \ldots 21/2$, for neutron energies $E_n = 0$–5 MeV. From Chiba and Iwamoto, 2010.

same overall behavior [cf. Fig. 7 of Escher and Dietrich (2006)].

Similar calculations were carried out by Chiba and Iwamoto (2010) for the decay of the odd compound nucleus ^{239}U. Figure 19 shows their results for positive-parity states with $J = 1/2$, $5/2$, $9/2$, $13/2$, $17/2$, $21/2$, for neutron energies $E_n = 0$–5 MeV. While ^{234}U and ^{236}U exhibit subthreshold fission, the compound nucleus ^{239}U does not. Consequently, for ^{239}U, all $G^{\mathrm{CN}}_{\mathrm{fission}}(E, J, \pi)$ are very small for $E_n < 1$ MeV. At the onset of fission, large variations in the fission probabilities are seen, a result that is in agreement with the earlier findings for ^{236}U and ^{234}U (Escher and Dietrich, 2006).

The calculated fission branching ratios $G^{\mathrm{CN}}_{\chi=\mathrm{fission}}(E, J, \pi)$ help us understand possible discrepancies between the directly measured cross sections and those extracted from a Weisskopf-Ewing analysis of the surrogate data: If the surrogate reaction populates the relevant compound nucleus, e.g., ^{236}U, with a spin-parity distribution that contains larger angular-momentum values than the population relevant to the neutron-induced reaction, then the measured decay probability $P_{\delta,\mathrm{fission}}(E_{\mathrm{ex}})$ of Eq. (4) contains larger contributions from those $G^{\mathrm{CN}}_{\chi=\mathrm{fission}}(E, J, \pi)$ associated with large J values than the cross section expression for the desired (n, f) reaction does. Consequently, the cross section extracted by using the Weisskopf-Ewing assumption and approximating $P_{\delta,\mathrm{fission}}(E_{\mathrm{ex}}) \approx \mathcal{G}^{\mathrm{CN}}_{\mathrm{fission}}(E_{\mathrm{ex}})$ gives too large of a result. The opposite will hold true for surrogate mechanisms that produce the compound nucleus with spin-parity distributions that are shifted to smaller J values relative to the distribution found in the neutron-induced reaction. In Sec. VI.C, we illustrate this effect using schematic surrogate spin-parity distributions.

In Fig. 18(b), a narrower range of angular-momentum values is considered for neutron energies up to 7 MeV. The associated branching ratios are seen to be very similar to each other for all but the lowest energies. The comparison of Figs. 18(a) and 18(b) illustrates an important point: It is not

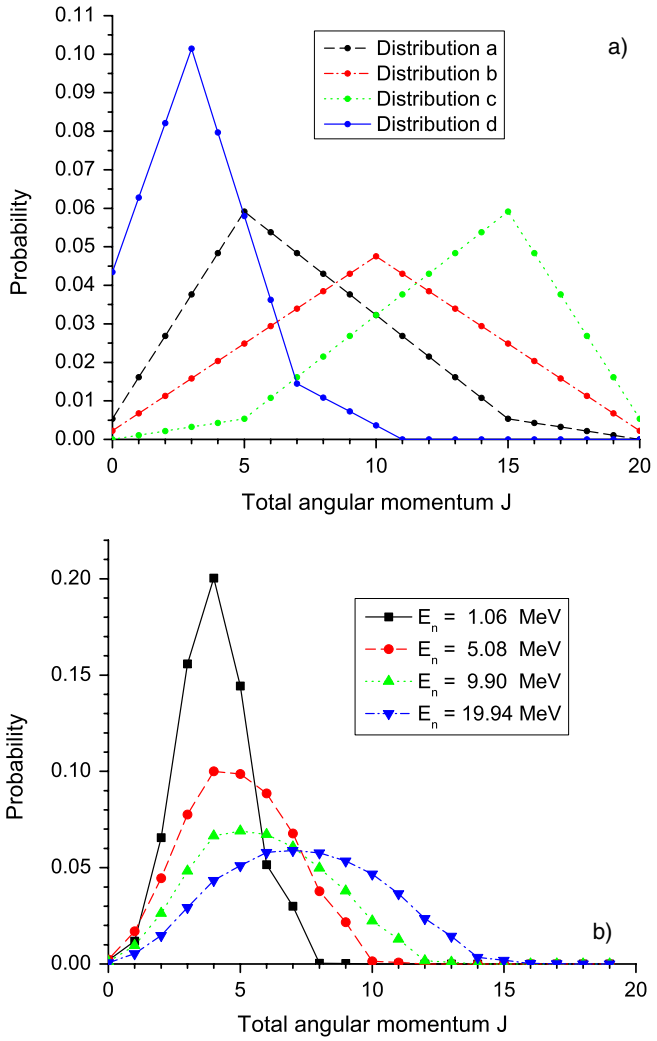

FIG. 20 (color online). (a) Schematic distributions of total angular momentum for the compound nucleus ^{236}U*. The mean angular momentum is $\langle J \rangle = 7.03$, 10.0, 12.97, and 3.30 for distributions a, b, c, and d, respectively; positive and negative parities are taken to be equally probable. The distributions were chosen solely to perform a sensitivity study. (b) Distributions of total angular momentum for ^{236}U* produced in the neutron-induced reaction $n + {}^{235}\mathrm{U}(n, f)$, for selected neutron energies.

a priori clear whether the Weisskopf-Ewing limit applies to a particular reaction in a given energy regime. While the Weisskopf-Ewing approximation may break down for a reaction that populates a wide range of $J\pi$ states, it may provide a valid description for a reaction that populates a narrow range of angular-momentum values. Thus, the spin-parity distributions for both the desired and surrogate reactions have to be considered.

For neutron-induced reactions, the spin and parity of the compound nucleus depends on the target spin and the energy of the neutron; the distribution can be calculated with an appropriate optical-model potential. An example for the case of $n + {}^{235}\mathrm{U}$ is shown in the right panel if Fig. 20. For the surrogate reaction, the spin-parity distribution depends on the reaction mechanism, the projectile-target combination considered, the energy of the projectile, and the angle of the outgoing direct-reaction particle. The ingredients needed for

predicting the spin-parity populations for surrogate are discussed in Sec. IX.

C. Fission cross sections from a Weisskopf-Ewing analysis

Employing the Weisskopf-Ewing assumption in the analysis of surrogate reactions for which this approximation is not valid will result in extracted cross sections that deviate from the desired true cross section. This was shown in Escher and Dietrich (2006), where the simulated branching ratios shown in Fig. 18 were taken to represent the "true" branching ratios and employed to simulate coincidence probabilities $P_\chi(E)$ with the help of several schematic CN spin-parity distributions. The calculated $P_\chi(E)$ correspond to the coincidence probabilities that are observed in typical surrogate experiments. These $P_\chi(E)$ were then analyzed in analogy to actual experimental results, and the Weisskopf-Ewing approximation was applied in the analysis. The resulting (n, f) cross sections were found to depend on the $J\pi$ distribution selected in the analysis, as can be seen in Fig. 21: Depending on the $J\pi$ distribution selected, the $^{235}\mathrm{U}(n, f)$ cross sections extracted from the simulated experiments differed from the expected results by as much as 40% for energies above 5 MeV and up to a factor of 2 for smaller energies. The schematic spin-parity populations used are shown in Fig. 20(a); the population associated with the $^{235}\mathrm{U}(n, f)$ reaction is shown in Fig. 20(b) for selected neutron energies.

It is clear that a larger mismatch between the $J\pi$ populations in the surrogate and desired reactions leads to a larger discrepancy between the cross section extracted in the Weisskopf-Ewing approximation and the reference cross section. The curve associated with distribution (c) can be considered an extreme outer limit, as surrogate-reaction conditions employed in recent experiments tend to populate lower spins.[1] The results for distribution *d* are in very close agreement with the expected cross section for $E_n =$ 0–8 MeV, and too large by about 10%–15% for higher energies. While the extracted cross sections are least sensitive to the underlying $J\pi$ distributions in the energy range $E_n =$ 13–20 MeV, they consistently overestimate the cross section by 10%–15%. These discrepancies are likely due to preequilibrium neutron emission in the neutron-induced reaction. Preequilibrium effects for the desired reaction, which reduce the reference cross section, have been included in the fit mentioned above, but are not contained in simulated surrogate observables $P_{\delta,\mathrm{fission}}(E_{\mathrm{ex}})$.

D. Fission cross sections from a ratio approach

To test the validity of the ratio approach, calculations similar to those employed for testing the Weisskopf-Ewing approximation can be carried out. Escher and Dietrich (2006) considered the cross section ratio

$$R(E) = \frac{\sigma[^{235}\mathrm{U}(n, f)](E)}{\sigma[^{233}\mathrm{U}(n, f)](E)}. \tag{19}$$

They treated $\sigma[^{235}\mathrm{U}(n, f)]$ as the desired ("unknown") cross section and $\sigma[^{233}\mathrm{U}(n, f)]$ as the known reference cross section. This choice has the advantage that all of the relevant cross sections are known from direct measurements. To simulate the quantity that is measured in a typical surrogate ratio experiment, namely, the ratio of coincidence probabilities, they calculated

$$R^{\mathrm{sim},p} = \frac{P^{^{236}\mathrm{U}(p)}_{\delta,\mathrm{fission}}(E)}{P^{^{234}\mathrm{U}(p)}_{\delta,\mathrm{fission}}(E)} = \frac{\sum_{J,\pi} F^{^{236}\mathrm{U}(p)}_{\delta}(E, J, \pi) G^{^{236}\mathrm{U}}_{\mathrm{fission}}(E, J, \pi)}{\sum_{J,\pi} F^{^{234}\mathrm{U}(p)}_{\delta}(E, J, \pi) G^{^{234}\mathrm{U}}_{\mathrm{fission}}(E, J, \pi)}, \tag{20}$$

where the superscript p indicates that the simulation employed one of the four schematic spin distributions $F^{(p)}_\delta$ shown in Fig. 20(a). The ^{236}U fission probabilities are those employed in the previous section, and the ^{234}U fission probabilities were taken from a Hauser-Feshbach calculation for the $^{233}\mathrm{U}(n, f)$, carried out in analogy to the one for $^{235}\mathrm{U}(n, f)$ case (Escher and Dietrich, 2006). For simplicity, the compound-nucleus formation cross section was assumed to be independent of the target nucleus, $\sigma^{\mathrm{CN}}_{n+^{233}\mathrm{U}} = \sigma^{\mathrm{CN}}_{n+^{235}\mathrm{U}}$, and the expressions occurring in the numerator and denominator of all ratios were matched at the same projectile energy.

Each $J\pi$ distribution considered, $p = a, b, c, d$, yields a ratio $R^{(p)}$, from which Escher and Dietrich (2006) deduced the desired cross section $\sigma^{(p)}[^{235}\mathrm{U}(n, f)] = R^{(p)}\sigma[^{233}\mathrm{U}(n, f)]$. The deviations of the resulting cross sections from each other provide a measure of how sensitive the ratio approach is to violations of the Weisskopf-Ewing approximation, while the comparison with the reference cross section allows for an assessment of the overall quality of the cross sections obtained from a ratio analysis.

Results are shown in Fig. 21(b). One observes that the $J\pi$ distributions have a much smaller effect on the cross sections deduced here than on the cross sections obtained from a surrogate analysis in the Weisskopf-Ewing limit; i.e., the ratio method is less sensitive to the details of the spin-parity distributions. Relatively good agreement is found between the simulated ratio results and the expected cross sections for energies above about 3 MeV. The largest discrepancies, which may be as large as 50%, occur at small energies ($E_n \leq 3$ MeV) and near the threshold for second-chance fission. Typical surrogate reactions populate spins significantly smaller than those occurring in distribution *c*, thus cross sections extracted from surrogate ratio experiments are expected to exhibit much closer agreement with the cross section of interest.

For situations in which the Weisskopf-Ewing limit provides at least a rough approximation, e.g., for $E_n =$ 5–20 MeV in the case considered here, the ratio method further reduces the discrepancies between the extracted and expected cross sections, thus providing significantly improved results. Effects that, in the surrogate Weisskopf-Ewing approach, cause deviations from the correct results cancel in part in the surrogate ratio treatment. This is, in particular, notable for the preequilibrium decays, the effects

[1]Information on the maximum spins populated in a reaction can be obtained from the γ rays observed in the decay of the relevant compound nucleus.

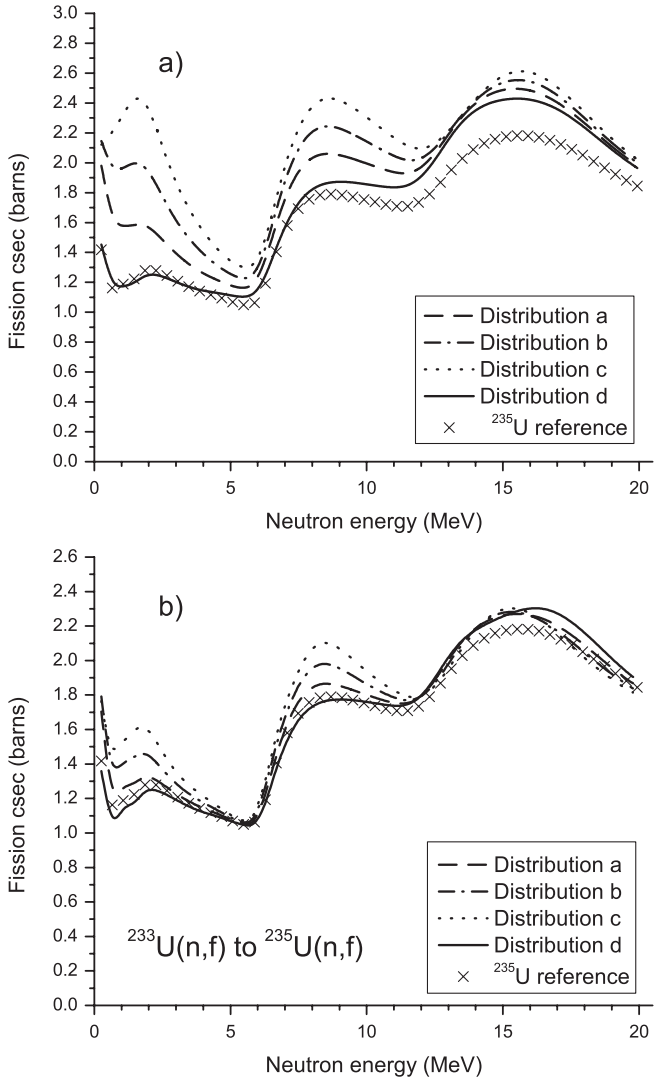

FIG. 21. (a) Weisskopf-Ewing and (b) ratio estimates of the ^{235}U(n, f) cross section, using the distribution of angular momenta shown in Fig. 20. The crosses represent the ''reference'' ^{235}U(n, f) cross section from the fit. From Escher and Dietrich, 2006.

of which were pronounced in the Weisskopf-Ewing approach and are significantly smaller here.

Chiba and Iwamoto (2010) came to qualitatively similar conclusions, but expected an overall closer agreement between the (n, f) cross section obtained from a surrogate ratio measurement and the actual (n, f) cross section than the calculations by Escher and Dietrich (2006) suggest. Based on a consideration of their calculated fission probabilities $G^{^{239}\mathrm{U}}_{\mathrm{fission}}(E, J, \pi)$ and ratios $G^{^{239}\mathrm{U}}_{\mathrm{fission}}(E, J, \pi)/G^{^{237}\mathrm{U}}_{\mathrm{fission}}(E, J, \pi)$, for individual $J\pi$ values, they predicted fission cross sections extracted from ratio measurements to be accurate to within 3%–5%.

VII. MODELING APPROACH

In the ''ideal approach'' outlined in Sec. III, one calculates the spin-parity distribution $F^{\mathrm{CN}}_{\delta}(E, J, \pi)$ and experimentally determines a set of coincidence data $P_{\delta\chi}(E)$, in order to extract the relevant $J\pi$-dependent branching ratios $G^{\mathrm{CN}}_{\chi}(E, J, \pi)$ from Eq. (4). In this approach, no assumptions about the form of the $G^{\mathrm{CN}}_{\chi}(E, J, \pi)$ are made (but the Bohr hypothesis is still considered to be valid). Note that the $F^{\mathrm{CN}}_{\delta}(E, J, \pi)$ depend not only on the direct-reaction mechanism selected, but also on the projectile energy and the angle of the outgoing direct-reaction particle. The beam energy and detection angle have to be varied in order to provide sufficient complementary information on the $J\pi$-dependent branching ratios $G^{\mathrm{CN}}_{\chi}(E, J, \pi)$. It is not *a priori* clear that experimental conditions can be selected that provide enough variation in the weights $F^{\mathrm{CN}}_{\delta}(E, J, \pi)$ to allow for an unambiguous determination of the branching ratios. This fact makes this approach challenging.

While the ''modeling approach'' is affected similarly by coincidence measurements that do not contain a wide range of complementary information on the $J\pi$-dependent branching ratios, it has the advantage that it can make use of independent information that constrains the $G^{\mathrm{CN}}_{\chi}(E, J, \pi)$. Specifically, a sensible modeling approach should include a model for the decay of the compound nucleus under consideration that makes use of the available nuclear-structure information for the region. In particular, neutron resonance spacings and average radiative widths may have been independently determined and there may be calculations or measurements for γ-ray strength functions and/or level densities. Reactions measured for nearby nuclei may also provide some constraints on the input parameters for the statistical reaction calculation. Combining such independent information with a surrogate measurement in order to place stringent constraints on a Hauser-Feshbach calculation for the desired reaction is the objective of the modeling approach. The approach is somewhat similar to that employed in data evaluations, where model parameters which were adjusted to fit measured cross sections in one energy regime, are extrapolated to calculate the cross section in another energy regime. In the surrogate modeling approach, the parameters are adjusted to reproduce measured coincidence probabilities and subsequently used to calculate the desired reaction cross section.

Important steps towards developing the surrogate modeling approach were taken by Back *et al.* (1974a, 1974b), Younes and Britt (2003b, 2003c), and Younes, Britt, and Becker (2004). Both groups employed simple direct-reaction calculations to predict the $J\pi$ distributions for compound nuclei formed in transfer reactions on actinide targets. Modeling the competition of the different decay channels for the relevant compound nuclei, and comparing the results to measured fission probabilities from direct-reaction experiments, allowed them to extract fission barrier parameters and, later on, deduce fission cross sections. Back *et al.* considered the energy region below the neutron separation energy; they did not attempt to determine fission cross sections, but focused on the competition of γ-ray emission and fission and employed the modeling approach to determine barrier heights and curvatures.

A. Modeling approach for low-energy (n, f) reactions

Younes and Britt (2003b, 2003c), and Younes, Britt, and Becker (2004) built on the work of Back *et al.* (1974a, 1974b) and extended it to higher energies in order to deduce

(n, f) cross sections from existing (t, pf), $(^3\mathrm{He}, df)$ and $(^3\mathrm{He}, tf)$ measurements. They revisited older data sets, published by Britt, Rickey, and Hall (1968), Cramer and Britt (1970a, 1970b), and by Back *et al.* (1974b), with the goal to improve on the previous surrogate analysis that had employed the Weisskopf-Ewing approximation.

Younes and Britt (2003b, 2003c) calculated the surrogate (t, pf) fission probabilities, $P_{(t,pf)}(E)$ as a function of energy by summing over the contributions from the individual $J\pi$ compound states $F^{\mathrm{CN}}_{(t,p)}(E, J, \pi)\, G^{\mathrm{CN}}_{\mathrm{fission}}(E, J, \pi)$ [see Eq. (4)]. The (t, p)-induced spin-parity distributions $F^{\mathrm{CN}}_{(t,p)}(E, J, \pi)$ were taken to be independent of energy and relied on the distorted-wave Born-approximation results of Back *et al.* (1974b). Younes and Britt modeled the decay of the compound nucleus of interest by developing a Hauser-Feshbach description for the statistical competition between γ decay, neutron emission, and fission. The γ decay was assumed to proceed solely by $E1$ transitions; the neutron-emission description employed a modern optical-model potential developed by Dietrich (described in the Appendix of Escher and Dietrich (2010). For the fission channel, a standard Hill-Wheeler formalism was employed, which included an inner barrier and two outer barriers with differing symmetry properties, discrete states in the first well and on top of the fission barriers. The discrete levels used are discussed in greater detail in Younes and Britt (2003b). In the γ, neutron, and fission channels, the level densities used were calculated in a macroscopic-microscopic approach, where single-particle states are generated by solving the Schrödinger equation for a nuclear potential that follows the shape of the nucleus, and the corresponding many-body states are counted in a partition-function approach (Bolsterli *et al.*, 1972). Width-fluctuation corrections were included as well.

In fitting their calculated $P_{(t,pf)}(E)$ probability to the surrogate data, Younes and Britt only allowed the heights of the fission barriers to vary. Discrete levels, level densities, γ-ray strength functions, and the neutron transmission coefficients were considered to be fixed. This somewhat constrained approach minimized the number of adjustable parameters. It produced calculated coincidence probabilities, that, after fitting the barrier heights, were in good agreement with the measured $P_{(t,pf)}$ for energies below the neutron separation energy, but showed deviations as large as 35% from the data above that energy. The discrepancy was interpreted as the fission model accounting for roughly the right proportions of transition states of a given spin and parity, but not necessarily their exact number and energies. Therefore, a renormalization procedure was introduced to account for the differences. Specifically, an energy-dependent (but $J\pi$-independent) factor was calculated as the ratio of measured and calculated fission probabilities $P_{(t,pf)}(E)$, and used to renormalize the calculated (n, f) cross sections.

For the $^{235}\mathrm{U}(n, f)$ test case considered, Younes and Britt deduced a cross section which is in good agreement with the ENDF/B-VI evaluation (Weston *et al.*, 1977) for neutron energies in the range of 0.5–2.5 MeV and too large by about 20% for energies from 0.1 to 0.5 MeV (see Fig. 22). The ENDF/B-VI evaluated cross section was estimated to be accurate within 2%. Overall, the approach developed by Younes and Britt, which includes corrections for the spin-parity mismatch, resulted in significantly improved low-energy (n, f) cross sections when compared to the earlier work (Cramer and Britt, 1970a) that relied on the Weisskopf-Ewing approximation [see, for example, the $^{235}\mathrm{U}(n, f)$ cross section in the upper right panel of Fig. 22]. The method tested for the $^{235}\mathrm{U}(n, f)$ case was subsequently applied to other available surrogate data. Younes and Britt (2003b) used it to predict the (n, f) cross section for the short-lived (26 min) isomeric state $^{235m}\mathrm{U}$ at $E = 77$ eV. The $^{235m}\mathrm{U}(n, f)$ cross section cannot be readily measured, and is therefore a good candidate for the surrogate approach. This cross section was also calculated by Lynn and Hayes (2003), using fission data on the $^{235}\mathrm{U}$ ground state as a surrogate for the isomer (n, f)

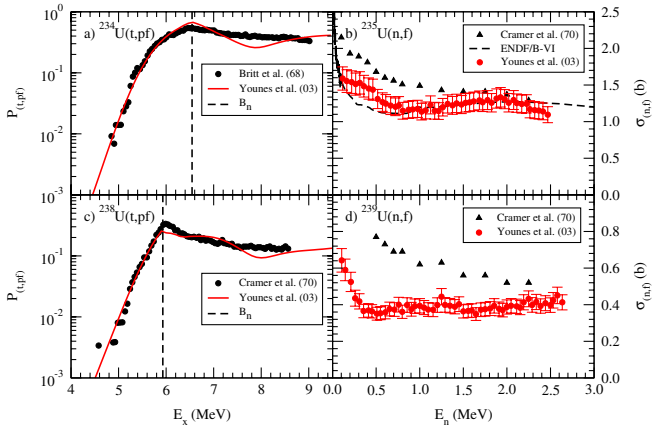

FIG. 22 (color online). Surrogate fission probabilities and (n, f) cross sections for $^{235}\mathrm{U}$ (top) and $^{239}\mathrm{U}$ (bottom). (a), (c) Measured and predicted (t, pf) coincidence probabilities and (b), (d) the extracted cross sections. (b) Results by Younes and Britt (2003c), whose analysis accounted for spin-parity differences between the desired and surrogate reactions, to the earlier analysis by Cramer *et al.*, which employed the Weisskopf-Ewing approximation, and to the ENDF/B-VI evaluation (Weston *et al.*, 1977). (d) The $^{239}\mathrm{U}(n, f)$ cross section, compared to the Weisskopf-Ewing result from Cramer *et al.* From Younes and Britt, 2003c.

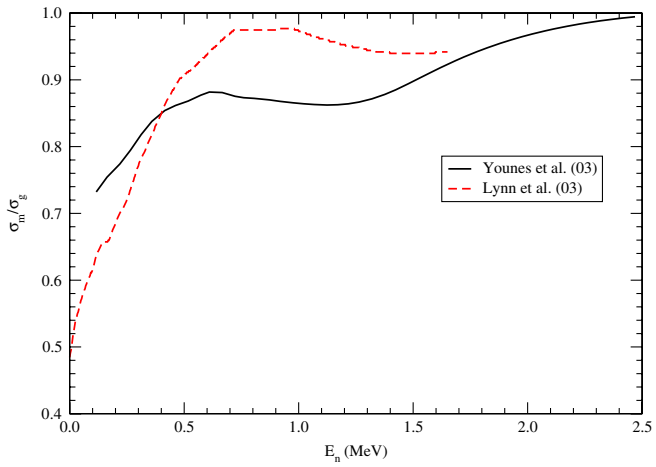

FIG. 23 (color online). Estimate of the isomer-to-ground state (n, f) cross section ratio for the $^{235}\mathrm{U}(n, f)$ reaction, deduced by Younes and Britt (2003b), from $^{234}\mathrm{U}(t, pf)$ surrogate fission probabilities and by Lynn and Hayes (2003) from $^{235}\mathrm{U}(d, pf)$ surrogate data. From Younes and Britt, 2004.

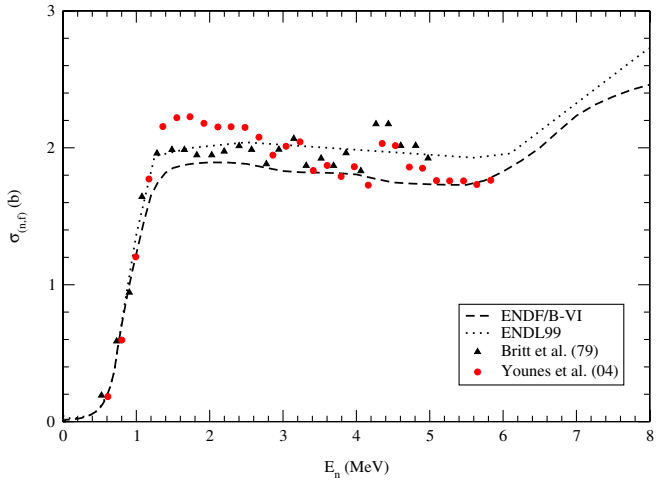

FIG. 24 (color online). Estimate of the ^{241}Am(n, f) cross section deduced from ^{242}Pu(^{3}He, tf) surrogate data (Britt and Wilhelmy, 1979; Younes, Britt, and Becker, 2004). The surrogate results are compared to the ENDF/B-VI and ENDL99 evaluations. From Younes, Britt, and Becker, 2004.

cross section. Despite some differences in the details of the fission model, the results for the ^{235m}U(n, f) cross section from Lynn and Hayes (2003) and Younes and Britt (2003b) are in qualitative agreement, with both predicting an inhibited fission cross section for the isomer relative to the ground state below $E_n \approx 2$ MeV (see Fig. 23). The surrogate method was also applied to the calculation of (n, f) cross sections from excited states for ^{235,237,239}U and ^{241,243}Pu targets (Younes and Britt, 2003a), but it was generally found that the difference between ground-state and excited-state cross sections was not as stark as in the ^{235m}U(n, f) case which involved greater differences in spins and parities ($7/2^-$ for the ground state and $1/2^+$ for the isomer). Younes and Britt (2003c) extracted (n, f) cross sections from (t, pf) data for neutron targets

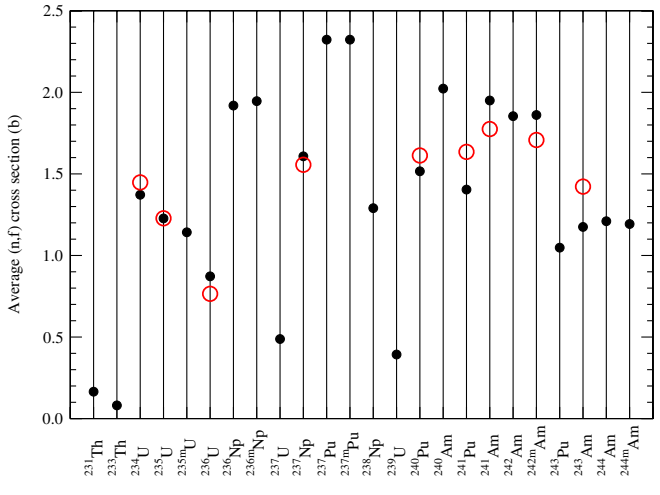

FIG. 25 (color online). Summary of surrogate-method (n, f) cross section results. For each target nucleus, the cross section was averaged over an energy range where it is relatively flat [E_n = 1–3 MeV for (t, pf), 1–6 MeV for (^{3}He, xf) results], and that single value is plotted as an open circle for the surrogate result, and a filled circle for directly measured data. From Younes and Britt, 2004.

^{240,241,243}Pu, ^{234,236,237,239}U, and ^{231,232}Th, for energies E_n = 0.1–2.5 MeV. All applications made use of the same approach, including the renormalization procedure. The accuracy of the results was estimated at 20% below $E_n \approx 0.5$ MeV, and 10% at higher energies, based on a comparison with known cross sections. Figure 25 summarizes the comparison between known actinide (n, f) cross sections and their surrogate-method estimates for low-energy fission.

In subsequent work, Younes, Britt, and Becker (2004) covered surrogate data from (^{3}He, df) and (^{3}He, tf) experiments carried out by Britt and Wilhelmy (1979) and by Gavron *et al.* (1976). They deduced (n, f) cross sections for neutron targets ^{236,236m,237,238}Np, ^{237,237m}Pu, and ^{240,241,242,242m,243,244,244m}Am, for energies E_n = 0–6 MeV. An example is shown in Fig. 24. For those cases for which direct measurements exist, the directly determined (n, f) cross section and the surrogate result agree within about 10% (see Fig. 25).

B. Extension of the method to higher neutron energy

Younes and collaborators developed a procedure for extrapolating the surrogate results to higher energies, and applied it to estimating the ^{235,237,239}U(n, f) cross sections for incident energies of up to 20 MeV (Younes *et al.*, 2003; Younes and Britt, 2005). In extending the surrogate results to higher energies, new phenomena must be accounted for such as multiple-chance fission (i.e., fission following neutron emission, so that the fissioning nucleus is different from the initial compound system), and preequilibrium neutron emission. The extrapolation procedure combines the surrogate predictions for the mass-A nucleus, which provides an estimate of the first-chance fission cross section, with known (n, f) cross sections on the $A - 1$ nucleus, which gives the second-chance and higher-chance contributions.

For the first-chance [e.g., in the case of ^{235}U(n, f), fission from the ^{236}U system] cross section, the surrogate predictions usually stop at a few MeV in equivalent neutron energy. In order to extend the predictions to 20 MeV, a linear extrapolation of the surrogate result was used. The surrogate data were used to fix the intercept of the linear extrapolation, and the slope was obtained from the ENDF/B-VI evaluation of the (n, f) cross section. That slope is determined, to a large extent, by the level density of transition states above the barriers, relative to the level density in the neutron-emission channel.

The second-chance [e.g., in the case of ^{235}U(n, f), fission from the ^{235}U system] fission cross section was decomposed into contributions from equilibrium and preequilibrium reactions. The second-chance equilibrium cross section was approximated as the difference between the compound formation and first-chance (n, f) cross sections. This difference gives the cross section for the equilibrium (n, n') process, which may then be followed by further neutron emission, γ decay, or fission. The preequilibrium (n, n') process was calculated using the Double Differential Hybrid Monte-Carlo Simulation (DDHMS) code (Chadwick, 2001), and its cross section was added to the equilibrium one. To extract the $(n, n'f)$ cross section, the total (n, n') cross section (equilibrium plus preequilibrium

contributions) was multiplied by the conditional probability $P_{f|(n,n')}$ that the nucleus fissions given that an (n, n') reaction has occurred. This conditional probability was calculated by invoking the Bohr hypothesis and assuming that the probability $P_{f|(n,n')}(A)$ for a target nucleus A is equal to the probability $P_{f|(n)}(A-1)$ of fission following neutron absorption on a target with mass $A-1$, and therefore leading to the same mass-A compound nucleus, provided the same excitation energy is reached in both reactions. In practice, the probability $P_{f|(n)}(A-1)$ was obtained from the measured (n, f) cross section on the $A-1$ nucleus. In principle, this procedure is designed to give the second-chance contribution to the cross section, but the use of the measured $A-1$ cross section introduces contributions from third-chance and higher-chance fission as well.

The dependence on emitted neutron energy for the second-chance fission process was assumed to follow a Maxwell distribution. The effective temperature in the distribution was the only adjustable parameter in the model. In a systematic study of the ^{235,237,239}U(n, f) cross sections, the Maxwell-distribution temperature was fixed by fitting the known ^{235}U(n, f) cross section with the model described above, and that same temperature was used to predict the ^{237,239}U(n, f) cross sections. The deduced ^{235,237,239}U(n, f) cross sections are shown in Fig. 26, where they are compared to the ENDF/B-VI evaluation. In the case of ^{239}U(n, f), no ENDF/B-VI evaluation was available, therefore the surrogate estimate was compared to a calculation using the Hauser-Feshbach code GNASH (Young, Arthur, and Chadwick, 1992). These surrogate results were incorporated into subsequent updates of the ENDF database, which are therefore not shown for comparison in Fig. 26.[2]

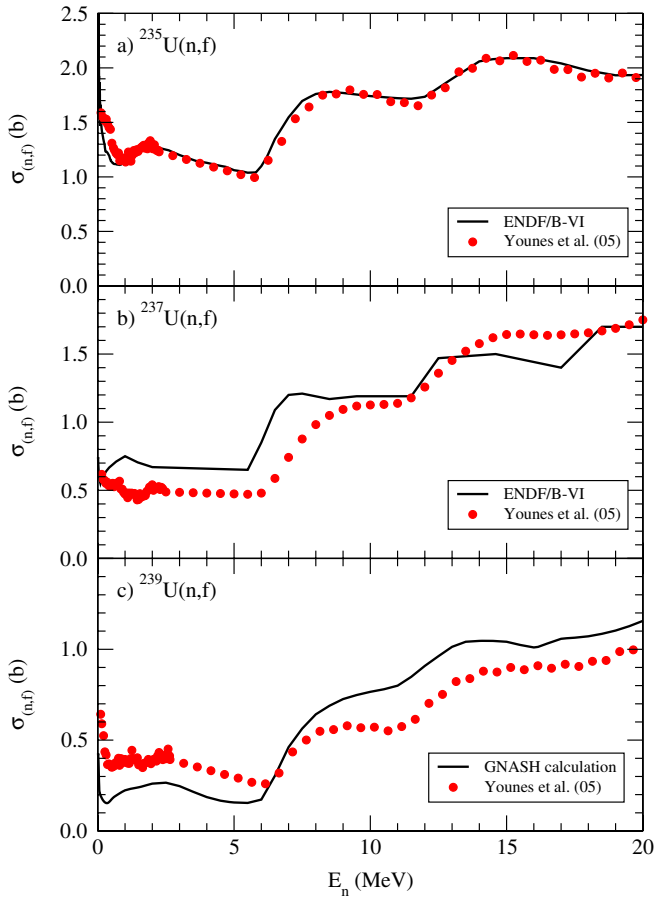

FIG. 26 (color online). Comparison of the calculated ^{235,237,239}U(n, f) cross sections with the ENDF/B-VI evaluation. From Younes and Britt, 2005.

C. Comments on the modeling approach

The work by Younes and collaborators clearly demonstrates that the accuracy of low-energy (n, f) cross sections can generally be improved by theoretically accounting for the spin-parity mismatch between the desired and surrogate reactions, and by using optical potentials that have been fit to scattering properties for nearby nuclei. The cross sections deduced in their modeling approach are in much better agreement with the available direct measurements than the older results, which employed the Weisskopf-Ewing approximation. Furthermore, some studies of interest, such as the ^{235m}U(n, f) cross section, require the explicit treatment of spin and parity in the surrogate method.

While the bulk of the work by Younes and Britt allowed only for a variation of very few parameters, namely, the fission barrier heights, a full modeling approach should relax the constraints on the level densities, strength functions, etc. Variation of some additional parameters was part of a sensitivity study carried out by Younes and Britt (2003b). Overall, it becomes important to balance the freedom gained by allowing additional parameters to vary, against the typically limited data that can be used to provide the necessary constraints. Although it may seem daunting, this program of continuing model and parameter improvements is already part and parcel of standard cross section evaluations, such as those found in the ENDF database.

The models used to predict $J\pi$ distributions of the compound nucleus were adapted from those used for studying properties of low-lying states, but seemed effective. The models did not take into account that nucleons were transferred to unbound states, nor did they include the possibility that the highly excited intermediate system might decay without forming a compound nucleus. The predicted $J\pi$ distributions were independent of energy, which might be a reasonable approximation for the 2.5 MeV range populated in the (t, pf) reactions, but might lead to additional uncertainties when considering wider energy ranges.

The calculated fission probabilities that resulted from the fitting procedure showed deviations from the surrogate data that had to be corrected for via an energy-dependent, but $J\pi$-independent normalization factor. The factor, which was seen to deviate from unity by as much as 15% for the ^{235}U(n, f) test case and 35% for the ^{235m}U application, indicates that further improvements in the method are possible. The goodness of the fit to the measured coincidence probabilities is an indication of how well the physics of the surrogate reaction, including the decay, is described by theory. Having an accurate description that requires no additional normalization factors is particularly important if one

[2]The ENDF ^{237}U(n, f) and ^{239}U(n, f) cross sections were updated with the surrogate results as of February 25, 2006.

wants to apply the method to reactions on nuclei which are a few nucleons off stability. Such an accurate description in the case of low-energy fission will require, in particular, a better understanding of the transition and class II states.

The predicted $J\pi$ populations were not independently tested. For the cases where directly measured (n, f) cross section data were available, the agreement between the surrogate results and the direct measurements was taken as an indication of the overall consistency of the approach and the models employed. However, developing experimental signatures that can test the predicted $J\pi$ populations would be useful for further tests and improvements of the surrogate method. Such signatures might be found in the γ-ray transitions of a decaying compound nucleus that was created in a surrogate reaction (see Sec. IX.C).

VIII. SURROGATE REACTIONS FOR (n, γ)

While a large number of surrogate experiments aimed at obtaining (n, f) cross sections have been carried out over the years, few experiments have been designed to determine (n, γ) cross sections. Still fewer experiments have attempted to provide information about the charged-particle or two-neutron exit channels. In this section, we focus on the prospects of determining (n, γ) cross sections from surrogate experiments.

A. Challenges for surrogate measurements of (n, γ) cross sections

Capture cross sections provide specific challenges for the surrogate approach: First, the level of precision required for the cross section is often higher than in the fission case. Recent advances in modeling the astrophysical *s* process have resulted in requests to determine capture cross sections to within a few percent and nuclear-energy applications require cross sections to within 5%–10% (Aliberti *et al.*, 2006; Käppeler and Mengoni, 2006; Colonna, 2009). On the other hand, cross section evaluations for cases without experimental data can show large deviations from each other (see the discussion in Sec. II).

Second, it is the low-energy regime that is relevant to many applications. For *s*-process applications, for example, one needs cross sections from a few keV to about 200 keV. Both calculations and measurements have shown that this is within the energy range for which the Weisskopf-Ewing approximation typically breaks down. Consequently, the mismatch between the spin-parity populations produced in the surrogate and desired reactions can be expected to play a more significant role than in the fission case. Here the question that needs to be addressed is whether corrections can be implemented to account for this mismatch.

Furthermore, cleanly identifying the γ-decay channel of interest in a surrogate experiment can be difficult. The signature is a complex γ-ray cascade from a highly-excited compound nucleus. Some experiments determine the relevant coincidence probability by measuring one or a few specific γ rays in the decaying residual nucleus. A model calculation or other experimental constraints have to be used to connect this measurement to the quantity of interest, namely, the sum of all γ cascades leading to the ground state of the residual nucleus. In the fission case, it is possible to directly measure the quantity of interest, namely, fission probabilities, by detecting the emitted fission fragments; angular anisotropies in the fission-fragment distributions can be accounted for by detecting the fission fragments over a wide range of angles.

Experiments that focus on measuring the sum of all γ rays in the decay cascade rather than a few specific γ rays come, in principle, closer to determining the relevant quantity. In practice, it becomes necessary to subtract contributions from sources other than the γ decay of the compound nucleus of interest. For example, backgrounds from target impurities (even if only at the percent level) are a concern because the γ-ray exit channel decreases rapidly with energy and can be orders of magnitude smaller than the cross section for unwanted nuclear reactions occurring within the target material. Also, neutron emission is typically followed by emission of γ rays that originate from a neighboring nucleus. In this case, the signal of interest can be isolated by experimentally restricting the energies of the γ rays that are counted (Goldblum *et al.*, 2008; 2010), or by estimating the contributions from the decay of other nuclei (Boyer *et al.*, 2006).

Furthermore, in applications to capture reactions the excitation energy of the compound nucleus must be precisely determined to avoid washing out the strong energy dependence of most (n, γ) cross sections. The resolution and calibration of the excitation-energy measurement also dictates how low in energy the experiment can probe before events from below the neutron separation energy compromise the surrogate data.

B. Experimental efforts for (n, γ)

Several experimental techniques have been developed to collect data to determine (n, γ) cross sections from surrogate reactions. The Livermore-Berkeley Array for Collaborative Experiments, which consist of an array of clover-type HPGe detectors (Duchene *et al.*, 1999) with bismuth-germanate-oxide Compton-suppression shields (Elekes *et al.*, 2003), have been used to identify the γ channel from a particular compound nucleus by detecting individual characteristic γ rays in coincidence with exit-channel particles. This detector array, described in detail in Lesher *et al.* (2010), is shown surrounding the target chamber and STARS detectors in Fig. 11. For experiments where individual transitions in the compound nucleus are identified using high-resolution γ-ray spectroscopy, the probability that the nucleus deexcites by γ-ray emission $P_{\delta\gamma}$ can be determined by modifying Eq. (5) as follows:

$$P_{\delta\gamma}(E_{\mathrm{ex}}) = \frac{1 + \alpha_{\mathrm{IC}}}{\epsilon_\gamma f(E_{\mathrm{ex}})} \frac{N_{\delta\gamma}(E_{\mathrm{ex}})}{N_\delta(E_{\mathrm{ex}})}, \tag{21}$$

where $N_{\delta\gamma}$ and N_δ denote the number of detected particle-gamma coincidences and scattered particles (singles), respectively, and the overall efficiency for identifying the γ-ray exit channel depends on f, the energy-dependent fraction of γ-ray cascades that pass through the transition of interest, and ϵ_γ and α_{IC}, the γ-ray detection efficiency and internal conversion (IC) coefficient for this transition. Typically ϵ_γ and α_{IC}

can be determined to the required precision with sealed-source measurements and calculations, respectively. The term f must be determined from experimental and/or theoretical constraints. The charged-particle detection efficiency cancels in the ratio.

Instead of focusing on identifying individual γ rays, one can count the number of γ-ray cascades in a manner that is independent of the particular γ-ray decay path. This approach is used for direct measurements at neutron beam facilities using sophisticated BaF_2 arrays with nearly 100% efficiencies (Ullmann *et al.*, 2005; Guerrero *et al.*, 2009) that act as calorimeters to identify neutron-capture events. For surrogate-reaction experiments, simpler detector arrays using C_6D_6 liquid scintillator arrays (Wilson *et al.*, 2003) or NaI (Guttormsen *et al.*, 1990) inorganic scintillator arrays have been used to detect the high-energy statistical γ rays emitted from the compound nucleus. In this case, the coincidence probability $P_{\delta\gamma}$ is obtained from

$$P_{\delta\gamma}(E_{\mathrm{ex}}) = \frac{N_{\delta\gamma}(E_{\mathrm{ex}})}{\epsilon_\gamma N_\delta(E_{\mathrm{ex}})}; \tag{22}$$

the efficiency ϵ_γ is typically determined from the number of γ-ray cascades detected below the neutron separation energy where γ emission is the only open (or overwhelmingly dominant) decay channel. However, this method cannot determine the source of the γ rays, so contributions from sources other than the compound nucleus of interest have to be eliminated or corrected.

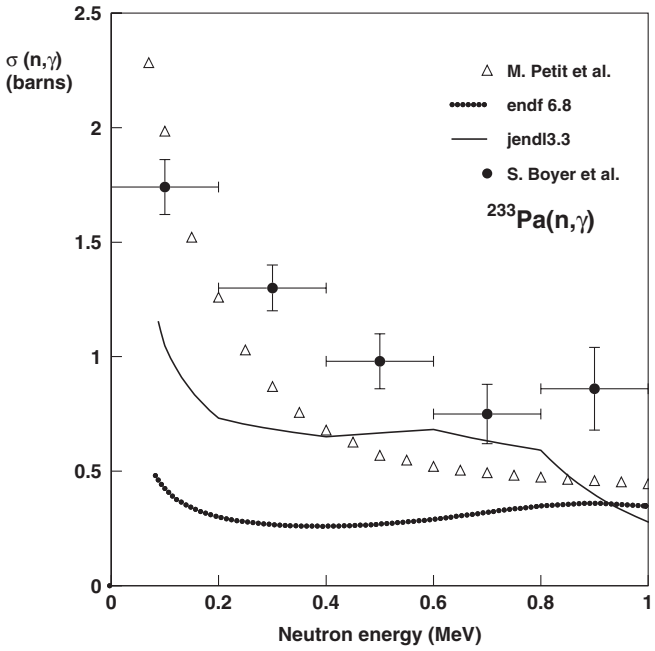

FIG. 27. ^{233}Pa(n, γ) cross section from two separate surrogate experiments, compared to evaluations. The triangles show the result of a Hauser-Feshbach calculation with parameters adjusted to fit the ^{233}Pa(n, f) cross section that was obtained from a ^{232}Th(^{3}He, pf) surrogate experiment. The large, filled circles show the results of a Weisskopf-Ewing analysis of a ^{232}Th(^{3}He, $p\gamma$) surrogate measurement. The solid and dotted curves show prior JENDL3.3 and ENDF/B-VI.6 results. Adapted from Boyer *et al.*, 2006.

1. Weisskopf-Ewing approach to (n, γ)

The French collaboration extracted the (n, γ) cross section for the short-lived ^{233}Pa isotope from two separate surrogate experiments.

The first experiment (Petit *et al.*, 2004) employed the (^{3}He, p) reaction on a ^{232}Th target and was designed to yield the ^{233}Pa(n, f) cross section. Cross sections for neutron-induced reactions on ^{233}Pa are important for nuclear-energy applications that focus on the thorium-uranium fuel cycle. Because of the short 27-day half-life of the isotope, direct cross section measurements are challenging and sparse. The collaboration used the charged-particle detectors discussed in Sec. V.A to measure the ^{234}Pa fission probabilities. The ^{233}Pa(n, f) cross section was obtained from a Weisskopf-Ewing analysis of the data, for neutron incident energies up to 10 MeV (the resulting cross section is compared to direct measurements in Fig. 9). Subsequently, a Hauser-Feshbach evaluation of the ^{233}Pa(n, f), ^{233}Pa(n, n'), and ^{233}Pa(n, γ) cross sections was carried out, with parameters adjusted to reproduce the new (n, f) results. The result of the ^{233}Pa(n, γ) cross section calculation is shown in Fig. 27.

The second experiment was specifically designed to determine the ^{233}Pa(n, γ) cross section. Boyer *et al.* (2006) measured p-γ coincidence probabilities using the ^{232}Th(^{3}He), $p\gamma$ reaction with a 24-MeV ^{3}He beam at the IPN Orsay Tandem facility. Their experimental setup included four Si telescopes for identifying the outgoing proton, and four liquid C^6D^6 scintillators for detecting γ-ray cascades. The approach made use of a previously developed technique to count the number of γ cascades in a manner that is independent of the particular γ-decay path (Wilson *et al.*, 2003). To avoid contamination by γ rays from fission fragments, the study was restricted to ^{234}Pa excitation energies below the fission barrier, which corresponds to neutrons incident on ^{233}Pa with energies of 0 to 1 MeV. In addition, contributions from the (n, $n'\gamma$) process were estimated and corrected. In the analysis of the data, the assumption was made that the angular momentum and parity population of the compound nucleus produced in the transfer reaction was similar to the spin-parity population relevant to the neutron-induced reaction. This simplified the extraction of the (n, γ) cross section (see Sec. III.B). The formation cross section was calculated using the same semimicroscopic neutron-nucleus optical potential (Bauge, Delaroche, and Girod, 1998; 2001) that was employed in the earlier fission work (Petit *et al.*, 2004).

In Fig. 27, the ^{233}Pa(n, γ) cross section obtained from this experiment is compared to the calculation discussed above and to prior evaluations. The results of the two surrogate experiments are within a factor of 2 of each other and of the JENDL-3.3 evaluation, but are larger than the ENDF/B-6.8 evaluation by up to a factor of 5. A clearer assessment of the indirect approaches is difficult, as no direct measurements are available in the energy regime of interest. While the fission experiments carried out by the French group normally include measurements of cross sections that are known, no such benchmark is available for the ^{233}Pa(n, γ) case.

Scielzo *et al.* (2010) used inelastic proton scattering on the even-even ^{154,156,158}Gd target nuclei as surrogates for the

^{153,155,157}Gd(n,γ) reactions. The experiment was designed to investigate various methods of analyzing surrogate data for (n,γ) applications. Gadolinium targets were bombarded with ≈ 2 nA of 22-MeV protons from the 88-inch Cyclotron and scattered protons and γ rays were detected using the STARS-LiBerACE experimental setup shown in Fig. 11.

The gadolinium region is well suited for tests of the surrogate nuclear reaction method because many stable Gd isotopes exist for which (n,γ) cross sections have been directly measured (Beer and Macklin, 1988; Voignier, Joly, and Grenier, 1992), and sufficient nuclear-structure information is available to carry out complementary cross section calculations. For the even-even compound nuclei, high statistics could be collected for the $E2$ transitions from the 8^+, 6^+, 4^+, and 2^+ states of the ground-state band. The validity and limitations of the Weisskopf-Ewing approximation were investigated by substituting the measured $P_{\delta\gamma}$ values for the branching ratio G_γ^{CN} and multiplying by a calculated σ_n^{CN} as prescribed by Eq. (9). In Sec. VIII.C.1, the ^{155}Gd(n,γ) cross sections obtained in this way are compared to directly measured results and to Hauser-Feshbach-type calculations.

2. Ratio measurements

The surrogate ratio approach introduced in Sec. III.B requires the (approximate) validity of the Weisskopf-Ewing limit. In this approach, the ratio $R(E)=\sigma_{\alpha_1\chi_1}/\sigma_{\alpha_2\chi_2}$ of the cross sections of two compound-nuclear reactions is measured, using two surrogate experiments. An independent determination of the cross section $\sigma_{\alpha_2\chi_2}$ can then be used to deduce $\sigma_{\alpha_1\chi_1}$. The ratio method eliminates the need to accurately measure the total number of surrogate-reaction events, which make it easier to correct for target impurities. In addition, for fission applications there are indications that small to moderate deviations from the Weisskopf-Ewing assumption might cancel in this approach [see the discussion in Sec. VI and Escher and Dietrich (2006, 2010); Chiba and Iwamoto (2010)].

For (n,γ) applications, two types of ratio measurements can be considered: A distinction is made between *internal* and *external* surrogate ratio approaches, based on whether the ratio under consideration involves *one* compound nucleus (but different decay channels) or two different compound systems, but identical exit channels.

The more widely employed variant is the *external surrogate ratio method*. The cross sections in the ratio $R(E)=\sigma_{\alpha_1\chi_1}^{\mathrm{CN1}}/\sigma_{\alpha_2\chi_2}^{\mathrm{CN2}}$ of Eq. (10) refer to two reactions with the same type of entrance channel, $\alpha_1=\alpha_2$ ($=n$ + target here), and the same type of exit channel, $\chi_1=\chi_2$ ($=\gamma$ decay here), but different compound nuclei, CN1 $\neq$ CN2. For instance, Scielzo *et al.* (2010) tested the ratio method by comparing $\sigma[M_Z{}^{157}\mathrm{Gd}(n,\gamma)]/\sigma[^{155}\mathrm{Gd}(n,\gamma)]$ determined from measurements of $P[^{158}\mathrm{Gd}(p,p'\gamma)]/P[^{156}\mathrm{Gd}(p,p'\gamma)]$ to the known cross section ratio. The comparison is shown in Fig. 33(a).

For neutron energies below about 1 MeV, the experimentally determined ratio is approximately unity, which is as much as a factor of 2 larger than the reference ratio. Therefore, if one extracted the low-energy ^{157}Gd(n,γ) cross section from this ratio, the result would be too large by this factor. In order to better assess the uncertainty that results from neglecting the J^π mismatch between desired and surrogate reactions, the ratios of the simulated Weisskopf-Ewing cross sections $R^p=\sigma_{n\gamma}^{^{157}\mathrm{Gd}(p)}/\sigma_{n\gamma}^{^{155}\mathrm{Gd}(p)}$ for the four schematic spin-parity distributions $p=1,2,3,4$ shown in Fig. 31 were calculated. The ratios, also plotted in Fig. 33(a), are seen to differ from each other by up to a factor of 2.5 for energies below about $E_n=0.7$ MeV; above that energy, they rapidly converge to the expected result. Thus, the ratio approach seems to somewhat reduce the effect of the J^π mismatch on the extracted cross sections for energies where the Weisskopf-Ewing approximation is not valid. These results indicate that deviations can be much smaller if the J^π differences between the desired and surrogate reactions are minimized. Clearly, it is preferable to carry out an experiment with a reaction mechanism and experimental conditions (projectile energy, angle of outgoing direct-reaction particle) that create J^π distributions similar to the one produced in the desired reaction.

Hatarik *et al.* (2010) determined the ratio $\sigma[^{171}\mathrm{Yb}(n,\gamma)]/\sigma[^{173}\mathrm{Yb}(n,\gamma)]$ from measurements of $P[^{171}\mathrm{Yb}(d,p\gamma)]/P[^{173}\mathrm{Yb}(d,p\gamma)]$. A 18.5-MeV deuteron beam was used to irradiate ^{171,173}Yb targets and γ-ray transitions characteristic for the decay of the compound nuclei ^{172,174}Yb were measured in coincidence with outgoing protons. In particular, the $6^+\rightarrow 4^+$ and $4^+\rightarrow 2^+$ were measured. The comparison of the cross section ratio $\sigma[^{171}\mathrm{Yb}(n,\gamma)]/\sigma[^{173}\mathrm{Yb}(n,\gamma)]$ extracted from the surrogate measurement to the ratio of directly measured cross sections showed differences of about 30% when the analysis was based on the $4^+\rightarrow 2^+$ transition, and 50% for the $6^+\rightarrow 4^+\gamma$ ray. The discrepancies were attributed to the mismatch between the spin-parity populations produced in the neutron-induced and stripping reactions. In addition, yrast transitions involving larger J values (such as $6^+\rightarrow 4^+$) can be more easily bypassed by γ cascades originating from compound-nuclear states with low angular momenta than yrast transitions involving lower J values (such as $2^+\rightarrow 0^+$). The low-energy ($E_\gamma<80$ keV) $2^+\rightarrow 0^+$ transition, which is expected to be populated by most γ cascades, could not be used in Hatarik's analysis; it was only weakly observed due to internal conversion and low detector efficiencies for this energy range. As the $4^+\rightarrow 2^+$ and $6^+\rightarrow 4^+$ yrast transitions were expected to predominantly sample cascades originating from higher compound-nuclear spins, a subtraction procedure was attempted to correct for this weighted sampling. This resulted in a better agreement of the extracted cross section ratio with the direct measurements for energies above about 90 keV, but did not satisfactorily resolve the discrepancies.

The ratio approach has also been used in analyses of experiments that measure a sum of γ rays, rather than specific discrete transitions. Goldblum *et al.* (2008, 2010) studied γ-ray spectra that had previously been measured in coincidence with outgoing particles in (^{3}He, ^{3}He$'$) and (^{3}He, α) experiments. The ^{170}Yb(n,γ) cross section was determined relative to the ^{160}Dy(n,γ) cross section, and the ^{161}Dy(n,γ) cross section was obtained relative to the ^{163}Dy(n,γ) and the ^{160}Dy(n,γ) cross sections. In principle, using a sum of γ rays circumvents the need for having to account for the fact that only a fraction of the γ cascade is detected in methods that

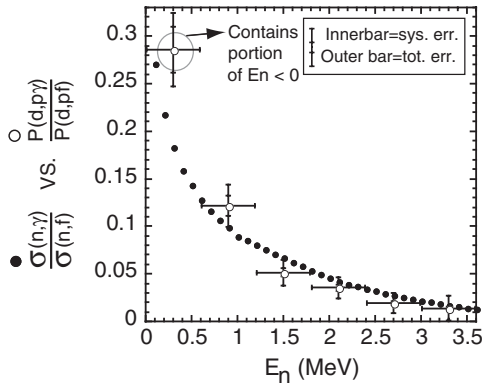

FIG. 28. Allmond *et al.* (2009) used the Internal Surrogate Ratio (ISR) approach to determine the ^{235}U(n, γ) cross section. Their measured coincidence ratio $P_{(d,p),\gamma}(E)/P_{(d,p),f}(E)$ is compared to the ratio $\sigma[^{235}\mathrm{U}(n, \gamma)]/\sigma[^{235}\mathrm{U}(n, f)]$ of cross sections from ENDF/B-VII evaluations. The latter are based on direct measurements. The comparison provides a test of the ISR method which is based on the assumption that the Weisskopf-Ewing is approximately valid. Under this circumstance, the cross section expressions factorize as shown in Eq. (11), and the measured coincidence ratio $P_{(d,p),\gamma}(E)/P_{(d,p),f}(E)$ should equal the cross section ratio for the neutron-induced reactions. Adapted from Allmond *et al.* (2009).

rely on specific γ rays. In practice, this method has its own challenges, such as determining in a reliable manner which portion of the γ-ray spectrum to exclude and how to properly normalize the number of coincidence events.

For actinides, the *internal surrogate ratio (ISR) approach* has also been considered. In this variant, the compound nuclei created in the two reactions of interest are identical, CN1 = CN2, the entrance channels are identical, $\alpha_1 = \alpha_2$, but the decay channels differ in type, $\chi_1 \neq \chi_2$. In the specific cases discussed below, the decay of a compound uranium nucleus by γ emission has been observed relative to the decay by fission; Allmond *et al.* (2009) measured the ratio $P[^{235}\mathrm{U}(d, p\gamma)]/P[^{235}\mathrm{U}(d, pf)]$ to determine $\sigma[^{235}\mathrm{U}(n, \gamma)]/\sigma[^{235}\mathrm{U}(n, f)]$, and Bernstein *et al.* (2006) employed inelastic scattering on ^{238}U to infer the cross section ratio $\sigma[^{237}\mathrm{U}(n, \gamma)]/\sigma[^{237}\mathrm{U}(n, f)]$.

The experiment by Allmond *et al.* (2009) made use of the (d, p) stripping reaction with 21-MeV deuterons on a ^{235}U target to produce the ^{236}U compound nucleus. Both p fission and p-γ coincidence probabilities were measured, as the objective of the experiment was to extract the ^{235}U(n, γ) cross section from an ISR analysis. A strong γ-ray transition in the γ decay of the ^{236}U compound nucleus was selected in order to infer the probability of the γ channel relative to the fission channel. The fraction of the γ cascade that proceeds through the transition studied was estimated by investigating the decay of the compound nucleus from excitation energies slightly below the neutron separation threshold and was accounted for in the ISR analysis. The resulting ^{235}U(n, γ) cross section is shown in Fig. 28. It is in agreement with the ENDF/B-VII evaluation, which is based on data from several direct ^{235}U(n, γ) measurements. They estimated the average deviation of the cross section to be somewhat less than 25%.

Bernstein *et al.* (2006) employed inelastic scattering with 55-MeV α particles as a surrogate mechanism to produce the ^{238}U compound nucleus. Both α fission and α-γ coincidence probabilities were measured. This made it possible to extract the ^{237}U(n, γ) cross section relative to the ^{237}U(n, f) cross section, using an ISR analysis and the ^{237}U(n, f) cross section determined by Burke *et al.* (2006). A set of characteristic γ-ray transitions was used to construct the total γ-channel probability, relative to the fission probability. Since the number of α-singles events was also determined, Bernstein *et al.* were also able to determine the ^{237}U(n, γ) cross section from a Weisskopf-Ewing analysis of the data. The results of both procedures were found to agree with each other (Bernstein *et al.*, 2006), but are larger than recent evaluations, by up to a factor of 5 [see Fig. 70 of Young *et al.* (2007)]. For this case, as for the ^{233}Pa(n, γ) case, there exists no direct cross section measurement, so assessing the success of employing the Weisskopf-Ewing and ratio approximations is difficult.

C. Theoretical case studies for (n, γ) cross sections

Several theoretical studies have been carried out to assess the feasibility of obtaining capture cross sections from surrogate measurements and to determine promising candidates for such measurements (Forssén *et al.*, 2007; Chiba and Iwamoto, 2010; Escher and Dietrich, 2010). The strategy followed in these investigations is to extract information from Hauser-Feshbach calculations that have been adjusted to reproduce known cross sections (capture and, where applicable, fission). The branching ratios (or "γ-channel probabilities") $G_\gamma^{\mathrm{CN}}(E, J, \pi)$ shown in Fig. 29 have been obtained via this procedure. These probabilities are defined in Eq. (2); the Weisskopf-Ewing limit is reached when they are approximately equal.

Figure 29(a) illustrates that the branching ratios can depend sensitively on angular momentum and parity of the decaying nucleus. In the energy regime considered, the decay of the compound nucleus ^{92}Zr proceeds by γ or neutron emission, with negligible contributions from other channels. Because of the low level density in the neighboring nucleus ^{91}Zr, few neutron decay channels are available; the opening of each new channel corresponds to a slope discontinuity in one or more γ-branching ratios. This, and the fact that the neutron decay is dominated by low partial waves (s and p), leads to γ-decay probabilities that are sensitive to the compound-nuclear $J\pi$ population. It is clear that the Weisskopf-Ewing approximation is not valid in this region.

For actinides, the behavior of the branching ratios $G_\gamma^{\mathrm{CN}}(E, J, \pi)$ is governed by the competition of fission, neutron emission, and γ decay. For ^{236}U, fission competes with γ emission below the neutron separation threshold, resulting in $G_\gamma^{\mathrm{CN}}(E, J, \pi) < 1$ at $E_{\mathrm{ex}} = 7.55$ MeV ($E_n = 0$), as seen in Fig. 29(c). While the $G_\gamma^{\mathrm{CN}}(E, J, \pi)$ for $J = 0 - 6$ are very similar to each other for $E_n > 1$ MeV, they differ more significantly below 1 MeV. For energies above $E_n \approx$ 1.5 MeV, all branching ratios exhibit roughly the same energy dependence, but the $G_\gamma^{\mathrm{CN}}(E, J, \pi)$ associated with the higher values $J = 9$, 12 differ from those for $J = 0$, 3 by factors ranging from 0.5 to 3. An increased probability for ^{236}U states with larger J values to decay via γ emission is not surprising, as s-wave neutron emission from these states is hindered at low energies due to angular-momentum selection

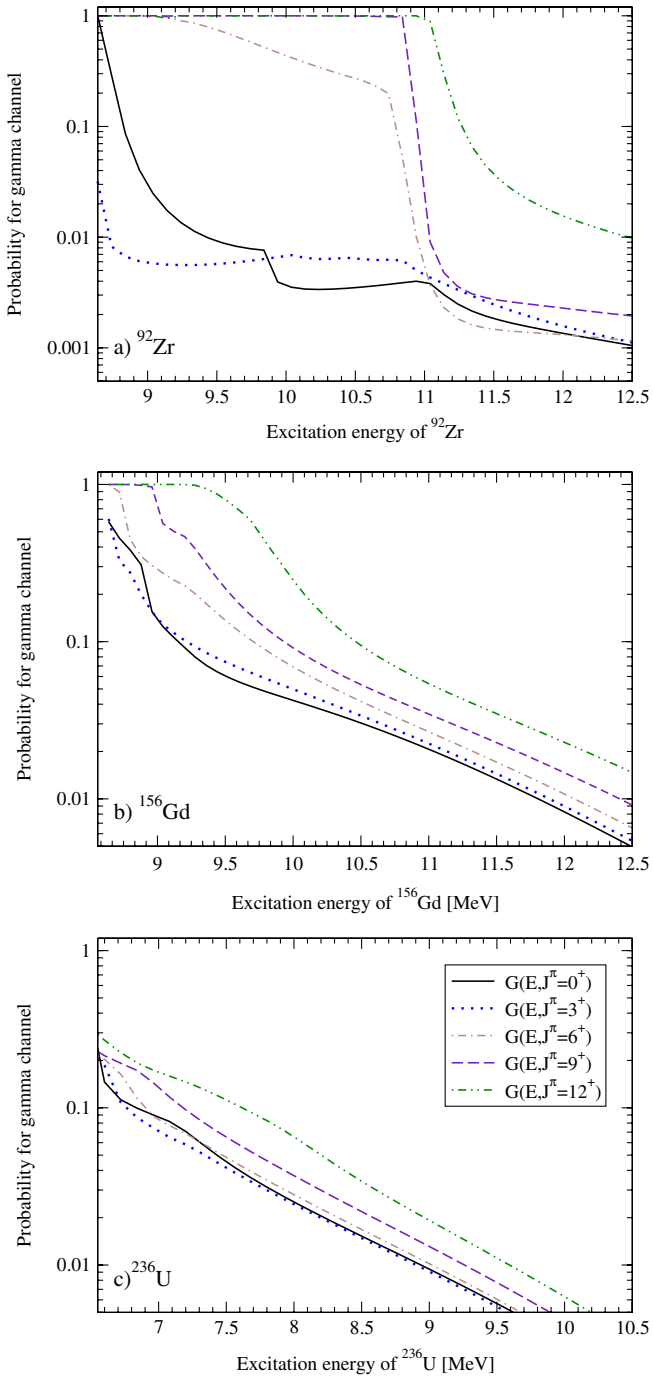

FIG. 29 (color online). Calculated γ-decay probabilities $G_\gamma^{\mathrm{CN}}(E, J, \pi)$, for ^{92}Zr, ^{156}Gd, and ^{236}U. Shown is the probability that the compound nucleus, when produced with a specific $J\pi$ combination, decays via the γ channel. The excitation energies shown correspond to incident-neutron energies of 0–4 MeV. The decay probabilities also depend on parity, only positive-parity results are shown here. More results can be found in Forssén *et al.* (2007); Escher and Dietrich (2010).

rules, but also not immediately obvious, as the fission channel has to be considered. The situation is clearer for the rare-earth case, where neutron and γ emission are the only significant decay modes. For actinides, we expect, based on these calculations, the cross sections obtained in the Weisskopf-Ewing approximation to be limited in accuracy.

In Fig. 29(b), calculated γ branching ratios $G_\gamma^{\mathrm{CN}}(E, J, \pi)$ are shown for the decay of ^{156}Gd. Since the fission channel is absent, and cross sections for charged-particle channels are very small, all $G_\gamma^{\mathrm{CN}}(E, J, \pi)$ equal 1 below the neutron separation energy; their behavior above S_n is governed by the competition of γ decay and neutron evaporation. The dependence on the spin of the decaying nucleus is stronger than in the actinide case, but significantly less than that found for the ^{92}Zr example. For energies below about 1 MeV, the branching ratios show effects of discrete levels in the neighboring nuclei; above that energy, the $G_\gamma^{\mathrm{CN}}(E, J, \pi)$ have a smooth energy dependence. While γ-branching ratios associated with small angular-momentum values ($J \leq 3$) are seen to drop rapidly right above the neutron separation energies, those related to larger J values remain high [$G_\gamma^{\mathrm{CN}}(E, J, \pi) = 1$] for several hundreds of keV above the neutron threshold. For these higher-J states, neutron evaporation is hindered at low energies, where s-wave neutron transmission dominates, since the residual ^{155}Gd nucleus contains few high-spin states to which the decay could occur. With increasing excitation energy, states with higher spins become available in the neighboring nuclei and p-wave transmission and d-wave transmission begin to compete—neutron evaporation becomes dominant. As the excitation energy increases, the $G_\gamma^{\mathrm{CN}}(E, J, \pi)$ begin to converge slowly, but no region can be identified for which the Weisskopf-Ewing limit is clearly reached.

Chiba and Iwamoto (2010) obtained γ-decay probabilities for ^{239}U that display larger variations than those shown in Fig. 29(c) for ^{236}U. Around $E_n = 5$ MeV, they found changes in $G_\gamma^{\mathrm{CN}}(E, J, \pi)$ of roughly a factor of 10 when they vary the angular momentum by $10\hbar$, from $J = 1/2$ to $J = 21/2$; at lower energies, the variations increase to factors larger than 20. Based on these results, they concluded that a surrogate analysis in the Weisskopf-Ewing approximation is not likely to produce reliable (n, γ) cross sections.

1. Spin-parity mismatch and Weisskopf-Ewing approximation for (n, γ) cross sections

Whether it is reasonable to employ the Weisskopf-Ewing approximation for a particular reaction depends not only on the energy regime considered, but also on the range of angular momenta populated in both the desired and surrogate reactions. The spin-parity population resulting from the absorption of a neutron can be calculated when reliable optical potentials are available (see the discussion in Sec. IX.D), while predicting the populations for the various surrogate mechanisms is more involved; the latter issue is discussed in Sec. IX.

The effects of the spin-parity mismatch on the extracted cross sections have been explored by Forssén *et al.* (2007) and Escher and Dietrich (2010). Schematic spin-parity distributions $F_\delta^{\mathrm{CN}}(E, J, \pi)$ were employed to simulate surrogate coincidence data $P_{\delta\gamma}^{sim}(E) = \sum_{J,\pi} F_\delta^{\mathrm{CN}}(E, J, \pi) G_\gamma^{\mathrm{CN}}(E, J, \pi)$. These were then used in a Weisskopf-Ewing "analysis" to yield the desired cross section, $\sigma_{n,\gamma}^{\mathrm{WE,sim}}(E) = \sigma_n^{\mathrm{CN}}(E) P_{\delta\gamma}^{\mathrm{sim}}(E)$; the investigation is analogous to the studies carried out for fission [see Sec. VI.C and Escher and Dietrich (2006)].

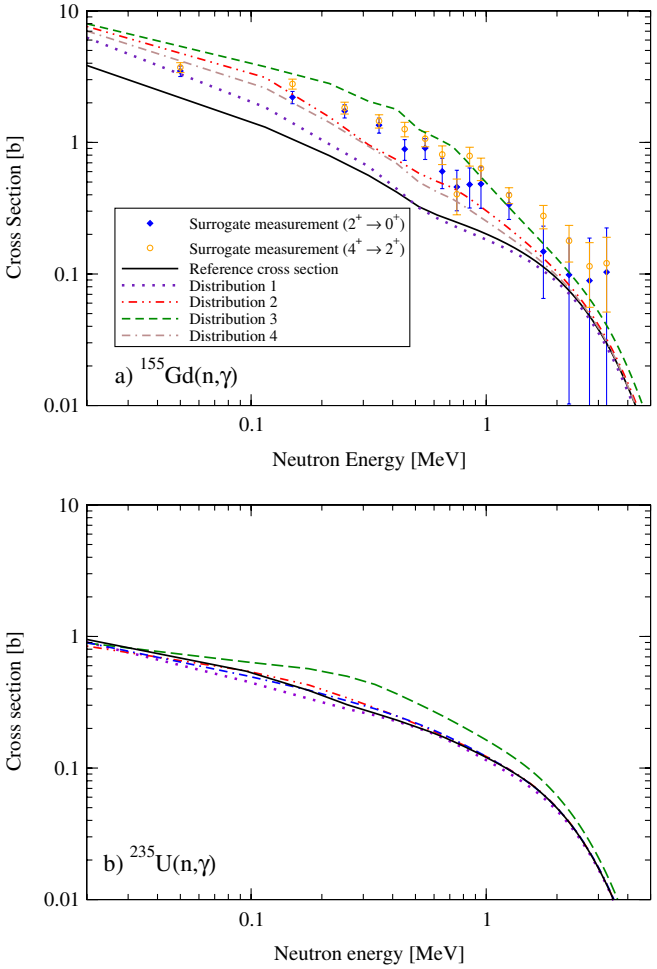

FIG. 30 (color online). Weisskopf-Ewing estimates for the (a) ^{155}Gd(n, γ) and (b) ^{235}U(n, γ) cross sections, extracted from analyses of simulated surrogate experiments, for the four different compound-nuclear $J\pi$ distributions shown in Fig. 31. For the gadolinium case, results from a Weisskopf-Ewing analysis of measured surrogate ^{156}Gd(p, p') data from Scielzo *et al.* (2010) are also shown. The reference cross sections were obtained by adjusting the parameters for the Hauser-Feshbach calculation to reproduce direct (n, γ) measurements.

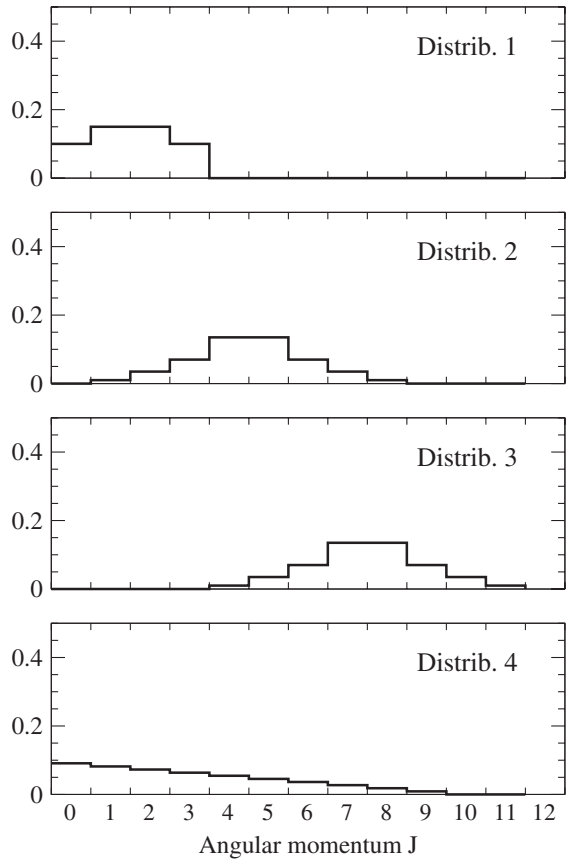

FIG. 31. Schematic spin-parity distributions, selected to simulate the compound nucleus created in the surrogate reaction. Positive and negative parity states are assumed to be populated with equal probability.

The range of cross sections $\sigma_{n,\gamma}^{\mathrm{WE,sim}}(E)$ obtained by varying the simulated spin distributions within reasonable limits provides a measure of the uncertainty in the extracted cross section due to the use of the Weisskopf-Ewing approximation. For the zirconium region, such sensitivity analysis was carried out by Forssén *et al.* (2007). An order-of-magnitude difference between the known reference cross section for ^{91}Zr(n, γ) and that extracted from the simulation was found, indicating that using the Weisskopf-Ewing approximation for this region of the nuclear chart is indeed not appropriate.

Discrepancies between extracted and reference (i.e., evaluated) cross sections are expected to be smaller for the deformed rare-earth and actinide cases, since the level densities in those regions are much higher than in the zirconium region. More recent studies (Escher and Dietrich, 2010) showed that this is indeed the case. Results for the ^{155}Gd(n, γ) and ^{235}U(n, γ) examples are shown in Fig. 30. Plotted are the reference cross sections, obtained by fitting Hauser-Feshbach calculations to direct measurements, and four cross sections extracted from simulated surrogate data; the corresponding spin distributions are shown in Fig. 31.[3]

The ^{235}U ground state has $J^\pi = 7/2^+$, and the compound nucleus ^{236}U produced in the neutron-induced reaction has an approximate spread in the J^π distribution of $2 \leq J \leq 6$ for $E_n \leq 0.1$ MeV, and $0 \leq J \leq 10$ for $E_n \approx 3$ MeV, i.e., there is significant overlap between those spin-parity distributions and the schematic distributions 1, 2, 4. The Weisskopf-Ewing analysis of the simulated surrogate data results indeed in cross sections that are similar to the reference cross section; in Fig. 30(b) the curves are seen to cluster around the (n, γ) reference result. The cross section extracted for distribution 3, however, shows clear deviations, illustrating the limitation of the Weisskopf-Ewing approximation for (n, γ) reactions in this mass region.

[3]To provide a better comparison, identical spin-parity distributions were selected for the gadolinium and uranium calculations. Inelastic scattering on a spin-0 target predominantly populates natural-parity $(0^+, 1^-, 2^+, 3^-,$ etc.) states. Replacing the distributions shown in Fig. 31 by similarly shaped "natural-parity-only" distributions yields results that differ little from those shown in Figs. 30) [cf. Figs. 16 and 19 in Scielzo *et al.* (2010)]. The effects of $J\pi$ distributions that include much larger spins have been studied for uranium by Escher and Dietrich (2010) (cf. Figure 5).

The spin distribution for the $n + {}^{155}$Gd case (the ^{155}Gd ground state has $J^\pi = 3/2^-$) has a spread of $1 \leq J \leq 4$ for E_n below about 1 MeV, and values between 0 and 6 for $E_n \approx$ 1.5 MeV, i.e., there is little overlap with distributions 2, 3, and 4 for the whole range of energies considered. This, and the fact that the $G_\gamma^{\rm CN}(E, J, \pi)$ are more sensitive to angular momentum and parity than those relevant to the uranium case, leads to cross sections that, when obtained in the Weisskopf-Ewing approximation, show poor agreement with the reference case, as can be seen in Fig. 30(a).

The cross sections obtained from the simulated surrogate data illustrate the effect of the spin-parity mismatch between the desired and surrogate reactions. The calculations give the total probability for the compound nucleus to decay via γ emission, i.e., they correspond to surrogate measurements that determine the total γ cascade resulting from the decay of the compound nucleus. Effects related to the experimental method used to identify the exit channel of interest have to be considered as well.

In Fig. 30(a) we compare ^{155}Gd(n, γ) results from the surrogate experiment by Scielzo *et al.* (2010) (see also Sec. VI.A) to the cross sections extracted from the simulated surrogate data and to the known reference cross section. In the experiment, protons inelastically scattered from a gadolinium target were detected in coincidence with discrete γ rays that are characteristic for the decay of ^{156}Gd. It was observed that almost all γ cascades proceed through the $2^+ \rightarrow 0^+$ transition [see the discussion in Scielzo *et al.* (2010)], i.e., this transition serves as a "collector" of γ cascades. The cross section extracted from a Weisskopf-Ewing analysis of this data was found to be a factor of 2 to 3 larger than the reference cross section, for most of the energy range considered. [Even larger deviations were found for the ^{157}Gd(n, γ) case, as can be seen in Fig. 8 of Scielzo *et al.* (2010)]. The ^{155}Gd(n, γ) result falls, for the most part, between the calculated curves, indicating that the surrogate reaction populated higher spins of the compound ^{156}Gd nucleus than a typical low-energy neutron-induced reaction. Also shown is the result that is obtained when using the $4^+ \rightarrow 2^+$ transition as the characteristic observable. While γ cascades originating from compound-nuclear states with low spins can bypass the $4^+ \rightarrow 2^+$ transition, thus leading to an estimate for the γ-channel probability that is too low, this effect is more than compensated for by the fact that the overall compound-nucleus spin distribution for the present example is shifted to higher J values, which results in an overestimate for the γ-channel probability relative to the neutron-induced reaction. The net effect of using the Weisskopf-Ewing approximation in this case is a cross section that is too large.

While the uranium case showed only moderate deviations from the reference cross section, both the simulation and the benchmark experiment for gadolinium indicate that the Weisskopf-Ewing approximation does not yield reliable cross section results for (n, γ) reactions on deformed rare-earth nuclei.

2. Ratios of coincidence probabilities

Cross sections for (n, f) reactions extracted in the ratio approximation have been found to be less affected by the spin-parity mismatch between the desired and surrogate reactions than results obtained from a Weisskopf-Ewing analysis. For (n, γ) reactions, the situation is more complex, as can be seen in Figs. 32 and 33. Figure 32 from Chiba and Iwamoto (2010) shows γ-decay probabilities for the compound nucleus ^{198}Au relative to those for ^{194}Ir. Ratios for individual spins $J\pi = 0^+, 2^+, \ldots, 10^+$ are compared to the ratio relevant to (n, γ) reactions. The former roughly reproduce the latter for energies above about 2 MeV, but deviate strongly for lower energies. It is unlikely that a surrogate reaction will populate the compound nuclei in a manner that the measured ratio will, on average, reproduce the ratio relevant to neutron capture. The spin effects are less pronounced in the uranium region [see Fig. 4 of Chiba and Iwamoto (2010)], but the energy range below 2 MeV remains problematic.

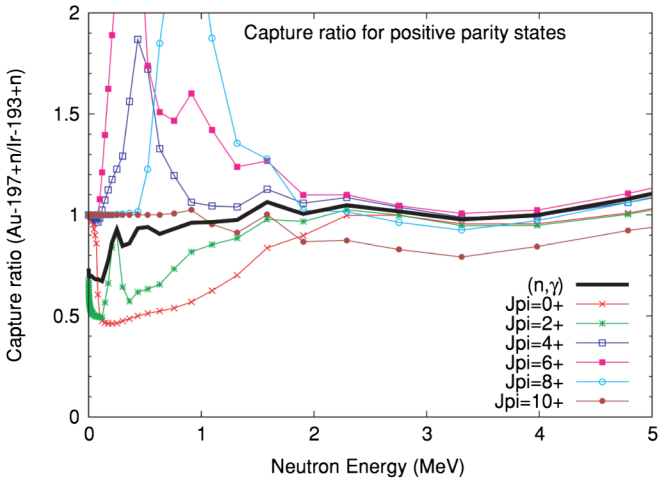

FIG. 32 (color online). Ratios $G_\gamma^{^{198}\rm Au}(E, J, \pi)/G_\gamma^{^{194}\rm Ir}(E, J, \pi)$ of decay probabilities for the compound nuclei ^{198}Au and ^{194}Ir, as a function of energy. Results for individual spins, $J\pi = 0^+, 2^+, \ldots, 10^+$, are compared to the ratio relevant to the neutron-capture reaction. From Chiba and Iwamoto, 2010.

Sensitivity studies that investigate the effect of the spin-parity distribution on the extracted cross section were carried out by Escher and Dietrich (2010). The $J\pi$ distributions of Fig. 31 were used to calculate cross section ratios from simulated ratio experiments; the results are compared to reference ratios that use known cross sections. Results for rare-earth and actinide nuclei are shown in Fig. 33. For the gadolinium example, the ratio approach was found to somewhat reduce, but not eliminate the effect of the spin-parity mismatch. Cross section ratios obtained from simulated data deviate from the reference cross section by as much as a factor of 2. Results for the surrogate ^{156,158}Gd(p, p') measurement (Scielzo *et al.*, 2010) track the theoretical curves, thus confirming that spin effects play an important role in low-energy capture reactions.

The situation seems better for the actinide region, where fission competes as a possible decay channel: Simulated surrogate results show better agreement with the reference ratios than in the gadolinium case, in particular, for neutron energies above about 0.6 MeV. The internal surrogate ratio approach [Fig. 33(c)] shows closer agreement than the external surrogate ratio method.

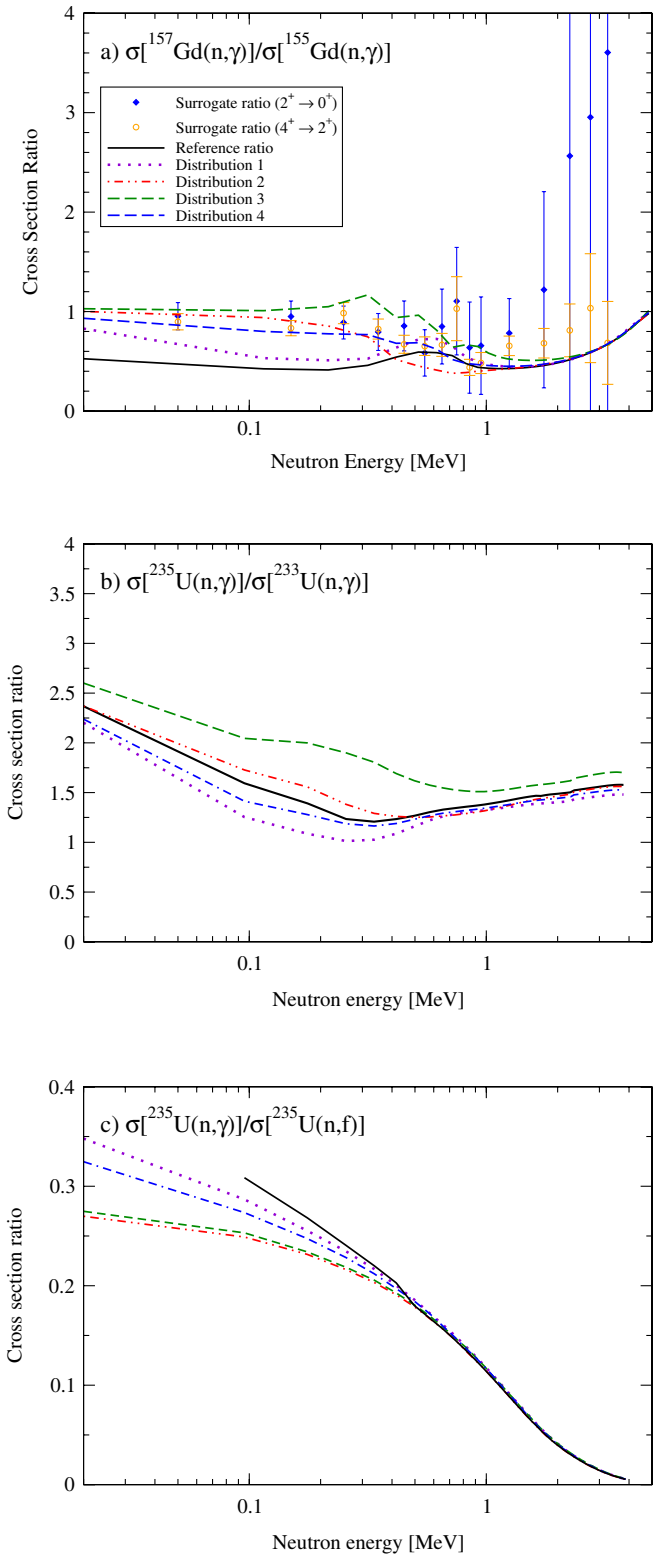

FIG. 33 (color online). Cross section ratios obtained from surrogate data are compared to ratios of evaluated cross sections. The four different compound-nuclear $J\pi$ distributions of Fig. 31 were used to simulate surrogate data. In addition, experimental results from the surrogate measurement by Scielzo *et al.* (2010) are plotted for gadolinium. (a) External surrogate ratio approach for the ^{157}Gd(n,γ) cross section, (b) external surrogate ratio approach for the ^{235}U(n,γ) cross section, and (c) internal surrogate ratio approach for the ^{235}U(n,γ) cross section.

3. Using surrogate data to normalize calculated cross sections

One might try to utilize the fact that surrogate experiments can, in principle, provide decay data for a wide range of energies, including energies for which the Weisskopf-Ewing limit is approximately valid. This approach was investigated for zirconium (Forssén *et al.*, 2007). As long as angular momenta below about $J = 6$ are involved, the Weisskopf-Ewing approximation was found to be roughly valid for $E_n \approx 3$ MeV [see Fig. 29(a)], making a fit to surrogate decay data in this region significantly less sensitive to the predicted $J\pi$ population than at lower energies. In addition, the sensitivity studies presented in Forssén *et al.* (2007) showed that modeling errors in the s-wave average radiative width $\langle\Gamma_\gamma\rangle_0$, or in the level spacing D_0, affect primarily the magnitude of the calculated cross section, but do not change the energy dependence of the cross section much. It was shown that several different decay models, representing typical uncertainties present in cross section evaluations, could be normalized to surrogate data in this energy region, despite incomplete information on surrogate spin-parity populations. The cross sections extracted using this procedure were found to be in remarkable agreement with results from an evaluation. The reason for the success of this approach was attributed to the linear relationship between variations of the level density formula, or γ-strength function, and the corresponding effect on the γ-decay branching ratios. This normalization approach is worth considering when it is possible to collect surrogate data with sufficient statistics in the relevant energy region.

IX. TOWARD A COMPREHENSIVE THEORY OF SURROGATE REACTIONS

The applications of the surrogate method discussed so far illustrate the relevance and usefulness of the method, as well as some of the limitations of its present implementations. We have observed that, in some situations, the use of the Weisskopf-Ewing and ratio approximations in the analysis of surrogate experiments can lead to large deviations from the true cross sections. To improve the accuracy of the cross sections extracted from surrogate data and to reliably extend the application of the method to new mass regions, e.g., several nucleons away from stability, a more detailed description of the reaction mechanisms involved is required. Specifically, we have to quantitatively account for the fact that the weights $F_\delta^{\mathrm{CN}}(E_{\mathrm{ex}}, J, \pi)$, by which the decay probabilities $G_\chi^{\mathrm{CN}}(E_{\mathrm{ex}}, J, \pi)$ are multiplied in Eq. (4), are different from the relative formation cross sections $F_\alpha^{\mathrm{CN}}(E_{\mathrm{ex}}, J, \pi) \equiv \sigma_\alpha^{\mathrm{CN}}(E_{\mathrm{ex}}, J, \pi)/\sum_{J'\pi'}\sigma_\alpha^{\mathrm{CN}}(E_{\mathrm{ex}}, J', \pi')$ that are directly related to Eq. (2).

In the desired reaction, the projectile a fuses with the target A to form the compound nucleus B, and the spin distribution can be predicted if the relevant a-nucleus optical-model potential is available and known to be sufficiently reliable. A number of optical potentials are available for the neutron-induced reactions that are of primary interest to the present review, i.e., we can obtain fairly reliable spin-parity information for the desired reaction.

Generating accurate predictions of the spin-parity distribution occurring in a surrogate reaction is more difficult, as it requires a model for the reaction mechanisms that are

involved in the formation of the compound nucleus. The surrogate reaction can be viewed as a process that produces initially a highly excited intermediate system. The system might consist, for instance, of a nucleon N (stripped from the projectile d in the reaction $d + D \rightarrow b + B^*$) plus the surrogate target nucleus D. For the surrogate approach to be valid, the $D + N$ system must subsequently fuse to produce the compound nucleus B^*, the decay of which one is interested in measuring. Decay of the intermediate system ($D + N$ in the example) by particle emission prior to reaching the equilibrated stage would invalidate the surrogate approach, since the measured coincidence probabilities would no longer be associated with the decay of the compound nucleus of interest, B^*. It is thus important to model how the configurations that are produced in the initial step evolve. Specifically, one needs to determine the probability for forming the desired compound nucleus B^*.

First steps towards predicting the spin-parity population in a surrogate reaction were taken by Andersen, Back, and Bang (1970), Back *et al.* (1974b), and, more recently, Younes and Britt (2003b and 2003c). They employed simple transfer calculations to estimate compound-nucleus spin-parity distributions following various stripping reactions on actinide targets. They neglected the possibility that the intermediate nucleus might decay prior to reaching equilibrium and took the resulting spin-parity distributions to be representative of those present in the compound nucleus created in the surrogate reaction of interest. Their work was reviewed in Sec. VII. Here we focus on what is needed to develop a more general description of the reaction mechanisms. We consider one-nucleon and two-nucleon transfer reactions, as well as inelastic scattering. In Sec. IX.A, we discuss the nuclear structure and reaction ingredients that are required to describe the formation of the compound nucleus in the surrogate reaction and summarize the insights gained from recent work in this area. In Sec. IX.B, we discuss briefly the issue of width-fluctuation correlations, which, in principle, affect both the desired and surrogate reaction.

Efforts to predict the spin-parity distributions for surrogate reactions need to be accompanied by the development of experimental methods that can test the predictions. In Sec. IX.C, we identify experimental observables that are sensitive to the $J\pi$ populations of the decaying compound nucleus.

Neutron-nucleus optical potentials are not only important for predicting the compound-nucleus spin-parity distributions in advanced applications of the surrogate approach, but are also needed for calculating the compound-formation cross section in applications that rely on the Weisskopf-Ewing or ratio approximation. The expected accuracy of this formation cross section is considered in Sec. IX.D. Information on preequilibrium neutron emission, which plays an important role in neutron-induced reactions at energies above a few MeV, can typically not be obtained from a surrogate experiment. How this contribution to the desired reaction can be accounted for is discussed in Sec. IX.E.

A. Theory of surrogate-reaction mechanisms

Predicting the compound-nuclear spin-parity distributions necessitates developing a quantitative description of the direct-reaction process that produces the highly excited intermediate nucleus, immediately following the direct reaction, as well as the subsequent competition between nonequilibrium particle emission and damping into the compound state. Such a description requires a framework for calculating cross sections of different reactions (stripping, pickup, charge exchange, and inelastic scattering) to continuum states, for a variety of projectiles (p, d, t, α, etc.) and targets (spherical, deformed, and transitional). The goal is to calculate the cross sections $\sigma_\delta^{\rm CN}(E_{\rm ex}, J, \pi, \theta_b)$ for forming the compound nucleus B^* with angular momentum J, parity π, and excitation energy $E_{\rm ex}$ for situations in which the outgoing particle b of the surrogate reaction $d + D \rightarrow b + B^*$ is emitted at an angle θ_b relative to the beam direction. Given these cross sections, we can then determine the spin-parity distribution for the surrogate reaction:

$$F_\delta^{\rm CN}(E_{\rm ex}, J, \pi, \theta_b) = \frac{\sigma_\delta^{\rm CN}(E_{\rm ex}, J, \pi, \theta_b)}{\sum_{J'\pi'} \sigma_\delta^{\rm CN}(E_{\rm ex}, J', \pi', \theta_b)}. \tag{23}$$

These quantities are the weights occurring in Eq. (4). Here we have made their dependence on the angle θ_b explicit. Varying the angle at which the ejectile b is observed is equivalent to sampling different angular-momentum transfers from the projectile to the target; consequently, the measured coincidence probability of Eq. (4) depends on this angle and needs to be written as $P_{\delta\chi}(E_{\rm ex}, \theta_b)$. Measurements over a wide range of angles is desirable in order to maximize the information that can be obtained from the experiment.

The calculation of the cross sections $\sigma_\delta^{\rm CN}(E_{\rm ex}, J, \pi, \theta_b)$ requires a suitable reaction model that captures the essential degrees of freedom of the reaction, while providing a clearly specified prescription for including higher-order corrections. The higher-order effects, such as collective rotational or vibrational excitations of the target, should be clearly identified and their structure (e.g., collective strength) needs to be known. To apply the reaction model to a given reaction, ingredients such as optical potentials describing the interaction of projectile d with the surrogate target D and of ejectile b with the remnant B are required. These can be estimated from regional or global parametrizations; ideally, they are tested against elastic scattering measurements at the energies relevant to the surrogate experiment. Furthermore, information on the effective interactions between relevant components of the target and the projectile is needed. In reactions that transfer a nucleon from the projectile to the target, this is the interaction between the transferred nucleon and the projectile remnant [e.g., the n-p interaction in a (d, p) reaction, where n refers to the transferred neutron and p to the outgoing proton]; for deuterons and other s-shell projectiles, these effective interactions are well known. For inelastic scattering reactions that lead to highly excited nuclei, the situation is more complicated: Target excitations induced by inelastic scattering can be described as superpositions of particle-hole excitations. In general, the effective interaction between the projectile and the target nucleons that are excited has an energy and density dependence that is not very well determined (Love *et al.*, 1980). This uncertainty is likely to affect the absolute magnitude of the predicted cross sections,

so comparisons for limiting cases, e.g., excitations which can also be described with collective models, are necessary. In all cases, comparisons with experiments are valuable. We discuss a series of surrogate-reaction mechanisms. In our descriptions, we proceed to increasingly complicated reactions, measured both by the amount of detailed target structure required and by the complexity of the required reaction model: We begin with the creation of holes in one-nucleon pickup reactions, and proceed through inelastic scattering, one-nucleon stripping, and charge-exchange reactions to two-nucleon transfer reactions. In all cases, we specifically consider the creation of an intermediate nucleus at excitation energies that are relevant to neutron-induced reactions on the neighboring isotope. For each reaction, we describe the basic reaction mechanisms, identify the nuclear-structure information that is needed for the calculations, and discuss the probability of nonequilibrium particle emission.

1. Pickup reactions

In pickup reactions, a nucleon deeply bound in the target is removed by the projectile, and is carried away in a bound ejectile state. For example, a ^{3}He nucleus incident on a ^{238}U target may pick up a neutron from the target to form an outgoing α particle, leaving behind an excited ^{237}U* nucleus. Such an experiment was performed by Lyles *et al.* (2007a), and the reaction theory has been outlined in Thompson and Escher (2006). If this reaction is to be a surrogate for $n + {}^{236}$U, the excitation energy in ^{237}U* needs to be at least 6–7 MeV to populate states above the neutron separation energy. That requires the hole state created by the pickup reaction to have a single-particle energy more than 12 MeV bound in the mean field of the target. The spin and parities J^π of the resulting ^{237}U* compound-nucleus states are therefore determined by the shell structure in the target at ≈ -12 MeV. That structure may be estimated by filling neutrons in a Hartree-Fock or Woods-Saxon mean field. The actinide and many rare-earth nuclei are well deformed, so, when the target deformation is known, a deformed mean field needs to be used as outlined, for example, in Thompson and Escher (2006). The single-particle binding energies in a mean field, whether spherical or deformed, do not take into account the residual interactions between the nucleons. Those residual interactions give a finite lifetime to any hole state (the deeper the hole state, the shorter the lifetime) and translate into nonzero widths for the hole states. These widths, also called ''spreading widths,'' reflect the fact that the initially pure single-particle configurations are ''spread out'' across much more complicated many-body states. The spreading effect can be approximated by assigning each single-particle state a Lorentzian form with a width that can be estimated, e.g., by the prescription given by Brown and Rho (1981). The result is a distribution of states that is smoothed out in energy.

One advantage of pickup reactions is that the initial states produced in such reactions consist entirely of bound particle states, so there is no significant escape of neutrons before the compound nucleus is formed. Also, the reaction does not depend on the details of correlations in excited states of the target. And finally, deep hole energies mean that there is reasonable to good energy matching in (^{3}He, α) pickup reactions, as the neutron separation energy in the α particle is 20.6 MeV. In contrast, deep hole states can only weakly be created in (p, d) reactions, as in this case the separation energy is only 2.22 MeV.

2. Inelastic scattering

Inelastic scattering is potentially an important surrogate mechanism for determining cross sections relevant to the astrophysical s process because (n, γ) reactions on unstable branch points often proceed through compound states of nuclei with stable ground states. Consequently, the compound states of interest can in principle be produced via an inelastic scattering reaction on a stable target. In inelastic scattering processes, nucleons in the target are excited from occupied to unoccupied states: from below the Fermi level to above it, either to unoccupied bound states or to continuum states (where the nucleons may escape). For example, beams of protons may create particle-hole excitations in ^{154}Gd*, so that compound-nucleus states are produced which are used to predict the ^{153}Gd(n, γ) cross section. The incident proton can be replaced by an incident α particle, which changes the reaction dynamics somewhat, but produces sets of excited states over similar ranges of energy.

The incident projectile may excite rotational bands or vibrational phonon states, but this is not sufficient to reach excitation energies relevant to surrogate applications. Instead, we rely on the projectile to excite particle-hole (ph) pairs in the target. In order to reach energies above the neutron separation threshold, $E_{\rm ex} > S_n$, the ph pairs must consist of deep holes, at energies $E_h \lesssim E_F - S_n/2$, and particles at energies $E_p \gtrsim E_F + S_n/2$, so that $E_{\rm ex} \equiv E_p - E_h > S_n$. If the particle states at $E_p \approx E_F + S_n/2$ are still bound, then there is no significant escape of neutrons before the compound nucleus is formed. Some neutron escape will result from excitations of nucleons near the Fermi surface. The spin of the resulting compound nuclei is the vector sum of the hole and particle spin states. Using spinless α-particle projectiles implies that only natural-parity states $(-1)^J = \pi$ can be excited, whereas using proton projectiles allows spin-dependent forces to also excite non-natural-parity states, albeit more weakly.

In nature, inelastic excitations are not individual particle-hole pairs, but linear combinations of all possible ph combinations that can couple to a given spin and parity of the excited nuclear state. Both the particle and the hole states have widths that contribute to the total spreading width of a given ph excitation. Individual ph excitations may be calculated using uncorrelated levels in a spherical or a deformed mean field, but a more realistic description requires a random phase approximation (RPA) excitation model. The RPA theory is designed to describe inelastic excitations up towards 100 MeV as general superpositions of all particle-hole excitations of an initial mean-field structure. RPA calculations can be carried out using spherical or deformed potentials; they may use harmonic-oscillator basis functions, or the eigenstates in a box of some radius larger than the nucleus; they may be built on Hartree-Fock mean fields, or on Hartree-Fock-Bogolyubov (HFB) structures that include the effects of pairing on the mean field (as in quasiparticle random-phase approximation descriptions).

Nobre *et al.* (2010) performed inelastic scattering calculations for a variety of target nuclei. In their work, they used a doorway approximation, which assumes that the total flux leaving the elastic channel to all possible first-order channels is independent of what happens afterwards, such as nucleon escape or damping into compound-nuclear resonances. Those calculations, therefore, do not actually predict the compound-nucleus production cross section, only the sum of the compound-nucleus cross section and the ''escape'' cross sections in each exit channel. To determine the compound-nucleus cross sections of interest to surrogate applications, extensions are needed to calculate the matrix elements of the exit-channel optical potentials with the outgoing wave functions in those channels. This is closely related to the ''partial fusion'' processes discussed in the context of stripping reactions.

3. Stripping reactions

One-nucleon stripping reactions, such as (d, p), play a prominent role in nuclear-stucture studies. They have been used extensively over the past several decades, and the formalism for stripping reactions that deposit a nucleon into a final bound state is well developed. The reaction model for deuteron stripping is well defined in terms of the Hamiltonian for a three-body model of a proton, a neutron, and the target nucleus. Higher-order effects such as deuteron breakup, and couplings between transfer states, can be modeled using currently available reaction codes; and (computationally intensive) extensions that included core excitations (Summers, Nunes, and Thompson, 2006a; 2006b) are possible. Further extensions that are specifically geared towards describing reactions on weakly bound nuclei are expected to address the needs arising from experiments at radioactive-beam facilities.

Radioactive-beam experiments are also expected to provide much-needed information on compound-nuclear reactions involving short-lived isotopes. Since free-neutron targets are not feasible, surrogate reactions, such as (d, p), will have to be used to study neutron-induced reactions in inverse kinematics. Intuitively, the process of transferring a neutron from a projectile, such as a deuteron, to a target seems very similar to bombarding that target with a neutron beam (we focus on neutron transfer here, proton-transfer can be treated analogously). Since the stripping reaction does not remove or excite target nucleons, no structure information about the occupied target states is needed to describe the process. On the other hand, since the nucleon is placed in a continuum state, one has to extend the standard stripping descriptions to properly describe this situation. Some techniques for describing reactions involving continuum wave functions have been developed (Vincent and Fortune, 1970; Sakuragi, Yahiro, and Kamimura, 1986); both breakup and transfers to narrow resonances are routinely described.

For surrogate applications, it is crucial to understand what happens after the neutron is removed from the projectile, since the neutron can escape rather than combining with the target to form the compound nucleus of interest. In other words, the reaction model needs to describe the competition between the equilibration (spreading) of the neutron-target system and neutron escape into the breakup phase space.

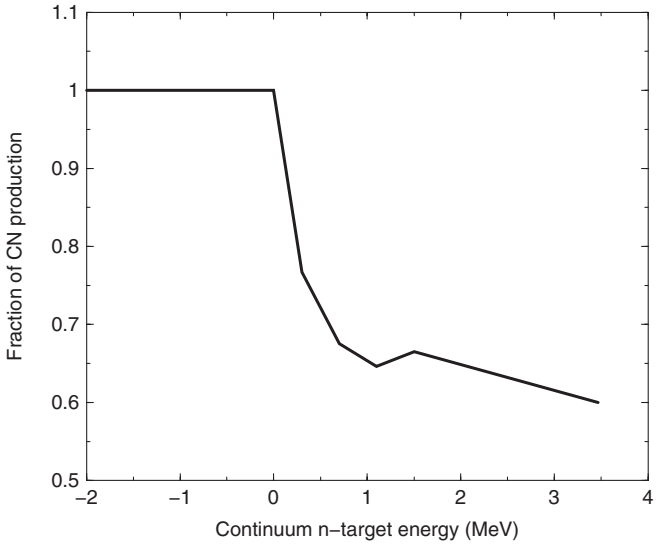

FIG. 34. Calculated probabilities from Thompson of compound-nucleus formation as a function of energy across the neutron escape threshold, for the reaction $d + {}^{239}\mathrm{Pu} \rightarrow p + {}^{240}\mathrm{Pu}$ at $E_d = 15$ MeV. This information is used to obtain the thick-dashed curve shown in Fig. 35.

In the literature, these reaction processes are also referred to as *partial fusion* reactions. Several models have been proposed to simultaneously describe the absorption of one part of a composite projectile by the target and the quantum-mechanical scattering of the other part, including those by Udagawa and Tamura (1980, 1981), Kerman and McVoy (1979) [based on work summarized in Kawai, Kerman, and McVoy (1973)], Baur *et al.* (1984), and Thompson and Diaz-Torres (2004). Applications to surrogate reactions, however, have only recently been considered by Thompson (2011) and Dietrich (2008). Thompson's calculations are based on the formalism by Udagawa and Tamura (1980, 1981), and Dietrich's approach, which is actually implemented for (n, γ) rather than (d, p), is based on a formalism developed in Parker *et al.* (1995).

Thompson calculated the probability of forming a compound nucleus in a ${}^{239}\mathrm{Pu}(d, p)$ reaction, shown in Fig. 34. The basic idea of the approach is to modify the standard (d, p) transfer description in a manner that allows one to follow the outgoing proton as well as to describe absorption of the neutron by the target. In the standard (d, p) formalism, one calculates the cross sections for a neutron being captured into a bound state around the target, with the proton escaping and being measured. The T matrix for this process has the standard form of

$$T_{dp}(\vec{k}_p) = \langle \psi^{(-)}(r_p; \vec{k}_p)\phi(r_n)|V|\phi_d(\vec{r})\Psi^{(+)}(\vec{R})\rangle, \qquad (24)$$

where $\phi(r_n)$ is the neutron final state in a real potential, $\phi_d(r)\Psi^{(+)}(R)$ is the wave function of the incoming deuteron, and V is the transfer interaction (in post or prior form). The usual partial-wave expansions can be applied to allow for proper angular-momentum coupling. For surrogate applications, we note that the neutron sees a complex potential $V(r_n) - iW(r_n)$, where the $-iW(r_n)$ term describes the loss of flux to compound-nucleus resonances. This ''spreading''

into compound-nucleus resonances is the key ingredient for calculating the partial fusion cross section of interest.

A suitable continuum wave function for the outgoing proton can be obtained by using a bin wave function, which is square integrable, i.e., it can be used as the final ''captured'' state in a standard transfer cross section calculation, without having to use techniques such as complex continuation for asymptotically large radii (Vincent and Fortune, 1970). This allows one to describe a situation in which the proton is detected far away from the target, as is done in surrogate applications. To describe the propagation of the neutron after transfer, one solves an inhomogeneous equation (here written in proper partial-wave form) with a source term that contains the proton bin function $\xi^{(-)}(r_p;\bar{k}_p)$ and the complex optical potential:

$$[H_n - E_n]\psi^J_{L_pL_d}(r_n;\bar{k}_p) = \langle \xi^{(-)}_{L_p}(r_p;\bar{k}_p)|V|\phi_d(r)\Psi^{(+)}_{L_d}(R)\rangle. \tag{25}$$

The compound-nucleus production cross section is then obtained using standard techniques. Integrating over all proton angles (summing over all L_p), one finds

$$\sigma^J_{\rm CN}(\bar{k}_p) = 4\pi\frac{2}{\hbar v_d}\sum_{L_dL_p}(2L_d+1) \times \int_0^\infty |\psi^J_{L_pL_d}(r_n;\bar{k}_p)|^2 W(r_n)dr_n, \tag{26}$$

which retains its dependence on the proton energy $E_p = \hbar^2\bar{k}_p^2/2\mu_p$.

An application of this formalism to the ^{239}Pu(d, p) reaction is shown in Fig. 34, where the probability for forming a compound nucleus in this reaction is plotted as function of ''equivalent neutron energy.'' Since a (d, p) reaction is considered, one can study ''negative neutron energies,'' i.e., the energy regime below the neutron separation energy in ^{240}Pu. As expected, the neutron cannot escape and the compound-nucleus formation probability is unity. Above the neutron separation threshold, the formation probability drops to about 60%.

This reduction of the compound-nucleus formation probability has clear implications for applications of the surrogate method, as can be seen in Fig. 35. Shown are measured fission probabilities from ^{239}Pu(d, pf) surrogate experiments (thin, dashed lines), carried out in the 1970s (Britt, Rickey, and Hall, 1968; Back *et al.*, 1971). Above the neutron separation threshold, these can be compared to the evaluated ^{239}Pu(n, f) cross section, divided by the compound-formation cross section for a neutron incident on ^{239}Pu (see thick solid line). The difference, which is clearly visible (it is about 40% at 2 MeV of equivalent neutron energy), can be attributed to the fact that the earlier surrogate work assumed 100% compound-nucleus formation in the (d, p) reaction. If one corrects for this, using the result shown in Fig. 34, one obtains the thick-dashed curve shown in Fig. 35, which is in much better agreement with the evaluated result. This illustrates that it is crucial to account for the competition between damping and escape in surrogate applications that use the (d, p) reaction to create the compound nucleus of interest.

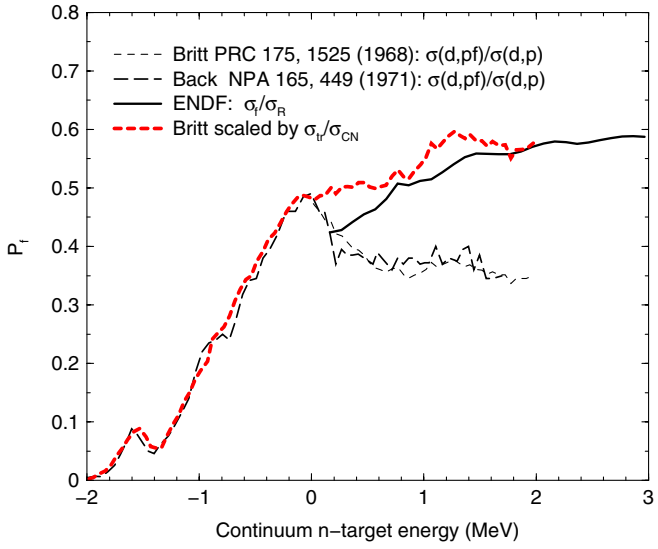

FIG. 35 (color online). Fission probabilities for ^{240}Pu* as extracted from surrogate (d, pf) experiments, compared with that obtained from evaluated (n, f) cross sections based on direct measurements, as a function of equivalent neutron energy (see text). The thick-dashed curve is the new result using the probabilities shown in Fig. 34.

The work by Dietrich (2008) further illustrates the importance of considering neutron decay before a compound nucleus is formed by looking at the evolution of the final state in the reaction ^{89}Y$(n, \gamma)^{90}$Y*, in which the direct-capture process deposits the neutron above the neutron separation energy in ^{90}Y by an amount E_n(esc), which is available for decay into the continuum (Dietrich, 2008). This reaction is similar to (d, p) since both direct reactions deposit the neutron mainly in the nuclear surface region. The results shown in Fig. 36 for the dependence of the compound-formation probability on the orbital angular momentum of the final-state (captured) neutron should be viewed as representative of what should be expected in a (d, p) reaction.

The average value of the compound-formation probability for energies above the escape threshold [i.e., $E_n(\text{esc}) > 0$] is in the neighborhood of 0.85 [see Parker *et al.* (1995) and Dietrich (2008) for details], somewhat higher than in the ^{239}Pu(d, p) case discussed above. However, there is a strong dependence on the orbital angular momentum L of the escaping neutron, as shown in the figure for three values of the decay energy, $E_n(\text{esc}) = 1$, 5, and 11 MeV. For high L values, the neutron is prevented from escaping by the centrifugal barrier. However, for low values there is significant competition between absorption and escape, and compound-formation probabilities can be as low as 0.5. We note that the radiative capture mechanism considered in Parker *et al.* (1995) and Dietrich (2008) can easily be replaced by the stripping process for further investigations; the treatment of the final state is the same in both cases.

This calculation as well as the one shown for ^{239}Pu(d, p) show quantitatively that it is crucial to consider the neutron escape process in surrogate reactions using (d, p) as the initial reaction. The escape mechanism not only significantly affects the average coincidence probability that is measured in a

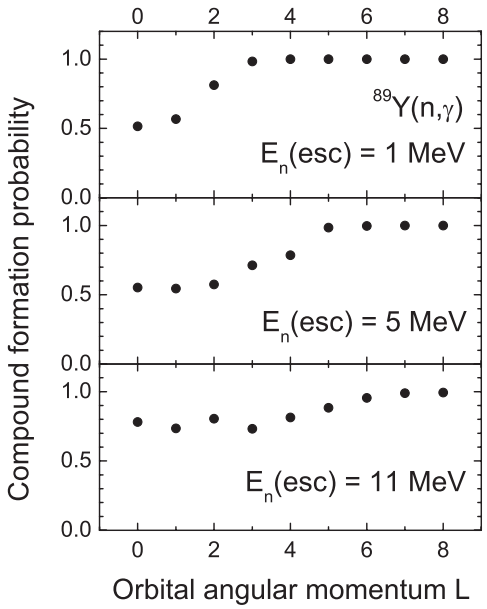

FIG. 36. Compound-formation probability for radiative capture of 19.6 MeV neutrons to unbound final states in the ^{89}Y$(n, \gamma)^{90}$Y* reaction as a function of the orbital angular momentum of the final-state neutron (Dietrich, 2008). This process is similar to deposition of the neutron in the (d, p) reaction. Results are shown for three values of the energy above the escape threshold for the final-state neutron.

surrogate reaction, but also distorts the spin-parity distribution in the compound nucleus because of the centrifugal barrier effect.

4. Charge-exchange reactions

Reactions such as (^{3}He, t) may be used to replace a neutron in the target by a proton by 2-nucleon charge exchange. For example, excited states in ^{240}Am* may be produced by the reaction ^{240}Pu(^{3}He, t)^{240}Am*, in order to indirectly measure reactions produced by neutrons incident on ^{239}Am. This approach has been used (Cramer and Britt, 1970a) to estimate (n, f) cross sections. These early results, however, used the Weisskopf-Ewing approximation, without the effect of any spin-parity distribution.

Predictions for the spin-parity distributions produced in charge-exchange reactions are more complicated than the previously discussed calculations for inelastic and transfer processes, as the effective interaction needed has many components (Osterfeld, 1992). The charge-exchange cross section for light nuclei is known to depend on a large number of single-particle matrix elements that contribute coherently (Guess *et al.*, 2009), and for heavy nuclei one needs more sophisticated approaches, such as (quasiparticle)RPA models (Terasaki *et al.*, 2005) to describe all particle-hole excited states that can be produced. The relevant reaction models for predicting the spin distributions are not yet implemented. In addition to the matrix elements required to describe the one-step process, at beam energies below 50 MeV/u one also needs to include two-step transfer contributions. For the (^{3}He, t) reactions, these two-step routes can proceed via (^{3}He, d, t) and (^{3}He, α, t) processes; the calculations require knowledge of one-nucleon overlap functions for several neighboring nuclei.

5. Two-nucleon transfer reactions

Two-nucleon transfer reactions may be used to travel further from the target nucleus in the Segré chart. For example, the fission cross section for neutrons incident on ^{239}U has been extracted by using a (t, p) reaction to transfer two neutrons from ^{238}U to make excited states in ^{240}U* (Younes and Britt, 2003c). The (^{18}O, ^{16}O) process has also been used (Burke *et al.*, 2011) for the same purpose. In addition, two-neutron pickup reactions (p, t) can be used to probe the states of nuclei that are more proton rich. We also need to consider (^{3}He, p) and (p, ^{3}He) reactions that transfer a proton and a neutron (in a superposition of different spin and isospin configurations).

In principle, all previous comments about pickup and transfer reactions apply here as well, because such reactions can be modeled as a di-nucleon transfer, but with additional complications since the di-nucleon is not strictly an inert particle. Transfer cross sections are small ($\approx$ 1–10 mb), so two-neutron transfers are even smaller ($\approx$ 10–100 μb).

The mechanisms for picking up two neutrons from a nucleus are essentially the same as two successive pickup reactions as described in Sec. IX.A.1, but there are also *simultaneous* transfer mechanisms that depend on the probability of correlated neutrons in relative s states in the target. Excitation energies relevant to neutron-induced reactions on neighboring nuclei can be achieved by removing neutrons from levels that are much less bound than in the one-neutron removal reactions discussed above; on average, the levels involved are only half as far below the Fermi energy as in the earlier case.

Transferring two neutrons to continuum states of a nucleus can result in states with rather high excitation energies. For example, in the ^{240}U case, the transfer can produce excitations on the order of 12 MeV above the ground state. In this case, it becomes necessary to calculate the probability for the neutrons appearing in the breakup channel rather than in a compound nucleus after their transfer. For applications, however, that involve the energy regime just above the neutron separation energy in ^{240}U (as is relevant, e.g., if the desired reaction is induced by a low-energy neutron on ^{239}U) one only needs to transfer an average two-neutron energy of -5 MeV on ^{238}U. This is not in the continuum, so the escape fraction that gives breakup should be much reduced.

The pair of transferred nucleons keeps (to first order) the same configuration that they have in the projectile: the same relative angular momentum, and the same distribution of radial separations. This means that (t, p) reactions, for example, where initially the two neutrons are almost entirely in a singlet $^1S_0$ state, only populate target states where they have the same relative motion. The angular momentum between the $2n$ and the target is not constrained, but, as in normal transfer reactions, may have any value as determined by the shell structure of the composite nucleus at the measured energies. One also needs to calculate two-step contributions from sequential transfers, the (t, d, p) or (^{18}O, ^{17}O, ^{16}O) routes, which again add coherently to the direct "simultaneous" transfer matrix element.

The reaction models for calculating *nn*, *np*, or *pp* two-nucleon transfers are available in principle for both simultaneous and sequential transfers, as long as we have available some structure models to calculate the various one-nucleon and two-nucleon overlap functions. Some additional work, though, may be needed to ensure convergence when we include continuum states as intermediate configurations in the sequential transfer of the nucleons.

B. Width-fluctuation corrections

The standard Hauser-Feshbach expression for a compound-nuclear reaction, such as the desired reaction in the present context, assumes independence of formation and decay for each total spin and parity $J\pi$. It is well known that this assumption is not strictly true, since there are correlations between the formation and decay widths of the microscopic compound-nuclear resonances, as well as between these widths and the total widths that appear in the Hauser-Feshbach denominators. There are a number of different treatments of this problem that vary according to the assumptions made about the statistical distributions of the widths, the degree to which the resonances overlap, and the approximations made to obtain the correction to the Hauser-Feshbach formula. These factors are usually expressed via width-fluctuation correction factors $W_{\alpha\chi}(J\pi)$, so that the corrected cross section for a reaction from channel α to channel χ becomes

$$\sigma_{\alpha\chi} = \pi\lambda^2 \sum_{J\pi} \omega_\alpha(J\pi) \frac{T_\alpha T_\chi}{\sum_\beta T_\beta} W_{\alpha\chi}(J\pi), \tag{27}$$

where $\omega_\alpha(J\pi)$ is a statistical factor and the T's are transmission coefficients for decay into the various channels. Hilaire, Lagrange, and Koning (2003) provided a recent review of this problem as well as numerical comparisons of three different approaches to generating the corrections.

Exactly the same issue arises in the surrogate problem. In this case, the expression for the observable coincidence probability $P_{\delta\chi}$ (where δ symbolizes the direct reaction used to form the compound nucleus) can be modified by inclusion of width-fluctuation factors $W'_{\delta\chi}(J\pi)$ as

$$P_{\delta\chi} = \sum_{J\pi} \frac{F_\delta(J\pi) T_\chi}{\sum_\beta T_\beta} W'_{\delta\chi}(J\pi). \tag{28}$$

In principle, the factors W' can be calculated with the same techniques as the W. In both cases there are correlations between the outgoing-channel widths and the denominator. In Eq. (27) there is also a correlation between the entrance channel and the denominator, but whether the entrance channel in Eq. (28) participates in the correlation will depend on the nature of the direct interaction. A theory for width-fluctuation effects for forming compound nuclei in one reaction that is being studied for surrogate reactions (d, p) has been given by Kerman and McVoy (1979), based on the formalism of Kawai, Kerman, and McVoy (1973). In one case, the analysis of fission probabilities following the (t, p) reaction (Younes and Britt, 2003b), numerical values for the W' factors have been calculated by the method of Moldauer (1961), under the assumption that the (t, p) formation factor does not participate in the correlation.

Width-correlation corrections are expected to be important at low energies in the desired reaction, where a limited number of channels is open. For example, corrections to (n, γ) reactions are typically in the 10%–20% range up to a few hundred keV, but become unimportant at significantly higher energies. The corrections in the fission probability analysis (Younes and Britt, 2003b) in some cases were as large as 30%. If simulations show that width-fluctuation effects are important in the desired reaction, it seems reasonable that they should be included in the analysis of the corresponding surrogate experiment.

C. Tests of the theory predictions

Theories describing transfer, inelastic scattering, and charge-exchange reactions that lead to final states with low excitation energies are well established (Satchler, 1983). Many experiments have been carried out over the years to test the theoretical predictions against cross section measurements. The angular and energy dependences of the cross sections have been measured, for various projectile-target combinations and bombarding energies, and used to improve the theories. As described in the preceding sections, for use in surrogate reactions these theories must be extended to treat highly excited, overlapping, unbound final states in the residual nucleus. It is highly desirable that these extended theories be tested by measuring absolute cross sections for the energy and angular distributions of the ejectile, even though this is not strictly necessary to carry out a surrogate measurement.

For applications of interest here, it is not sufficient to calculate only the angular and energy dependence of the differential cross sections of the outgoing particle; reliable predictions for the spin-parity population of the residual compound nucleus are needed. Consequently, to test surrogate-reaction models it is necessary to also identify observables that are sensitive to the $J\pi$ distribution of the compound nuclei created. Candidates include the yields of discrete γ-ray transitions of the decaying compound nucleus, as well as angular distributions of fission fragments, for systems that decay via this mode.

The path of the γ cascade of a decaying compound nucleus is known to depend on the initial spin of the nucleus. While this fact can complicate the detection of the decay channel of interest in surrogate applications (see the discussion in Sec. VIII.A), it is also a source of useful information. Simultaneously measuring the yields of several such γ-ray transitions can provide signatures for the spin-parity distribution of the compound nucleus prior to decay. An example for this is shown in Fig. 37, where we have plotted the relative yields of several ground-state band transitions for ^{236}U, for the four schematic $J\pi$ distributions shown in Fig. 31. We find that different $J\pi$ distributions lead to markedly different relative γ-ray yields. These observables can be employed to test and constrain theories that predict compound-nuclear spin-parity distributions. Relative γ-ray yields for the decay of even-even gadolinium nuclei have recently been measured (Scielzo *et al.*, 2010) and methods are being developed to use

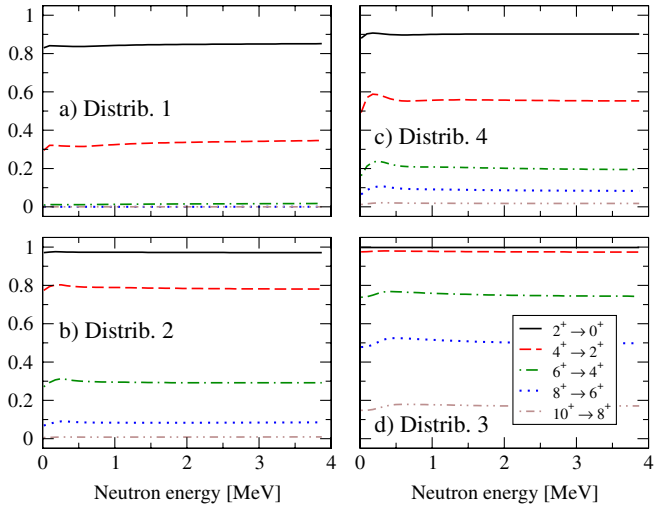

FIG. 37 (color online). Ratios of the yields of various γ-ray transitions in the ground-state band of ^{236}U to the total production of ^{236}U, for the four schematic spin distributions shown in Fig. 31.

this information in order to improve the (n, γ) cross sections determined from surrogate experiments.

Similarly, anisotropic distributions of fission fragments can both complicate the measurements of total fission probabilities in surrogate applications, and provide valuable information on the properties of the nucleus that undergoes fission. These anisotropies must be measured (and extrapolated) to infer the total number of fission fragments when the fission detectors cover only a portion of 4π. Distributions both within and perpendicular to the reaction plane have to be considered.

Angular correlations between the outgoing direct-reaction particle and fission fragments were studied in the 1960s for (d, pf), (t, pf), (t, df), and (α, α') reactions (Wilkins, Unik, and Huizenga, 1964; Britt *et al.*, 1965; Britt and Plasil, 1966; Vandenbosch *et al.*, 1967; Britt, Rickey, and Hall, 1968; Wolf, Vandenbosch, and Loveland, 1968; Britt and Cramer, 1969). For a given projectile-target combination, the fragment distributions were found to depend on a variety of parameters: (i) the energy E_{ex} to which the nucleus B^* was excited in the direct reaction; (ii) properties of the transition states populated in B^*, such as the parity π of the relevant state, as well as the angular momentum J and its projections K and M on the body-fixed and laboratory-fixed axes, respectively; and (iii) the angle of the outgoing direct-reaction particle with respect to the beam direction. Both the stripping and the inelastic scattering studies found the anisotropies in the fission-fragment distribution to be particularly large near the fission threshold. At about 2 MeV above the threshold the number of states increases significantly and many different spin states are populated, which dilutes the strength of any one particular spin and the anisotropy disappears. For situations in which transition states with known K values are populated, measured fission-fragment anisotropies may provide useful information about the mechanisms that populate these states in direct reactions (Casperson *et al.*, 2011). This can then be used to verify the accuracy of direct-reaction models that describes these mechanisms.

D. Accuracy of compound-nucleus formation cross sections

In this section, we comment on the accuracy with which neutron compound-nucleus formation cross sections can be determined from optical potentials. The compound-nucleus formation cross section, also called the absorption cross section, is related to cross sections calculated by a spherical or coupled-channels optical-model code by

$$\sigma_{\text{cmpd}} = \sigma_{\text{tot}} - \sigma_{\text{elas}} - \sigma_{\text{inel}}, \tag{29}$$

where σ_{tot} is the total cross section, σ_{elas} is the shape elastic cross section, and σ_{inel} is the sum of the cross sections for inelastic excitation of the coupled states, if any. σ_{cmpd} is used directly in a Weisskopf-Ewing analysis of a surrogate reaction, and is also a weighted sum of the transmission coefficients required for a full Hauser-Feshbach treatment.

We focus on neutrons because most surrogate-reaction experiments to date are intended as indirect measurements of neutron-induced reactions such as (n, f) or (n, γ). The surrogate experiment itself provides no constraints on the absorption cross section or transmission coefficients. These quantities must be obtained independently from an optical-model calculation with potentials that can be extrapolated with sufficient accuracy from neighboring nuclei where the observables can be checked against experiment. A useful summary of available optical potentials can be found in Capote *et al.* (2009) and on the Reference Input Parameter Library (RIPL-3) website.

For incident energies above the region of isolated resonances, direct measurements of the compound-formation cross section are difficult, the experimental data are sparse, and there is significant scatter among available measurements on a given nucleus that is not consistent with the slow energy dependence expected from an optical potential. Thus, the optical-model values for the compound cross section are largely a prediction based on fits of the model parameters to other quantities more easily measured, such as total cross sections and elastic angular distributions. The predicted compound-formation cross sections from various phenomenologically determined potentials vary by amounts in the 5%–7% range, and the experimental data [see, for example, the CSISRS/EXFOR database (CSISRS, 2010)] do not clearly choose among them. One set of direct measurements that appears to provide a useful constraint on the compound cross sections is a set of measurements (MacGregor, Ball, and Booth, 1957; 1963) across the periodic table at 14.1 MeV, in which the scatter about a smooth behavior with A is approximately 3%–5%.

At low energies (below about 100 keV) the compound cross sections are closely related to the s-wave and p-wave strength functions obtained from the analysis of neutron resonance data. These quantities, which are equivalent to the s-wave and p-wave transmission coefficients, are available for a wide variety of stable targets across the periodic table (Mughabghab, 2006; Capote *et al.*, 2009). The strength functions are important for constraining the optical potential at low energies, particularly the strength of the imaginary component. However, caution should be exercised near closed shells (for example, near $A = 90$ and 120), where global optical potentials such as that of Koning and

Delaroche (2003) do not fit the strength function data well. There is also significant scatter in the strength function data, particularly evident in the $A = 120$ region, which may indicate the importance of doorway states (Shakin, 1963; Feshbach, Kerman, and Lemmer, 1967) that are beyond the scope of the single-channel optical model.

Statically deformed nuclei are a particularly favorable case. They are far from closed shells, and structural features (such as the deformation parameters) vary slowly with Z and A. Recent investigations (Dietrich, Thompson, and Kawano, 2012) also show that the calculated σ_{cmpd} are very insensitive to the spin and K value of the target state. Potentials used in analysis of recent surrogate experiments in the actinides [the phenomenological FLAP 2.2 (Escher and Dietrich, 2010), a deformed-nucleus folding model (Bauge *et al.*, 2000) based on a reparametrization of the JLM (Jeukenne-Lejeune-Mahaux) nuclear-matter optical potential (Bauge, Delaroche, and Girod, 1998)], as well as an additional phenomenological potential fit to a wide variety of neutron and proton data (Sukhovitskii *et al.*, 2000), show differences in the energy dependence of σ_{cmpd}, particularly below 10 MeV. Nevertheless, these potentials are in agreement to roughly 5% below 10 MeV, and 3% above. These values, if taken as the optical-model uncertainty, are significantly smaller than the total uncertainties in currently available surrogate experiments.

For nuclei near the valley of stability that can be treated with a spherical, single-channel optical model, extrapolations to nuclei that are one or two nucleons away from nuclei where optical potentials adequately reduce experimental data are likely to be possible. However, this is subject to the qualifications noted above for nuclei very close to closed shells. For a specific case, the global potential by Koning and Delaroche (2003) may yield satisfactory results, or may serve as a useful starting point for the determination of a regional potential that yields better results in the neighborhood of the nucleus of interest.

For future experiments away from valley of stability with rare-isotope beams, the assumption that the optical model is sufficiently well known for surrogate-reaction analysis will likely not be satisfactory. Since little data will be available to determine the parameters of a phenomenological potential, this will require further development of microscopically based potentials. It will also be important in each case to check the fundamental assumptions of the optical model, such as the requirement that the level density in the compound system be sufficiently high for the energy averaging implicit in the model to yield well-defined results.

E. Preequilibrium neutron emission in the desired reaction

Preequilibrium neutron emission is important for neutron-induced reactions at incident energies above a few MeV, and is normally included in calculations of (n, f), $(n, 2n)$, etc., cross sections.

The discussions here assume that a unique compound nucleus is formed in a given surrogate reaction. In this picture, the contributions to the desired (n-induced) cross section due preequilibrium processes cannot be obtained from surrogate measurements. One might argue that at least in cases of one-neutron transfer reactions to the target, processes similar to those in traditional preequilibrium reactions occur, but it is not clear how the escape events in stripping reactions, such as the (d, p) case discussed above, are quantitatively related to the preequilibrium emission in a neutron-induced reaction. However, some estimates of the effects of preequilibrium emission on the (n, f) cross section can be made. For neutron capture, we expect the effects to be negligible, as preequilibrium emission typically occurs at neutron energies above at least 5–6 MeV.

Figure 38 shows a typical Hauser-Feshbach calculation for the $^{235}\mathrm{U}(n, f)$ cross section including a preequilibrium component (solid line), together with the same calculation without preequilibrium but identical parameters otherwise (dashed line).

The principal effect of preequilibrium neutron emission is on first-chance fission; i.e., fission of the compound nucleus formed by fusion of the incident neutron with the target. Preequilibrium neutron emission corresponds to a fast (n, n') process that bypasses this stage. The sum of cross sections for all reaction processes induced by the incident neutron, both preequilibrium and compound, must be approximately the area of the nucleus. Consequently, the compound-nucleus formation cross section (which would correspond to the nuclear area in the absence of prequilibrium) must be reduced by the calculated preequilibrium emission cross section. This is reflected in a reduction of first-chance fission.

In the region ($\lesssim 7$ MeV) where first-chance fission dominates, the correction to the total fission is less than 10%. At the highest energies (≈ 20 MeV), the depletion of first-chance fission is quite large, in the neighborhood of 40%. However, second-chance and third-chance fission are dominant in this region, so the net correction to the total fission is much less, not exceeding $\approx 15\%$ over the entire energy range.

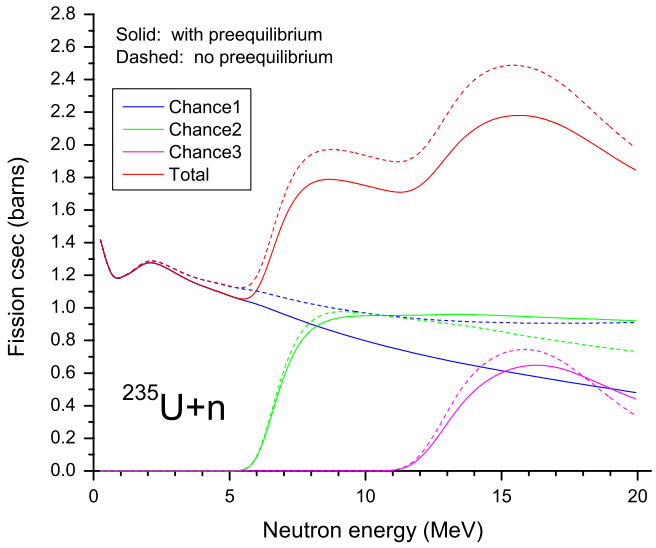

FIG. 38 (color online). Hauser-Feshbach calculation illustrating the effect of preequilibrium neutron emission. The solid lines represent the fit to the known $^{235}\mathrm{U}(n, f)$ cross section, as discussed by Escher and Dietrich (2006). The dashed lines are a calculation with identical parameters except that preequilibrium is turned off.

The effects of preequilibrium on second-chance and third-chance fission are much smaller than for first chance. Although the preequilibrium (n, n') process bypasses the first compound nucleus, for sufficiently low energies of the inelastically scattered neutrons the residual nucleus will be sufficiently excited to be able to fission. This component of the fission cross section originates from the same residual nucleus that is reached by neutron emission from the first compound nucleus, and thus must be added to the fission component (second-chance fission) arising from purely compound processes. The net result is that second-chance and higher-chance fission cross sections are much less sensitive to the inclusion of preequilibrium than the first-chance process.

Because the interplay between the preequilibrium and compound parts of the reaction is complicated, it is not possible to make a straightforward correction for preequilibrium emission in the simple Weisskopf-Ewing picture of the surrogate reaction or in the ratio method based on it. However, we have noted above that the total fission cross sections calculated with and without preequilibrium are within 15% of each other. Moreover, we expect that the corrections for preequilibrium should be very similar for targets differing only by two neutrons [^{233}U(n, f) vs ^{235}U(n, f) as studied here, or ^{235}U(n, f) vs ^{237}U(n, f) as typically inferred from experiments using the ratio method]. Therefore, the errors incurred by ignoring preequilibrium emission are likely to be much smaller than 15% when the ratio method is used.

With our present knowledge, it appears that the best way to account for the missing preequilibrium contribution in a surrogate reaction is to make model calculations of the desired reaction with and without preequilibrium (as done in Fig. 38), and then multiply the result of the surrogate-reaction analysis by the ratio of the two model calculations. We will not discuss this issue further, but note that the effects can be large enough that a correction is essential. This issue deserves further attention in a more complete treatment of surrogate reactions.

X. CONCLUDING REMARKS

Surrogate experiments carried out so far illustrate both the potential and the current limitations of the method. We reviewed the present status of the surrogate method, with a focus on applications involving neutron-induced reactions. We showed successful applications from the early surrogate experiments, carried out at Los Alamos in the 1970s, and more recent experiments carried out by research groups in France, India, and the United States. In particular, we have seen that (n, f) cross sections extracted from surrogate measurement show reasonable agreement with directly measured cross sections for neutron energies above 1–2 MeV, can help to distinguish discrepancies between different direct measurements and extend known cross sections to energy regimes for which no data exist. Moreover, they are able to provide cross sections for reactions that cannot be measured directly.

We have also discussed the limitations of the surrogate method as it is presently implemented. Almost all applications of the method so far have relied on approximation schemes which ignore the fact that the compound nucleus that is produced in the surrogate reaction is characterized by a spin-parity distribution that can be very different from the spin-parity distribution of the compound nucleus occurring in the desired, neutron-induced reaction. Ignoring this ''spin-parity mismatch'' is not only formally incorrect, it also has practical implications: it reduces the accuracy of the cross sections extracted from surrogate measurements and it limits the reach of the surrogate approach. We illustrated this with examples of measured low-energy (n, f) cross sections and theoretical sensitivity studies. We also showed the improvements that can be attained when correcting for the spin-parity mismatch. We furthermore demonstrated that (n, γ) cross sections extracted from surrogate experiments tend to be much more sensitive to the spin-parity distribution of the compound nucleus than (n, f) cross sections. The examples indicate that it is crucially important to correct for the spin-parity mismatch when considering (n, γ) reactions.

A comprehensive theoretical treatment of the surrogate approach involves a description of direct reactions that populate highly excited, unbound states, the damping of these doorway states into more complicated configurations that lead to a compound nucleus (or nonequilibrium particle emission), the dependence and influence of these processes on angular momentum, parity, and energy, and (when necessary) width-fluctuation corrections to the Hauser-Feshbach-type formalism. This has to be carried out for multiple direct-reaction mechanisms (stripping, pickup, inelastic scattering, and charge exchange) and various projectile-target combinations. We outlined the steps that will improve the accuracy and reliability of the surrogate approach and extend its applicability to reactions that cannot be approached with the present implementation of the method. It is crucial that the theory developments be accompanied by suitable experiments that test their predictions; we identified some observables to address this need.

Ultimately, to study isotopes further from stability, experiments performed in ''inverse kinematics,'' where a heavy-ion beam will impinge on a low-mass target, will be required. For neutron-induced reactions, surrogate-reaction techniques will have to be used in place of the desired neutron-induced reactions as free-neutron targets are not feasible. Studies at the Holifield Radioactive Ion Beam Facility (HRIBF) at Oak Ridge National Laboratory have begun to investigate some of the challenges associated with performing this type of measurement (Cizewski *et al.*, 2006). Reactions such as (d, p) look promising for generating the exotic compound nuclei needed to determine cross sections and sophisticated detector arrays, such as the Helical Orbit Spectrometer (HELIOS) at Argonne National Laboratory (Lighthall *et al.*, 2010), have been developed for high-resolution studies of these reactions. Using surrogate reactions, a wide range of cross sections for exotic and short-lived isotopes will be accessible to study at the many existing and future high-intensity radioactive-beam facilities around the world.

ACKNOWLEDGMENTS

We wish to express our gratitude to all those colleagues who have contributed to our understanding of the physics

summarized here. In particular, we thank L. A. Bernstein for initiating the experimental surrogate research effort at LLNL, E. P. Hartouni for his support in establishing the research program, H. C. Britt and A. K. Kerman for frequent discussions on the subject. We thank R. D. Hoffman, S. Goriely, F. Herwig, and J. J. Ressler for constructive input on the manuscript, and M. Aiche, B. Jurado, and J. M. Allmond for providing us with modified figures of their published work. We are grateful to R. J. Casperson for his work on Fig. 1. Partial support was provided by the Department of Energy's NNSA, Office of Nonproliferation Research and Development (NA-22). This work was performed under the auspices of the U.S. Department of Energy by Lawrence Livermore National Laboratory under Contract No. DE-AC52-07NA27344.

REFERENCES

Ahearne, J. F., *et al.*, 2006, "Scientific Opportunities with a Rare-Isotope Facility in the United States," Rare-Isotope Assessment Committee, Board on Physics and Astronomy, Washington, D.C. (unpublished).

Aliberti, G., G. Palmiotti, M. Salvatores, T. Kim, T. Taiwo, M. Anitescu, I. Kodeli, E. Sartori, J. Bosq, and J. Tommasi, 2006, Ann. Nucl. Energy **33**, 700.

Allmond, J. M., *et al.*, 2009, Phys. Rev. C **79**, 054610.

Andersen, B. L., B. B. Back, and J. M. Bang, 1970, Nucl. Phys. **A147**, 33.

Arnould, M., and S. Goriely, 2003, Phys. Rep. **384**, 1.

Arnould, M., S. Goriely, and K. Takahashi, 2007, Phys. Rep. **450**, 97.

Azhari, A., V. Burjan, F. Carstoiu, H. Dejbakhsh, C. A. Gagliardi, V. Kroha, A. M. Mukhamedzhanov, L. Trache, and R. E. Tribble, 1999, Phys. Rev. Lett. **82**, 3960.

Back, B. B., J. P. Bondorf, G. A. Otroschenko, J. Pedersen, and B. Rasmussen, 1971, Nucl. Phys. **A165**, 449.

Back, B. B., H. C. Britt, O. Hansen, B. Leroux, and J. D. Garrett, 1974a, Phys. Rev. C **10**, 1948.

Back, B. B., O. Hansen, H. C. Britt, and J. D. Garrett, 1974b, Phys. Rev. C **9**, 1924.

Basunia, M., *et al.*, 2009, Nucl. Instrum. Methods Phys. Res., Sect. B **267**, 1899.

Bauge, E., J. P. Delaroche, and M. Girod, 1998, Phys. Rev. C **58**, 1118.

Bauge, E., J. P. Delaroche, and M. Girod, 2001, Phys. Rev. C **63**, 024607.

Bauge, E., J.-P. Delaroche, M. Girod, G. Haouat, J. Lachkar, Y. Patin, J. Sigaud, and J. Chardine, 2000, Phys. Rev. C **61**, 034306.

Baur, G., 1986, Phys. Lett. B **178**, 135.

Baur, G., C. A. Bertulani, and H. Rebel, 1986, Nucl. Phys. **A458**, 188.

Baur, G., K. Hencken, and D. Trautmann, 2003, Prog. Part. Nucl. Phys. **51**, 487.

Baur, G., and H. Rebel, 1996, Annu. Rev. Nucl. Part. Sci. **46**, 321.

Baur, G., F. Rösel, D. Trautmann, and R. Shyam, 1984, Phys. Rep. **111**, 333.

Baur, G., and S. Typel, 2004, Prog. Theor. Phys. Suppl. **154**, 333.

Beer, H., and R. L. Macklin, 1988, Astrophys. J. **331**, 1047.

Bender, P. C., *et al.*, 2009, Phys. Rev. C **80**, 014302.

Bernstein, L. A., *et al.*, 2006, "Deducing the ^{237}U(n,γ) and $(n,2n)$ Cross Sections Using a New Surrogate Ratio Method," Technical Report, Lawrence Livermore National Laboratory, Livermore, CA.

Beun, J., J. C. Blackmon, W. R. Hix, G. C. McLaughlin, M. S. Smith, and R. Surman, 2009, J. Phys. G **36**, 025201.

Blons, J., B. Fabbro, C. Mazur, D. Paya, M. Ribrag, and Y. Patin, 1988, Nucl. Phys. **A477**, 231.

Blons, J., C. Mazur, D. Paya, M. Ribrag, and H. Weigmann, 1984, Nucl. Phys. **A414**, 1.

Bolsterli, M., E. O. Fiset, J. R. Nix, and N. J. L., 1972, Phys. Rev. C **5**, 1050.

Boyer, S., *et al.*, 2006, Nucl. Phys. **A775**, 175.

Britt, H. C., and J. D. Cramer, 1969, Phys. Rev. **181**, 1634.

Britt, H. C., and J. D. Cramer, 1970, Phys. Rev. C **2**, 1758.

Britt, H. C., W. R. Gibbs, J. J. Griffin, and R. H. Stokes, 1965, Phys. Rev. **139**, B354.

Britt, H. C., and F. Plasil, 1966, Phys. Rev. **144**, 1046.

Britt, H. C., F. A. Rickey, and W. S. Hall, 1968, Phys. Rev. **175**, 1525.

Britt, H. C., and J. B. Wilhelmy, 1979, Nucl. Sci. Eng. **72**, 222.

Brown, G. E., and M. Rho, 1981, Nucl. Phys. **A372**, 397.

Burbidge, E. M., G. R. Burbidge, W. A. Fowler, and F. Hoyle, 1957, Rev. Mod. Phys. **29**, 547.

Harke, J. T., *et al.*, 2006, Phys. Rev. C **73**, 054604.

Burke, J. T., *et al.*, 2011, "Surrogate two-neutron transfer reactions to populate ^{240}U," unpublished.

Capote, R., *et al.*, 2009, Nucl. Data Sheets **110**, 3107.

Casperson, R., J. Burke, I. Thompson, J. Escher, J. Ressler, and N. Scielzo, 2011, Bull. Am. Phys. Soc. **55**, JG.6, http://meetings.aps.org/Meeting/DNP11/Event/150618.

Chadwick, M., 2001 (private communication).

Chiba, S., and O. Iwamoto, 2010, Phys. Rev. C **81**, 044604.

Cizewski, J., *et al.*, 2006, AIP Conf. Proc. **819**, 209.

Clark, R. M., *et al.*, 2005, Phys. Rev. C **72**, 054605.

Colonna, N., 2009, J. Phys. Conf. Ser. **168**, 012024.

Colonna, N., *et al.*, 2010, Energy and Environmental Science **3**, 1910.

Committee on the Physics of the Universe (National Research Council), 2003, *Connecting Quarks with the Cosmos: Eleven Science Questions for the New Century* (National Academies Press, Washington, D.C.), http://books.nap.edu/catalog.php?record_id=10079.

Cramer, J. D., and H. C. Britt, 1970a, Nucl. Sci. Eng. **41**, 177.

Cramer, J. D., and H. C. Britt, 1970b, Phys. Rev. C **2**, 2350.

CSISRS, the Cross Section Information Storage and Retrieval System, 2010, Database available at www.nndc.bnl.gov and mirror web sites.

Dabbs, J. W. T., C. H. Johnson, and C. E. Bemis, 1983, Nucl. Sci. Eng. **83**, 22.

David, P., J. Hartfiel, H. Janszen, R. von Mutius, J. Arvieux, L. Farvacque, B. Berthier, B. Bonin, and J. C. Lugol, 1987, Z. Phys. A **326**, 367.

Dean, D., J. Dobaczewski, K. Langanke, F. Nunes, and W. Ormand, 2005, *RIA Theory Bluebook: A Road Map* (RIA Theory Group), http://fribusers.org/3_GROUPS/20_THEORY/3_DOCUMENTS/Blue_Book_FINAL.pdf.

Descouvemont, P., and T. Rauscher, 2006, Nucl. Phys. **A777** (Special Issue on Nuclear Astrophysics), 137.

Dietrich, F. S., I. J. Thompson, and T. Kawano, 2012, Phys. Rev. C (in press).

Dietrich, F. S., 2008, AIP Conf. Proc. **1005**, 125.

Duchene, G., *et al.*, 1999, Nucl. Instrum. Methods Phys. Res., Sect. A **432**, 90.

Elekes, Z., T. Belgya, G. L. Molnár, A. Z. Kiss, M. Csatlós, J. Gulyás, A. Krasznahorkay, and Z. Máté, 2003, Nucl. Instrum. Methods Phys. Res., Sect. A **503**, 580.

Escher, J., L. A. Bernstein, J. T. Burke, F. S. Dietrich, C. Forssén, and B. Lyles, 2007, in *International Conference on Nuclear Data*

for Science and Technology (ND2007), Nice, France, 2007, pp. 325–329.
Escher, J. E., and F. S. Dietrich, 2006, Phys. Rev. C **74**, 054601.
Escher, J. E., and F. S. Dietrich, 2010, Phys. Rev. C **81**, 024612.
Feshbach, H., A. K. Kerman, and R. H. Lemmer, 1967, Ann. Phys. (N.Y.) **41**, 230.
Fomushkin, E. F., Y. I. Vinogradov, V. V. Gavrilov, G. F. Novoselov, 1990, Sov. At. Energy **69**, 889.
Forssén, C., F. Dietrich, J. Escher, R. Hoffman, and K. Kelley, 2007, Phys. Rev. C **75**, 055807.
Fröbrich, P., and R. Lipperheide, 1996, *Theory of Nuclear Reactions* (Clarendon Press, Oxford).
Fursov, B. I., *et al.*, 1997, *Conf. Nucl. Data for Sci. And Techn.*, Trieste, p. 488.
Gagliardi, C. A., *et al.*, 1999, Phys. Rev. C **59**, 1149.
Gavron, A., H. C. Britt, E. Konecny, J. Weber, and J. B. Wilhelmy, 1975, Phys. Rev. Lett. **34**, 827.
Gavron, A., H. C. Britt, E. Konecny, J. Weber, and J. B. Wilhelmy, 1976, Phys. Rev. C **13**, 2374.
Gibelin, J., *et al.*, 2008, AIP Conf. Proc. **1005**, 77.
Goldblum, B. L., S. G. Prussin, U. Agvaanluvsan, L. A. Bernstein, D. L. Bleuel, W. Younes, and M. Guttormsen, 2008, Phys. Rev. C **78**, 064606.
Goldblum, B. L., S. G. Prussin, L. A. Bernstein, W. Younes, M. Guttormsen, and H. T. Nyhus, 2010, Phys. Rev. C **81**, 054606.
Goldblum, B. L., *et al.*, 2009, Phys. Rev. C **80**, 044610.
Goriely, S., 1997, Astron. Astrophys. **325**, 414, http://aa.springer.de/papers/7325001/2300414.pdf.
Goriely, S., 1998, Phys. Lett. B **436**, 10.
Guerrero, C., *et al.*, 2009, Nucl. Instrum. Methods Phys. Res., Sect. A **608**, 424.
Guess, C. J., *et al.*, 2009, Phys. Rev. C **80**, 024305.
Guttormsen, M., *et al.*, 1990, Phys. Scr. **T32**, 54.
Hatarik, R., *et al.*, 2010, Phys. Rev. C **81**, 011602.
Hauser, W., and H. Feshbach, 1952, Phys. Rev. **87**, 366.
Herman, M., R. Capote, B. V. Carlson, P. Oblozinsky, M. Sin, A. Trkov, H. Wienke, and V. Zerkin, 2007, Nucl. Data Sheets **108**, 2655.
Herwig, F., 2005, Annu. Rev. Astron. Astrophys. **43**, 435.
Hilaire, S., C. Lagrange, and A. J. Koning, 2003, Ann. Phys. (N.Y.) **306**, 209.
Jurado, B., *et al.*, 2008, AIP Conf. Proc. **1005**, 90.
Käppeler, F., and A. Mengoni, 2006, Nucl. Phys. **A777**, 291.
Kawai, M., A. K. Kerman, and K. W. McVoy, 1973, Ann. Phys. (N.Y.) **75**, 156.
Kerman, A. K., and K. W. McVoy, 1979, Ann. Phys. (N.Y.) **122**, 197.
Kessedjian, G., *et al.*, 2010, Phys. Lett. B **692**, 297.
Koning, A. J., and J.-P. Delaroche, 2003, Nucl. Phys. **A713**, 231.
Kreisler, M., 2007, in *Particle Accelerator Conference, 2007. PAC. IEEE*, pp. 124–126, http://accelconf.web.cern.ch/AccelConf/p07/PAPERS/MOZBC01.PDF.
Lesher, S. R., *et al.*, 2009, Phys. Rev. C **79**, 044609.
Lesher, S. R., L. Phair, L. A. Bernstein, D. L. Bleuel, J. T. Burke, J. A. Church, P. Fallon, J. Gibelin, N. D. Scielzo, and M. Wiedeking, 2010, Nucl. Instrum. Methods Phys. Res., Sect. A **621**, 286.
Lesko, K., 1984, *Energy Loss and Straggle Tool* [adapted from the Computer program ENELOSS, written by H. Ernst (1981) with stopping power routines by K. Lesko (1984)].
Lighthall, J., *et al.*, 2010, Nucl. Instrum. Methods Phys. Res., Sect. A **622**, 97.
Love, G., *et al.*, 1980, in *Conference on the* (p, n) *Reaction and the Nucleon-Nucleon Force, Telluride, Colorado 1979*, edited by C. D. Goodman, (Plenum, New York).
Lugaro, M., F. Herwig, J. C. Lattanzio, R. Gallino, and O. Straniero, 2003, Astrophys. J. **586**, 1305.
Lyles, B. F., *et al.*, 2007a, Phys. Rev. C **76**, 014606.
Lyles, B. F., *et al.*, 2007b, Phys. Rev. C **76**, 019905.
Lynn, J. E., and A. C. Hayes, 2003, Phys. Rev. C **67**, 014607.
MacGregor, M. H., W. P. Ball, and R. Booth, 1957, Phys. Rev. **108**, 726.
MacGregor, M. H., R. Booth, and W. P. Ball, 1963, Phys. Rev. **130**, 1471.
Mathews, G. J., A. Mengoni, F.-K. Thielemann, and W. A. Fowler, 1983, Astrophys. J. **270**, 740.
May, M., *et al.*, 2008, *Nuclear Forensics: Role, State of the Art, Program Needs*, Technical Report, Nuclear Forensics Working Group of the American Physical Society's Panel on Public Affairs and the American Association for the Advancement of Science.
McNally, J. H., J. W. Barnes, B. J. Dropesky, P. A. Seeger, and K. Wolfsberg, 1974, Phys. Rev. C **9**, 717.
Meadows, J., 1983, Report No. ANL/NDM-83.
Meadows, J. W., 1988, Ann. Nucl. Energy **15**, 421.
Micron Semiconductor Ltd., 2010, http://www.micronsemiconductor.co.uk/.
Moldauer, P. A., 1961, Phys. Rev. **123**, 968.
Mortensen, F. N., J. M. Scott, and S. A. Colgate, 2003, Los Alamos Sci. **28**, 38.
Moses, E., *et al.*, 2009, Fusion Sci. Technol. **56**, 547.
Mughabghab, S. F., 2006, *Atlas of Neutron Resonances, Resonance Parameters and Thermal Cross Sections* $Z = 1$–100 (Elsevier, Amsterdam), 5th ed..
Muir, D. W., and L. R. Veeser, 1971, in *Proceedings of the Third International Conference on Neutron Cross Sections and Technology, Knoxville, 1971*, Vol 1, p. 292.
Mukhamedzhanov, A. M., C. A. Gagliardi, and R. E. Tribble, 2001, Phys. Rev. C **63**, 024612.
Nayak, B. K., A. Saxena, D. C. Biswas, E. T. Mirgule, B. V. John, S. Santra, R. P. Vind, R. K. Choudhury, and S. Ganesan, 2008, Phys. Rev. C **78**, 061602.
Nobre, G. P. A., F. S. Dietrich, J. E. Escher, I. J. Thompson, M. Dupuis, J. Terasaki, and J. Engel, 2010, Phys. Rev. Lett. **105**, 202502.
Northrop, J. A., R. H. Stokes, and K. Boyer, 1959, Phys. Rev. **115**, 1277.
Osterfeld, F., 1992, Rev. Mod. Phys. **64**, 491.
Parker, W. E., *et al.*, 1995, Phys. Rev. C **52**, 252.
Petit, M., *et al.*, 2004, Nucl. Phys. **A735**, 345.
Pignatari, M., R. Gallino, M. Heil, M. Wiescher, F. Kaeppeler, F. Herwig, and S. Bisterzo, 2010, Astrophys. J. **710**, 1557.
Pizzone, R. G., and C. Spitaleri, 2008, AIP Conf. Proc. **972**, 270.
Plattard, S., *et al.*, 1981, Phys. Rev. Lett. **46**, 633.
Plettner, C., *et al.*, 2005, Phys. Rev. C **71**, 051602(R).
Rauscher, T., 2005, Nucl. Phys. **A758**, 655.
Rauscher, T., 2008, J. Phys. G **35**, 014026.
Ressler, J. J., *et al.*, 2011, Phys. Rev. C **83**, 054610.
Ressler, J. J., *et al.*, 2010, Phys. Rev. C **81**, 014301.
Rolfs, C. E., and S. Rodney, 1988, *Cauldrons in the Cosmos* (University of Chicago Press, Chicago).
Sakuragi, Y., M. Yahiro, and M. Kamimura, 1986, Prog. Theor. Phys. Suppl. **89**, 136.
Satchler, G. R., 1983, *Direct nuclear Reactions* (Oxford University Press, New York).
Schatz, H., *et al.*, 1998, Phys. Rep. **294**, 167.
Scielzo, N. D., *et al.*, 2008, AIP Conf. Proc. **1005**, 109.
Scielzo, N. D., *et al.*, 2010, Phys. Rev. C **81**, 034608.
Shakin, C. M., 1963, Ann. Phys. (N.Y.) **22**, 373.

Shcherbakov, O., *et al.*, 2002, J. Nucl. Sci. Tech., Suppl. **2**, 230, http://wwwndc.jaea.go.jp/nd2001/proc/pdf/1_0230.pdf.
Sinha, A. K., P. David, H. Hanscheid, F. Risse, C. Rosel, and W. Schrieder, 1992, J. Phys. G **18**, L105.
Specht, H. J., J. S. Fraser, and J. C. D. Milton, 1966, Phys. Rev. Lett. **17**, 1187.
Sukhovitskii, E. S., O. Iwamoto, S. Chiba, and T. Fukahori, 2000, J. Nucl. Sci. Technol. **37**, 120.
Summers, N. C., F. M. Nunes, and I. J. Thompson, 2006a, Phys. Rev. C **73**, 031603.
Summers, N. C., F. M. Nunes, and I. J. Thompson, 2006b, Phys. Rev. C **74**, 014606.
Surman, R., J. Beun, G. C. McLaughlin, and W. R. Hix, 2009, Phys. Rev. C **79**, 045809.
Surman, R., and J. Engel, 2001, Phys. Rev. C **64**, 035801.
Tanaka, K., 2009, Nucl. Fusion **49**, 104004.
Terasaki, J., J. Engel, M. Bender, J. Dobaczewski, W. Nazarewicz, and M. Stoitsov, 2005, Phys. Rev. C **71**, 034310.
Thompson, I., and J. Escher, 2006, "Theory of (3He,alpha) surrogate reactions for deformed uranium nuclei," Technical Report UCRL-TR-225984, Lawrence Livermore National Laboratory.
Thompson, I. J., 2011, J. Phys. Conf. Ser., **312**, 082041.
Thompson, I. J., and A. Diaz-Torres, 2004, Prog. Theor. Phys. Suppl. **154**, 69.
Thompson, I. J., and F. Nunes, 2009, *Nuclear Reactions for Astrophysics : Principles, Calculation and Applications Of Low-Energy Reactions* (Cambridge University Press, Cambridge).
Timofeyuk, N. K., and P. Descouvemont, 2005, Phys. Rev. C **71**, 064305.
Timofeyuk, N. K., R. C. Johnson, and A. M. Mukhamedzhanov, 2003, Phys. Rev. Lett. **91**, 232501.
Tovesson, F., *et al.*, 2004, Nucl. Phys. **A733**, 3.
Tovesson, F., and T. S. Hill, 2007, Phys. Rev. C **75**, 034610.
Tovesson, F., *et al.*, 2002, Phys. Rev. Lett. **88**, 0.
Travaglio, C., R. Gallino, E. Arnone, J. Cowan, F. Jordan, and C. Sneden, 2004, Astrophys. J. **601**, 864.
Typel, S., and G. Baur, 2003, Ann. Phys. (N.Y.) **305**, 228.
Udagawa, T., and T. Tamura, 1980, Phys. Rev. Lett. **45**, 1311.
Udagawa, T., and T. Tamura, 1981, Phys. Rev. C **24**, 1348.
Ullmann, J., *et al.*, 2005, AIP Conf. Proc. **769**, 918.
Vandenbosch, R., K. L. Wolf, J. Unik, C. Stephan, and J. R. Huizenga, 1967, Phys. Rev. Lett. **19**, 1138.
Van Der Plicht, J., M. N. Harakeh, A. V. D. Woude, P. David, J. Debrus, H. Janszen, and J. Schulze, 1980, Nucl. Phys. **A346**, 349.
Vincent, C. M., and H. T. Fortune, 1970, Phys. Rev. C **2**, 782.
Vogt, E. W., 1968, in *The Statistical Theory of Nuclear Reactions* in Advances in Nuclear Physics, edited by M. Baranger, E. W. Vogt (Plenum, New York), Vol. 1, pp. 261–342.
Voignier, J., S. Joly, and G. Grenier, 1992, Nucl. Sci. Eng. **112**, 87.
Vorotnikov, P., *et al.*, 1984, Sov. J. Nucl. Phys. **40**, 726.
Wallerstein, G., *et al.*, 1997, Rev. Mod. Phys. **69**, 995.
Wanajo, S., 2007, Astrophys. J. **666**, L77.
Weston, L. W., P. G. Young, W. P. Poenitz, and C. Lubitz, 1977, *ENDF/B-VI Evaluation, Revision 5* (National Nuclear Data Center, Brookhaven National Laboratory, Upton, NY).
Wiedeking, M., *et al.*, 2008a, Phys. Rev. C **77**, 054305.
Wiedeking, M., *et al.*, 2008b, Phys. Rev. Lett. **100**, 152501.
Wilkins, B. D., J. P. Unik, and J. R. Huizenga, 1964, Phys. Lett. **12**, 243.
Wilson, J. N., B. Haas, S. Boyer, D. Dassie, G. Barreau, M. Aiche, S. Czajkowski, C. Grosjean, and A. Guiral, 2003, Nucl. Instrum. Methods Phys. Res., Sect. A **511**, 388.
Wolf, K. L., R. Vandenbosch, and W. D. Loveland, 1968, Phys. Rev. **170**, 1059.
Wolter, H. H., and S. Typel, 2003, Nucl. Phys. **A722**, C215.
Wu, J. R., J. R. Beene, C. E. Bemis, F. E. Bertrand, E. E. Gross, D. J. Horen, and W. P. Jones, 1981, Phys. Rev. C **24**, 500.
Xu, H. M., C. A. Gagliardi, R. E. Tribble, A. M. Mukhamedzhanov, and N. K. Timofeyuk, 1994, Phys. Rev. Lett. **73**, 2027.
Younes, W., and H. C. Britt, 2003a, "Neutron Fission of ^{235,237,239}U and ^{241,243}Pu: Cross Sections, Integral Cross Sections and Cross Sections on Excited States," Technical Report UCRL-ID-154206, Lawrence Livermore National Laboratory, Livermore, CA.
Younes, W., and H. C. Britt, 2003b, Phys. Rev. C **67**, 024610.
Younes, W., and H. C. Britt, 2003c, Phys. Rev. C **68**, 034610.
Younes, W., and H. C. Britt, 2004, "Simulated (n, f) cross sections on various Th, U, Np, Pu, and Am targets," Technical Report UCRL-PROC-206823, Lawrence Livermore National Laboratory, Livermore, CA (unpublished).
Younes, W., and H. C. Britt, 2005, "Estimates of the ^{237,239}U(n, f) Cross Sections for $0.1 < E_n(\mathrm{MeV}) \leq 20$," Technical Report UCRL-TR-212600, Lawrence Livermore National Laboratory, Livermore, CA.
Younes, W., H. C. Britt, and J. A. Becker, 2004, "Estimated (n, f) cross sections for ^{236,236m,237,238}Np, ^{237,237m}Pu, and ^{240,241,242,242m,243,244,244m}Am isotopes," Technical Report UCRL-TR-201913, Lawrence Livermore National Laboratory, Livermore, CA.
Younes, W., H. C. Britt, J. A. Becker, and J. B. Wilhelmy, 2003, "Initial estimate for the ^{237}U(n, f) cross section for $0.1 \leq E_n(\mathrm{MeV}) \leq 20$," Technical Report UCRL-ID-154194, Lawrence Livermore National Laboratory, Livermore, CA.
Young, P. G., 2003 (private communication).
Young, P. G., M. B. Chadwick, R. E. MacFarlane, P. Talou, T. Kawano, D. G. Madland, W. B. Wilson, and C. W. Wilkerson, 2007, Nucl. Data Sheets **108**, 2589.
Young, P. E., E. D. Arthur, and M. B. Chadwick, 1992, "Comprehensive Nuclear Model Calculations: Introduction to the Theory and Use of the GNASH Code," Los Alamos National Laboratory Technical Report LA-12343-MS.
Ziegler, J. F., 2004, Nucl. Instrum. Methods Phys. Res., Sect. B **219**, 1027.